

# Global Biogeochemical Cycles<sup>\*</sup>








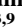














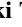


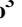


## RESEARCH ARTICLE

10.1029/2024GB008141

## Carbon and Greenhouse Gas Budgets of Europe: Trends, Interannual and Spatial Variability, and Their Drivers

### Key Points:

- We provide a bottom-up estimate of CO<sub>2</sub>, CH<sub>4</sub>, N<sub>2</sub>O emissions of 3.9 Pg CO<sub>2</sub>-eq. yr<sup>-1</sup> over Europe, 2010–2019
- Terrestrial ecosystems acted as a greenhouse gas net sink of 0.9 Pg CO<sub>2</sub>-eq. yr<sup>-1</sup>, dominated by CO<sub>2</sub> sink
- Net-greenhouse gas emissions decreased by ~1/4 since the 1990s, but land carbon sink is weakening since the 2000s

Ronny Lauerwald<sup>1</sup> , Ana Bastos<sup>2</sup> , Matthew J. McGrath<sup>3</sup>, Ana Maria Roxana Petrescu<sup>4</sup>, François Ritter<sup>3</sup>, Robbie M. Andrew<sup>5</sup>, Antoine Berchet<sup>3</sup> , Grégoire Broquet<sup>3</sup>, Dominik Brunner<sup>6</sup>, Frédéric Chevallier<sup>3</sup> , Alessandro Cescatti<sup>7</sup> , Sara Filipek<sup>8</sup> , Audrey Fortems-Cheiney<sup>3,9</sup> , Giovanni Forzieri<sup>10</sup> , Pierre Friedlingstein<sup>11,12</sup>, Richard Fuchs<sup>13</sup>, Christoph Gerbig<sup>2</sup>, Sander Houweling<sup>4</sup> , Piyu Ke<sup>11,14</sup> , Bas J. W. Lerink<sup>8</sup> , Wanjing Li<sup>14</sup>, Wei Li<sup>14</sup> , Xiaojun Li<sup>15</sup>, Ingrid Luijckx<sup>16</sup> , Guillaume Monteil<sup>17</sup>, Saqr Munassar<sup>2</sup>, Gert-Jan Nabuurs<sup>8</sup>, Prabir K. Patra<sup>18,19</sup> , Philippe Peylin<sup>3</sup>, Julia Pongratz<sup>20,21</sup> , Pierre Regnier<sup>22</sup>, Marielle Saunois<sup>3</sup> , Mart-Jan Schelhaas<sup>8</sup> , Marko Scholze<sup>17</sup> , Stephen Sitch<sup>11</sup> , Rona L. Thompson<sup>23</sup> , Hanqin Tian<sup>24</sup> , Aki Tsuruta<sup>25</sup> , Chris Wilson<sup>26,27</sup> , Jean-Pierre Wigneron<sup>15</sup>, Yitong Yao<sup>3</sup> , Sönke Zaehle<sup>2</sup> , and Philippe Ciais<sup>3</sup> 

### Supporting Information:

Supporting Information may be found in the online version of this article.

### Correspondence to:

R. Lauerwald,  
ronny.lauerwald@inrae.fr

### Citation:

Lauerwald, R., Bastos, A., McGrath, M. J., Petrescu, A. M. R., Ritter, F., Andrew, R. M., et al. (2024). Carbon and greenhouse gas budgets of Europe: Trends, interannual and spatial variability, and their drivers. *Global Biogeochemical Cycles*, 38, e2024GB008141. <https://doi.org/10.1029/2024GB008141>

Received 15 FEB 2024

Accepted 17 JUL 2024

### Author Contributions:

**Conceptualization:** Ronny Lauerwald, Ana Bastos, Ana Maria Roxana Petrescu, Philippe Ciais

**Data curation:** Ronny Lauerwald, Ana Maria Roxana Petrescu, Robbie M. Andrew, Antoine Berchet, Grégoire Broquet, Dominik Brunner, Frédéric Chevallier, Sara Filipek, Audrey Fortems-Cheiney, Pierre Friedlingstein, Richard Fuchs, Christoph Gerbig, Sander Houweling, Bas J. W. Lerink, Wanjing Li, Wei Li, Xiaojun Li, Ingrid Luijckx, Guillaume Monteil, Saqr Munassar, Gert-Jan Nabuurs, Prabir K. Patra, Philippe Peylin, Julia Pongratz, Pierre Regnier, Marielle Saunois, Mart-Jan Schelhaas, Marko Scholze,

<sup>1</sup>Université Paris-Saclay, INRAE/AgroParisTech UMR EcoSys, Palaiseau, France, <sup>2</sup>Max-Planck-Institute for Biogeochemistry, Jena, Germany, <sup>3</sup>CEA/CNRS/UVSQ Laboratoire des Sciences du Climat et de l'Environnement, Université Paris-Saclay, Gif-sur-Yvette, France, <sup>4</sup>Department of Earth Sciences, Vrije Universiteit Amsterdam, Amsterdam, The Netherlands, <sup>5</sup>CICERO Center for International Climate Research, Oslo, Norway, <sup>6</sup>Swiss Federal Laboratories for Materials Science and Technology, EMPA, Dübendorf, Switzerland, <sup>7</sup>European Commission, Joint Research Centre (JRC), Ispra, Italy, <sup>8</sup>Wageningen Environmental Research, Wageningen University and Research (WUR), Wageningen, The Netherlands, <sup>9</sup>Science Partners, Paris, France, <sup>10</sup>Department of Civil and Environmental Engineering (DICEA) Via di Santa Marta 3, University of Florence, Firenze, Italy, <sup>11</sup>Faculty of Environment, Science and Economy, University of Exeter, Exeter, UK, <sup>12</sup>Laboratoire de Meteorologie Dynamique, Departement de Geosciences, Institut Pierre-Simon Laplace, CNRS-ENS-UPMC-X, Ecole Normale Supérieure, Paris, France, <sup>13</sup>Land Use Change & Climate Research Group, IMK-IFU, Karlsruhe Institute of Technology (KIT), Garmisch-Partenkirchen, Germany, <sup>14</sup>Department of Earth System Science, Ministry of Education Key Laboratory for Earth System Modeling, Institute for Global Change Studies, Tsinghua University, Beijing, China, <sup>15</sup>INRAE, UMR 1391 ISPA, Université de Bordeaux, Villenave d'Ornon, France, <sup>16</sup>Meteorology and Air Quality Group, Wageningen University, Wageningen, The Netherlands, <sup>17</sup>Department of Physical Geography and Ecosystem Science, Lund University, Lund, Sweden, <sup>18</sup>Research Institute for Global Change, JAMSTEC, Yokohama, Japan, <sup>19</sup>Research Institute for Humanity and Nature, Kyoto, Japan, <sup>20</sup>Department of Geography, Ludwig-Maximilians-Universität München, Munich, Germany, <sup>21</sup>Max Planck Institute for Meteorology, Hamburg, Germany, <sup>22</sup>Department Geoscience, Environment & Society-BGEOSYS, Université Libre de Bruxelles, Bruxelles, Belgium, <sup>23</sup>Norwegian Institute for Air Research (NILU), Kjeller, Norway, <sup>24</sup>Department of Earth and Environmental Sciences, Center for Earth System Science and Global Sustainability, Schiller Institute for Integrated Science and Society, Boston College, Chestnut Hill, MA, USA, <sup>25</sup>Finnish Meteorological Institute, Helsinki, Finland, <sup>26</sup>National Centre for Earth Observation, University of Leeds, Leeds, UK, <sup>27</sup>School of Earth & Environment, University of Leeds, Leeds, UK

**Abstract** In the framework of the RECCAP2 initiative, we present the greenhouse gas (GHG) and carbon (C) budget of Europe. For the decade of the 2010s, we present a bottom-up (BU) estimate of GHG net-emissions of 3.9 Pg CO<sub>2</sub>-eq. yr<sup>-1</sup> (using a global warming potential on a 100 years horizon), which are largely dominated by fossil fuel emissions. In this decade, terrestrial ecosystems acted as a net GHG sink of 0.9 Pg CO<sub>2</sub>-eq. yr<sup>-1</sup>, dominated by a CO<sub>2</sub> sink that was partially counterbalanced by net emissions of CH<sub>4</sub> and N<sub>2</sub>O. For CH<sub>4</sub> and N<sub>2</sub>O, we find good agreement between BU and top-down (TD) estimates from atmospheric inversions. However, our BU land CO<sub>2</sub> sink is significantly higher than the TD estimates. We further show that decadal averages of GHG net-emissions have declined by 1.2 Pg CO<sub>2</sub>-eq. yr<sup>-1</sup> since the 1990s, mainly due to a reduction in fossil fuel emissions. In addition, based on both data driven BU and TD estimates, we also find that the land CO<sub>2</sub> sink has weakened over the past two decades. A large part of the European CO<sub>2</sub> and C sinks is located in Northern Europe. At the same time, we find a decreasing trend in sink strength in Scandinavia, which can be attributed to an increase in forest management intensity. These are partly offset by increasing CO<sub>2</sub> sinks in parts of Eastern Europe and Northern Spain, attributed in part to land use change. Extensive regions of high CH<sub>4</sub> and N<sub>2</sub>O emissions are mainly attributed to agricultural activities and are found in Belgium, the Netherlands and the southern UK. We further analyzed interannual variability in the GHG budgets. The drought year of 2003 shows the highest net-emissions of CO<sub>2</sub> and of all GHGs combined.

© 2024. The Author(s).

This is an open access article under the terms of the [Creative Commons Attribution License](https://creativecommons.org/licenses/by/4.0/), which permits use, distribution and reproduction in any medium, provided the original work is properly cited.

Stephen Stich, Rona L. Thompson,  
Hanqin Tian, Aki Tsuruta, Chris Wilson,  
Jean-Pierre Wigneron, Yitong Yao,  
Sönke Zaehle

**Formal analysis:** Ronny Lauerwald,  
Ana Bastos, Matthew J. McGrath, Ana  
Maria Roxana Petrescu, François Ritter,  
Robbie M. Andrew, Giovanni Forzieri,  
Piyu Ke, Philippe Ciais

**Investigation:** Ronny Lauerwald,  
Ana Bastos, Matthew J. McGrath, Ana  
Maria Roxana Petrescu, François Ritter,  
Philippe Ciais

**Methodology:** Ronny Lauerwald,  
Ana Bastos, Matthew J. McGrath, Ana  
Maria Roxana Petrescu, François Ritter,  
Philippe Ciais

**Supervision:** Philippe Ciais

**Validation:** Ronny Lauerwald,  
Ana Bastos, Matthew J. McGrath, Ana  
Maria Roxana Petrescu, Philippe Ciais

**Visualization:** Ronny Lauerwald,  
Ana Bastos, Matthew J. McGrath,  
François Ritter, Piyu Ke

**Writing – original draft:**  
Ronny Lauerwald, Ana Bastos, Matthew  
J. McGrath, Ana Maria Roxana Petrescu,  
François Ritter, Giovanni Forzieri,  
Philippe Ciais

**Writing – review & editing:**  
Ronny Lauerwald, Ana Bastos, Matthew  
J. McGrath, Ana Maria Roxana Petrescu,  
François Ritter, Robbie M. Andrew,  
Antoine Berchet, Grégoire Broquet,  
Dominik Brunner, Frédéric Chevallier,  
Alessandro Cescatti, Sara Filipek,  
Audrey Fortems-Cheiney,  
Giovanni Forzieri, Pierre Friedlingstein,  
Richard Fuchs, Christoph Gerbig,  
Sander Houweling, Bas J. W. Lerink,  
Wanjing Li, Wei Li, Xiaojun Li,  
Ingrid Luijkx, Guillaume Monteil,  
Saqr Munassar, Gert-Jan Nabuurs, Prabr  
K. Patra, Philippe Peylin, Julia Pongratz,  
Pierre Regnier, Marielle Saunois, Mart-  
Jan Schelhaas, Marko Scholze,  
Stephen Stich, Rona L. Thompson,  
Hanqin Tian, Aki Tsuruta, Chris Wilson,  
Jean-Pierre Wigneron, Yitong Yao,  
Sönke Zaehle, Philippe Ciais

**Plain Language Summary** We have synthesized the European budgets of carbon and the greenhouse gases (GHG) carbon dioxide, methane and nitrous oxide. This synthesis includes estimates of direct emissions from fossil fuel burning, industrial production, waste management and agriculture, as well as of sources and sinks in the terrestrial biosphere. Summing up the sources and sinks of the three GHGs, we estimate for the decade of the 2010s an average annual net-emission of 3.9 billion tons of carbon dioxide equivalents. These net-emissions are dominated by carbon dioxide from fossil fuel emissions (4.1 billion tons of carbon dioxide). In contrast, the terrestrial biosphere acts as a net sink of carbon dioxide, the effect of which is only partly counterbalanced by net emissions of methane and nitrous oxide. The net-effect of the terrestrial biosphere's GHG budget is a sink of 0.9 billion tons of carbon dioxide equivalents per year. Over the last three decades, European GHG emissions have declined by 1.2 billion tons carbon dioxide equivalents per year, mainly due to reductions in fossil fuel emissions. However, the sink capacity of the terrestrial biosphere has diminished since the 2000s.

## 1. Introduction

The REgional Carbon Cycle Assessment and Processes Phase 2 (RECCAP2) initiative of the Global Carbon Project aims at re-assessing the carbon (C) and greenhouse gas (GHG) budgets of the land and oceans over the recent decade 2010–2019, including their component fluxes. This goal is to be achieved based on an ensemble of 10 regional budget analyses at the (sub-)continental scale, which in total cover the entire global land mass. The first phase of this initiative (RECCAP1), launched more than 10 years ago (Canadell et al., 2011), featured budget analyses of nine large land regions and focused on the period 2000–2009. While in RECCAP1 most regional budget analyses were limited to carbon dioxide (CO<sub>2</sub>), the second phase of RECCAP (RECCAP2) now explicitly focuses on the three main GHGs: carbon dioxide (CO<sub>2</sub>), methane (CH<sub>4</sub>) and nitrous oxide (N<sub>2</sub>O). The delineation of land regions has been updated as well, distinguishing now 10 land regions (see Ciais et al., 2022). In this study, we present the European GHG and C budget for the decades 1990–1999, 2000–2009, and 2010–2019 in the framework of RECCAP2.

For RECCAP1, the European GHG and C budget had been presented by Luysaert et al. (2012). Different from other land budgets of RECCAP1, it already considered the budgets of the three main GHGs CO<sub>2</sub>, N<sub>2</sub>O, and CH<sub>4</sub>. Their budget analysis focused on the two 5-year-periods 1996–2000 and 2001–2005. The paper presented here is an update on Luysaert et al. (2010, 2012) focusing on the more recent period 2010–2019, including more recent and improved data sets, and additionally considering interannual variability (IAV) of GHG budgets. Note also, that the European region for RECCAP2 is defined differently to that of RECCAP1. The RECCAP2 region of Europe includes the countries of Austria, Albania, Andorra, Belarus, Belgium, Bulgaria, Bosnia and Herzegovina, Croatia, Cyprus, Czech Republic, Denmark, Estonia, Faroe Islands, Finland, France, Germany, Greece, Greenland, Hungary, Iceland, Ireland, Italy, Liechtenstein, Lithuania, Latvia, Luxembourg, North-Macedonia, Malta, Moldova, Montenegro, Netherlands, Norway, Poland, Portugal, Romania, San Marino, Serbia, Slovakia, Slovenia, Spain, Sweden, Switzerland, Ukraine, and United Kingdom—all in their boundaries as accepted by the UN, but excluding oversea territories outside of continental Europe. In contrast, the European region used in RECCAP1 excluded the East European countries of Moldova, Ukraine and Belarus.

More recently, the European GHG budgets for CO<sub>2</sub>, CH<sub>4</sub>, and N<sub>2</sub>O have been reassessed in the framework of the project VERIFY, first covering the periods 1990–2017 (Petrescu McGrath, et al., 2021; Petrescu et al., 2021), and now extended to the periods 1990–2019 for CH<sub>4</sub> and N<sub>2</sub>O (Petrescu et al., 2023) and 1990–2020 for CO<sub>2</sub> (McGrath et al., 2023). VERIFY focused on the comparison of national GHG inventories against other, partially independent estimates from global data sets, models and atmospheric inversions, but also investigated temporal trends in emissions and the contribution from different sectors. The spatial domain of VERIFY was more restricted, with most of the analysis focusing on the 27 EU Member States plus the UK. However, VERIFY also featured a number of analyses additionally including Norway, Switzerland, Moldova, Ukraine, and Belarus. This larger region is more comparable to the European region as defined in RECCAP2, but excluding Iceland and the non-EU countries in the Balkans (Serbia, Albania, Bosnia-Herzegovina, North-Macedonia, Montenegro, and Kosovo). For our analysis of the European C and GHG budgets in the framework of RECCAP2, we use many data sets that have already been used by or prepared for VERIFY, with the aim to deepen our understanding of trends,

IAV and spatial patterns in GHG and C fluxes. While VERIFY has investigated long-term trends of GHG emissions with a specific focus on anthropogenic emissions, in RECCAP2 we investigate in more detail spatial patterns and IAV of GHG and C budgets within Europe, which are mainly driven by climate variability and landscape processes. Both these research foci are novel and will help to deepen our process understanding with regard to large-scale dynamics of C and GHG budgets and their feedbacks with climate variability and change.

In the spirit of RECCAP, and analogous to other studies mentioned above, we assess the European GHG and C budgets using two approaches: (a) a top-down (TD) approach using atmospheric inversion estimates, and (b) a bottom-up (BU) approach using inventory-based estimates, eddy covariance flux measurements and outputs of various mechanistic models, including Dynamic Global Vegetation Models (DGVMs) and more specialized models. We analyze different types of biospheric C stock change and flux estimates (inventories, upscaled eddy-covariance measurements, DGVMs) to evaluate their agreement with regard to spatial distribution of biospheric C gains and losses. We additionally use independent maps of C gains and losses related to harvest, land use change, fire and other disturbances, which will shed more light on the spatial drivers of the European land C sink, and bookkeeping models to isolate the effect of land-use change. For the analysis of the interannual variability of European GHG budgets, we extend the work of Bastos et al. (2016) who were able to link the IAV of the land CO<sub>2</sub> budget to large-scale climate patterns such as the North Atlantic Oscillation (NAO) and the East Atlantic pattern (EA). In our study, we also included CH<sub>4</sub> and N<sub>2</sub>O budgets and finally assessed the global warming potential (GWP) of these three GHGs and their IAV.

In the following section, we look first into the GHG (Section 3) and carbon (Section 4) budgets for the entirety of Europe. We start this analysis with a budget of the most recent decade 2010–2019, before we compare the budgets of the last three decades, analyzing temporal trends and identifying sectors and fluxes that are responsible for those trends. Then, we investigate spatio-temporal variability in GHG sources and sinks within Europe and during the last decade based on regional inversions (Section 5), focusing on IAV, recent trends and local hotspots of sinks and sources. Then, we take a closer look at the IAV of the different GHG budgets, exploring to what extent they are driven by climate modes (Section 6). In the later part of our study, we investigate how much different spatialized BU estimates of C stock changes agree among each other and with TD approaches on large-scale spatial patterns in the European land C sink, and what we can learn about the main environmental drivers of the temporal trends in the land C sink (Section 7). In a final section, we investigate how far forest disturbances have affected the European C balance over the past decades (Section 8).

## 2. Methods and Materials

### 2.1. GHG Budgets From Bottom-Up Estimates

We aim to establish BU GHG budgets based on a range of flux estimates for different sectors and flux components, and then compare these to the TD budget estimates of atmospheric inversions. We distinguish between direct anthropogenic emissions of GHG (Section 2.1.1) and the land fluxes that focus on GHG exchange between the continental biosphere and the atmosphere (Section 2.1.2), largely following the guidelines proposed by Ciais et al. (2022). Our primary focus lies on the land budgets and the question of how GHG sinks and sources in continental ecosystems are distributed in space and time and how they evolved over the past decades. This includes managed lands and terrestrial ecosystem-atmosphere exchange fluxes affected by human intervention. Anthropogenic emissions that are not related to ecosystem-atmosphere exchange fluxes are treated separately as direct anthropogenic emissions ( $F_{\text{direct}}$ , Equation 1).

When several estimates exist for a GHG sink or source, we calculate their median. We further calculate a lower and upper bound estimate, which are either based on an uncertainty estimate reported in the original data, on the spread of individual results where ensembles of DGVMs or inversions are used, or on an uncertainty estimate based on expert judgment. For the latter, we largely adopted estimates of relative uncertainties used in RECCAP1 (Ciais et al., 2021; Luysaert et al., 2012).

#### 2.1.1. Direct Anthropogenic Emissions

For anthropogenic emissions, we use the main sectors proposed by IPCC (2006): Energy ( $F_{\text{energy}}$ ), industrial processes and product use ( $F_{\text{IPPU}}$ ), Waste ( $F_{\text{waste}}$ ), and Agriculture, Forestry and Other Land Use ( $F_{\text{AFOLU}}$ ).  $F_{\text{energy}}$  includes all emissions related to exploration, exploitation, transformation, distribution, and use of fossil

fuels.  $F_{\text{IPPU}}$  comprises a variety of industrial processes that release GHGs from chemical or physical transformation of materials.  $F_{\text{waste}}$  comprises all emissions related to disposal and treatment of solid waste and wastewater, including burning of waste.  $F_{\text{AFOLU}}$  comprises both all anthropogenic GHG emissions and also all sink removals on managed lands, where managed lands are broadly defined as ecosystems where humans intervene and over which countries claim responsibility for AFOLU fluxes (IPCC, 2006). Note that national inventories in Europe use land designated as “managed” as a proxy for anthropogenic emissions and removals from all land, in order to avoid attempting to separate out, for example, background growth in young forests from growth due to increased atmospheric  $\text{CO}_2$  concentrations. Thus,  $F_{\text{AFOLU}}$  accounts for all GHG exchanges between terrestrial ecosystems and the atmosphere.  $F_{\text{AFOLU}}$  can further be split into sub-categories “Agriculture” ( $F_{\text{agri}}$ ) and “Land Use, Land-Use Change, and Forestry” ( $F_{\text{LULUCF}}$ ), which facilitates integration of these estimates with other BU estimates focusing only on one of these two sub-categories. Soil carbon changes on agricultural land are counted as part of  $F_{\text{LULUCF}}$ , which further comprises vegetation and soil carbon changes related to land-use changes and forestry, and  $F_{\text{agri}}$  thus includes only GHG emissions from urea applications and liming ( $\text{CO}_2$ ), enteric fermentation ( $\text{CH}_4$ ), manure management ( $\text{CH}_4$ ,  $\text{N}_2\text{O}$ ), and burning of crop residues ( $\text{CO}_2$ ,  $\text{CH}_4$  and  $\text{N}_2\text{O}$ ). Note, however, that we only consider  $F_{\text{agri}}$  as part of  $F_{\text{direct}}$  (Equation 1), while we consider  $F_{\text{LULUCF}}$  to be an anthropogenic perturbation of exchange fluxes between terrestrial ecosystems and the atmosphere (Section 2.1.2). For our definition of  $F_{\text{agri}}$  as a component of direct anthropogenic emissions, we further excluded  $\text{N}_2\text{O}$  emissions from agricultural soils and  $\text{CO}_2$  emissions related to changes in soil C stocks, as those are included in the land budgets as well.

$$F_{\text{direct}} = F_{\text{energy}} + F_{\text{IPPU}} + F_{\text{waste}} + F_{\text{agri}} \quad (1)$$

For  $F_{\text{energy}}$ ,  $F_{\text{IPPU}}$ ,  $F_{\text{waste}}$ ,  $F_{\text{agri}}$ , and  $F_{\text{LULUCF}}$ , we use several inventory-based assessments that follow the definition of the sectors proposed by IPCC (2006): EDGAR v6.0, GAINS, and UNFCCC (Table 1). These data cover at least the period since 1990, and we can thus calculate consistent budgets for the three decades of the 1990s, 2000s, and 2010s. UNFCCC data are a collection of national GHG inventories that use national activity data with different levels of sophistication, ranging from default emission factors (Tier 1), country- and technology-specific parameters (Tier 2), to more complex methods that may include calibrated, process-based models (Tier 3). UNFCCC data include uncertainty estimates that take into account uncertainties in both emission factors and activity data. More information on these data can be found in Petrescu, Qiu, et al. (2021), Petrescu, McGrath et al. (2021), Petrescu et al. (2023) and McGrath et al. (2023). The inventory-based estimates of EDGAR v6.0 and GAINS are based on global activity data but country- and technology-specific emission factors (Tier 2). For EDGAR, uncertainties were assessed by Solazzo et al. (2021). For UNFCCC data, depending on the tiers used for emission estimates in the national reporting, GHG budgets are better constrained for certain countries but not in a manner consistent across Europe. Note further that there are slight differences in the spatial reference of the inventories. For instance, EDGAR v6.0 lists GHG budgets of overseas territories separately, which makes it easy for us to exclude those from the budget. In contrast, the national reports for the UNFCCC give the emissions for the whole economic zone of each country, and it is not possible to separate the contributions from overseas territories. However, the data in EDGAR v6.0 demonstrate that the contributions from overseas territories are marginal (<1% of  $F_{\text{direct}}$  for  $\text{CO}_2$ ,  $\text{CH}_4$ , and  $\text{N}_2\text{O}$ ).

In addition, we use an ensemble of fossil-fuel  $\text{CO}_2$  emission ( $F_{\text{fossil}}$ ) estimates assembled by Andrew (2020). In agreement with that study, we consider  $F_{\text{fossil}}$  as the sum of  $F_{\text{energy}}$  and  $F_{\text{IPPU}}$  of  $\text{CO}_2$ . For a detailed description of these data sets, see Andrew (2020). Note that we excluded estimates based on EDGAR and UNFCCC from Andrew (2020) to avoid redundancies. Finally, we included Tier 1 estimates from FAOSTAT for  $F_{\text{AFOLU}}$ ,  $F_{\text{agri}}$ , and  $F_{\text{LULUCF}}$  (Tubiello et al., 2013), while the latter flux is used for the land budget. Those estimates are based on the global activity data from the FAOSTAT database, which are sourced from national statistical services reporting this information annually to the FAO, and from generalized emission factors proposed by the IPCC (2006).

### 2.1.2. Land Budgets

While we kept uniformity for anthropogenic emission sectors with the definitions used by the IPCC, we adapted the land budgets in a way that was deemed most suitable for each GHG (Figure 1). In general, we sub-divided the land systems further into terrestrial ecosystems (vegetation-soil systems), inland waters, and coastal ecosystems

**Table 1**  
List of Bottom-Up Data Sets Used in This Study

Data set	Parameters, Sectors	Substances	Period	Temp. resol.	Spatial resol.
<b>Inventories</b>					
UNFCCC	$F_{\text{direct}}, F_{\text{LULUCF}}, \Delta C_{\text{GL}}, \Delta C_{\text{CL}}$	CO <sub>2</sub> , CH <sub>4</sub> , N <sub>2</sub> O	1990–2019	Annual	Country
GAINS	$F_{\text{direct}}, F_{\text{LULUCF}}$	CH <sub>4</sub> , N <sub>2</sub> O	1990–2015	Annual	Country
EDGAR v6.0	$F_{\text{direct}}, F_{\text{AFOLU}}$	CO <sub>2</sub> , CH <sub>4</sub> , N <sub>2</sub> O	1970–2018	Annual	Country
FAOSTAT	$F_{\text{AFOLU}}, F_{\text{agri}}, F_{\text{LULUCF}}, F_{\text{soil N}_2\text{O,man}}, \Delta C_{\text{GL}}, \Delta C_{\text{CL}}, \Delta C_{\text{FL}}$	CO <sub>2</sub> , CH <sub>4</sub> , N <sub>2</sub> O	1961–2019	Annual	Country
Andrew (2020)	$F_{\text{fossil}}$	CO <sub>2</sub>	Various	Annual	Country
FAOSTAT	$F_{\text{wood harvest}}, F_{\text{crop harvest}}, F_{\text{wood trade}}, F_{\text{crop trade}}$	Mass of products	1961–2019	Annual	Country
Hirschler and Oldenburg (2022)	$F_{\text{peat harvest}}, F_{\text{peat trade}}, F_{\text{peat use}}$	Mass of products	2013–2017	None	Country
<b>Land surface models</b>					
TRENDYv10	NPP, GPP, Rh, Ra, NBP	CO <sub>2</sub>	1901–2019	Monthly	0.5°
Global N <sub>2</sub> O budget ensemble	$F_{\text{soil N}_2\text{O}}$	N <sub>2</sub> O	1901–2015	Monthly	0.5°
O-CN (Zaehle & Friend, 2010, ext. for NMIP2)	$F_{\text{soil N}_2\text{O}}$	N <sub>2</sub> O	1901–2019	Monthly	0.5°
GMB2020, BU models	$F_{\text{peat CH}_4}$	CH <sub>4</sub>	2005–2019	Monthly	0.5°
ORCHIDEE-GMv3.2 (Chang et al., 2021)	$F_{\text{grazing}}$	C	1861–2012	Monthly	0.5°
<b>Other process based models</b>					
MeMo	$F_{\text{methanotrophy}}$	CH <sub>4</sub>	1990–2009	Monthly	1°
VPRM (Gerbig & Koch, 2021)	NEE <sub>C</sub>	CO <sub>2</sub>	2006–2020	–	7.5'
<b>Bookkeeping models</b>					
H&N (as in Friedlingstein et al., 2022)	$F_{\text{LUC}}$	CO <sub>2</sub>	1990–2020	Annual	RECCAP2
BLUE (Ganzenmüller et al., 2022)	$F_{\text{LUC}}$	CO <sub>2</sub>	1960–2019	Annual	0.25°
<b>Land cover data</b>					
HILDA+	Land cover, land cover change	–	1960–2019	Annual	0.01°
<b>Data driven estimates</b>					
FLUXCOM (Jung et al., 2020 BG) - RS v006	GPP, $Re_{\text{terr}}$	CO <sub>2</sub>	2001–2020	Monthly	5'
FLUXCOM (Jung et al., 2020 BG)—ERA	GPP, $Re_{\text{terr}}$	CO <sub>2</sub>	1990–2018	Monthly	5'
GLASS	GPP, NPP	CO <sub>2</sub>	2001–2018	8 Day	500 m
Madani and Parazoo (2020)	GPP	CO <sub>2</sub>	1982–2016	Monthly	8 km
MODIS	NPP	CO <sub>2</sub>	2001–2020	8 Day	500 m
BESS	GPP	CO <sub>2</sub>	2001–2016	8 Day	1 km
Yao et al. (2020)	$Rh_{\text{terr}}$	CO <sub>2</sub>	1985–2013	Annual	0.5°
GFEDv4 (extended.)	$F_{\text{fire}}$	C	1997–2019	Monthly	0.25°
GFASv1.2	$F_{\text{fire}}$	C, CO <sub>2</sub> , CH <sub>4</sub> , N <sub>2</sub> O	2003–2020	Daily	0.1°
Mendonca et al. (2017)	$\Delta C_{\text{burial}}$	C		None	COSCAT
Lauerwald et al. (2023)	$F_{\text{IW}}$	CO <sub>2</sub> , CH <sub>4</sub> , N <sub>2</sub> O	present day	None	RECCAP2
Rosentreter et al. (2023)	$F_{\text{Cwa}}, F_{\text{CWL}}$	CO <sub>2</sub> , CH <sub>4</sub> , N <sub>2</sub> O	present day	None	RECCAP2
Zscheischler et al. (2017)	$F_{\text{weathering}}, F_{\text{litho2river}}, F_{\text{river export}}, \Delta C_{\text{litho}}$	C, CO <sub>2</sub>	present day	None	1°
Etiopie et al. (2019), updated for Petrescu et al. (2023)	$F_{\text{geo}}$	CH <sub>4</sub>	present day	None	1°
EMEP	$F_{\text{soil N}_2\text{O,Ndep}}$	N	2000–2019	Daily	0.1°
EFISCEN	$\Delta C_{\text{FL}}$	Biomass	2000–2020	5 Year	Country
EFISCEN, gridded version	$\Delta C_{\text{FL}}$	Biomass	2000–2020	Annual	7.5'
L-VOD	$\Delta C_{\text{FL}}$	Biomass	2011–2021	Quarterly	25 km

**Table 1**  
Continued

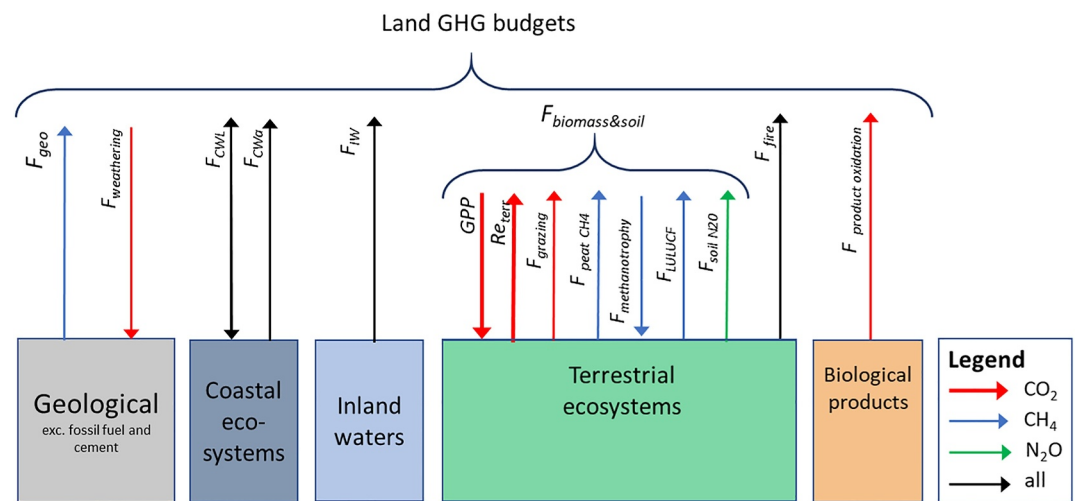
Data set	Parameters, Sectors	Substances	Period	Temp. resol.	Spatial resol.
Byrne et al. (2023)	$F_{\text{wood harvest}}$ , $F_{\text{crop harvest}}$ , $F_{\text{wood use}}$ , $F_{\text{crop use}}$	C	1961–2019	Annual	5'

Note. Spatial resolution refers to pixel size of gridded product, or to regions, which can be country areas, COSCAT regions (based on coastal segments and their catchments, Meybeck et al., 2006), or the entire study area (RECCAP2).

(waters and wetlands). Before we describe the land budget of each GHG further below, we first describe here which flux components and data sources are shared between those budgets. In contrast to terrestrial ecosystems, the emissions from inland waters ( $F_{\text{IW}}$ ), coastal waters ( $F_{\text{Cwa}}$ ) and coastal wetlands ( $F_{\text{CWL}}$ ) are treated similarly in each land GHG budget, which means that similar processes, subdivisions, and data sources are considered for each GHG. For these fluxes, we use syntheses of estimates that have been developed within the RECCAP2 initiative (Lauerwald et al., 2023 for  $F_{\text{IW}}$ ; Rosentreter et al., 2023 for  $F_{\text{Cwa}}$  and  $F_{\text{CWL}}$ ). All these estimates are climatologies of average annual fluxes, which we assumed to be constant and representative for the last three decades.

Another flux, which is included in all three land GHG budgets, is fire emissions ( $F_{\text{fire}}$ ), which relates to in situ burning of biomass and is thus distinguished from incineration of waste, which belongs to  $F_{\text{waste}}$ ; the burning of crop residues, which is part of  $F_{\text{agri}}$ ; and the burning and decay of crop, wood and peat products ( $F_{\text{product oxidation}}$ ), which is a separate flux component in the  $\text{CO}_2$  and C budgets (see below).  $F_{\text{fire}}$  represents the gross emissions, and does not account for the net  $\text{CO}_2$  uptake through vegetation recovery over the subsequent years. These effects of vegetation recovery are implicitly included in our estimates of primary production (see subsection on *Land  $\text{CO}_2$  budget*), and cannot be easily separated from them. Thus, we do not give estimates of net fire emissions in this study.

$F_{\text{fire}}$  is derived from two data-driven estimates: the CAMS Global Fire Assimilation System (GFAS) (Kaiser et al., 2012) and the global fire emission database (GFED) v4 (van der Werf et al., 2017). GFAS is based on fire radiative power observations from satellite-based sensors. GFED is based on remotely sensed data (Moderate Resolution Imaging Spectroradiometer—MODIS and Visible Infrared Imaging Radiometer Suite—VIIRS) of burned area and emission factors. Both GFED and GFAS give estimates of emissions of total C,  $\text{CO}_2$ ,  $\text{CH}_4$ , and  $\text{N}_2\text{O}$ . GFAS fully covers the last two decades. For GFEDv4, estimates of GHG emissions could only be derived for years until 2016, and the decadal estimates were derived as average of the first 7 years of the 2010s. For total C



**Figure 1.** Greenhouse gas fluxes included for the land budget, adapted from Ciais et al. (2022) to include  $\text{N}_2\text{O}$  fluxes and coastal waters. This land GHG budget excludes direct anthropogenic emissions (see text) such as  $\text{CH}_4$  emissions from agriculture and waste, industrial processes and fossil emissions.

emissions, in contrast, beta-versions of emission estimates were also available at the end of the 2010s. For the GHG budgets of the 1990s, we assumed that fire emissions equaled those of the 2000s.

Note that we do not explicitly estimate CO<sub>2</sub> emissions from other forest disturbances such as windthrows, pests, or diseases. However, these emissions are implicitly included in UNFCCC carbon stock change inventories established by countries, just as fire emissions. This is in particular the case where the gain-loss method is employed, that is, approximately half of the countries in the European Union. A specific estimate of decadal forest carbon stock loss and gain from forest disturbances is given in Section 8.

The major fluxes between terrestrial ecosystems and the atmosphere are defined and treated differently for each land GHG budget, as detailed in the following.

### 2.1.2.1. Land CO<sub>2</sub> budget

$$F_{\text{land CO}_2} = \text{GPP} + \text{Re}_{\text{terr}} + F_{\text{IW}} + F_{\text{product oxidation}} + F_{\text{grazing}} + F_{\text{fire}} + F_{\text{Cwa}} + F_{\text{CWL}} + F_{\text{weathering}} \quad (2)$$

$$\text{Re}_{\text{terr}} = \text{Ra} + \text{Rh} \quad (3)$$

At the center of the land CO<sub>2</sub> budget, we put the balance between gross primary production (GPP) and terrestrial ecosystem respiration Re<sub>terr</sub>, which is itself the sum of autotrophic (Ra) and heterotrophic (Rh) respiration in the terrestrial biosphere (Equation 3). Note that CO<sub>2</sub> emissions from inland waters (F<sub>IW</sub>) are largely fed by terrestrial ecosystem respiration (Battin et al., 2023), which is not explicitly included in the flux Re<sub>terr</sub>. We treat emissions/uptake from coastal water (F<sub>Cwa</sub>) and coastal wetlands (F<sub>CWL</sub>) separately in this budget, as we assume that they are not included in the estimates of GPP, Ra, Rh, or F<sub>IW</sub>. Note that we did not distinguish F<sub>LULUCF</sub> in the land CO<sub>2</sub> budget of Equation 2, as we assume this flux to be implicitly included in the other fluxes in that equation. F<sub>fire</sub> includes emissions from both natural and anthropogenic fires in the landscape. For GPP and net primary production (NPP = GPP – Ra), we used several different estimates for the period 2010–2019 (Table 1). These include estimates from MODIS that are based on remote sensing data on leaf area index (LAI) and the fraction of photosynthetically active radiation (FPAR), from which estimates of GPP and NPP are derived in a semi-empirical way involving a light use efficiency model and gridded information on meteorological drivers as predictors (Zhao et al., 2005). We further used estimates from the Breathing Earth System Simulator (BESS, Jiang & Ryu, 2016) and Madani and Parazoo (2020) that are based on the same remote sensing data but use different approaches to estimate GPP. Madani and Parazoo (2020) used a light use efficiency model that was optimized based on flux tower data and inventories (Madani et al., 2017), while BESS uses a more process-based approach representing the continuous exchange of carbon, water and energy between the biosphere and atmosphere. Finally, we included GLASS data that is based again on the semi-empirical approach of Zhao et al. (2005) but uses improved LAI and FPAR estimates from combining MODIS and Advanced Very High Resolution Radiometer (AVHRR) remote sensing data.

From FLUXCOM data, we derived estimates of GPP and Re<sub>terr</sub> that are based on flux-tower observations from the Fluxnet network and upscaled based on machine learning algorithms and meteorological predictor data (Jung et al., 2020). More precisely, we used two versions of this data set: one that was extrapolated based on remote sensing data only (RS v006), and one that was extrapolated based on both remote sensing data and meteorological forcing data (ERA5). From Yao et al. (2021), we use global estimates of annual soil heterotrophic respiration that are upscaled from 455 observed annual fluxes from the soil respiration database SRDB distributed over 290 sites based on machine learning using meteorological variables, soil moisture and other soil properties, GPP and land cover as predictors. This data set represents an ensemble of 126 alternative estimates based on different combinations of predictor data sets. We use the mean and range of these estimates as the best estimate and uncertainty range, respectively.

For the land CO<sub>2</sub> budget of the 2010s, we present the median of the GPP estimates mentioned above. A median Re<sub>terr</sub> was derived from the two FLUXCOM estimates and an alternative data-driven estimate, which we calculated as the sum of Ra after GLASS and Rh from Yao et al. (2021). For the comparison of land CO<sub>2</sub> budgets of the last three decades, we only used GPP and Re<sub>terr</sub> from the ERA version of FLUXCOM, since it is the only data set that covers this entire period (Table 1). Moreover, for the budget of the 2010s decade, this flux estimate

was found to be close to the ensemble median of estimates described above (Table S1 in Supporting Information S2), which further supports this choice. For comparison, we also derived the median and range of GPP, Rh, Ra, and  $Re_{terr}$  for all three decades as simulated by the TRENDY v10 land surface model ensemble that were originally prepared for the Global Carbon Budget 2021 (Friedlingstein et al., 2022). We do not include TRENDY simulations in our budget directly as DGVM simulations tend to be biased by the poor representation of perturbation, anthropogenic appropriation of biomass, and lateral export fluxes (Ciais et al., 2021). Moreover, we only used simulations from ORCHIDEE v2 (in the following simply referred to as ORCHIDEE), OC-N, LPJwsl, ISBA, ISAM, DLEM, CLM5, and CABLE for which the actual resolution was sufficiently high (0.5°). We excluded ORCHIDEE v3 and SDGVM models from the selection as the spatial patterns of their simulated land-atmosphere net C exchange did not correlate at all with those of the other TRENDY models (see Figure S1 in Supporting Information S1).

Harvesting vegetation biomass for wood and crop products as well as extraction of peat increases the gap between GPP and  $Re_{terr}$  because this extracted organic matter does not feed directly into  $Re_{terr}$  according to our definition of that flux. The same is true for the biomass that is taken out by grazing livestock ( $F_{grazing}$ ). While we assume  $F_{grazing}$  to represent a flux of C instantaneously and completely returned to the atmosphere, the return of C from the use, decay or burning of wood, crop or peat products ( $F_{product\ oxidation}$ ) is partly delayed and altered by import and export fluxes across the boundaries of our study area (Table 2). The calculation of  $F_{product\ oxidation}$  and  $F_{grazing}$  is explained in detail in Section 2.3.

$F_{grazing}$  is derived from modeled flux rates based on the ORCHIDEE model with prescribed livestock densities and simulated grassland management intensity (Chang et al., 2021). As those simulations cover only the period 1901–2012, we scaled the average flux rates from the last 10 years of simulation (2003–2012) to average areas of intensively and extensively managed pastures over the period 2010–2019 derived from HILDA+ (Winkler et al., 2021). For the decades of the 1990s and 2000s, we used the simulation results from Chang et al. (2021) directly. A final flux which is specific to the land  $CO_2$  budget is the atmospheric  $CO_2$  sink related to rock weathering ( $F_{weathering}$ ), which binds  $CO_2$  as dissolved inorganic C, which is then exported by rivers to the coast (see C section). For our budget, we used the estimate of average annual  $F_{weathering}$  from Zscheischler et al. (2017) after the empirical model developed by Hartmann et al. (2009), assumed to be constant over the last three decades. The individual estimates used for the 2010s' budget are listed in Table S1 in Supporting Information S2 in the supplement. Those used for all three decades are listed in Table S2 in Supporting Information S2.

### 2.1.2.2. Land $CH_4$ budget

$$F_{land\ CH_4} = F_{peat\ CH_4} + F_{methanotrophy} + F_{LULUCF} + F_{fire} + F_{IW} + F_{CWA} + F_{CWL} + F_{geo} \quad (4)$$

For the land  $CH_4$  budget, we distinguish between peatlands as  $CH_4$  source ( $F_{peat\ CH_4}$ ) and terrestrial ecosystems with well-aerated soils, which act as  $CH_4$  sinks due to their methanotrophy ( $F_{methanotrophy}$ ) (Equation 4). In addition, we have  $F_{LULUCF}$  as net-emission of  $CH_4$ , which is related to land use change and land management, and which is neither included in the estimates of  $F_{peat\ CH_4}$  nor  $F_{methanotrophy}$  we use. As data-driven estimates of  $F_{peat\ CH_4}$  and  $F_{methanotrophy}$  are scarce, we resorted to the diagnostic DGVM simulations as synthesized by the Global  $CH_4$  Budget (Saunois et al., 2020) to quantify  $F_{peat\ CH_4}$  and to the mechanistic methanotrophy model MeMo (Murguia-Flores et al., 2018) to quantify  $F_{methanotrophy}$ . Note that the MeMo simulations only cover years until 2009, and thus we had to assume the average  $F_{methanotrophy}$  over the last 10 years of simulation (2000–2009) to be representative for our budget period. For the 2000s and 1990s, we used the published MeMo simulation results directly. Similarly, the DGVM results assembled for the Global  $CH_4$  Budget allowed us to derive ensemble medians and ranges for all three decades. The estimates of  $F_{LULUCF}$  were taken from the national inventories collected by UNFCCC. Finally, we include geological emissions of  $CH_4$  ( $F_{geo}$ ) using data-driven estimates from Etiope et al. (2019), which were recently updated for the VERIFY  $CH_4$  and  $N_2O$  budgets (Petrescu et al., 2023). These estimates represent a climatology of average annual fluxes that do not represent interannual variability or trends at the decadal time scale. We assumed them to be representative of the last three decades. The individual estimates used for the 2010s' budget are listed in Table S3 in Supporting Information S2. Those used for all three decades are listed in Table S4 in Supporting Information S2.



**Table 2**  
Best Estimates for the Flux Components of the European GHG Budget 2010–2019<sup>a</sup>

Flux	CO <sub>2</sub> emissions		CH <sub>4</sub> emissions		N <sub>2</sub> O emissions		GWP <sub>100</sub> (as CO <sub>2</sub> equivalents)				
	Tg yr <sup>-1</sup>	Conf.	Tg yr <sup>-1</sup>	Conf.	Gg yr <sup>-1</sup>	Conf.	Tg yr <sup>-1</sup>	Conf.	CO <sub>2</sub>	CH <sub>4</sub>	N <sub>2</sub> O
Direct anthropogenic emission											
<i>F</i> <sub>energy</sub>	3,792	***	6.66	*	108	*	4,020	***	94%	4%	1%
<i>F</i> <sub>IPPU</sub>	321	***	0.08	*	106	--	353	**	91%	1%	8%
<i>F</i> <sub>waste</sub>	5	*	6.37	*	52	-	191	*	3%	90%	7%
<i>F</i> <sub>agri</sub>	11	***	10.72	**	78	*	322	***	3%	90%	7%
Total	4,130	***	23.83	*	343	*	4,867	***	85%	13%	2%
Land budget											
GPP	-20,085	**	-	-	-	-	-	-	-	-	-
Re <sub>terr</sub>	16,740	**	-	-	-	-	-	-	-	-	-
<i>F</i> <sub>LULUCF</sub>	-	-	0.61	*	-	-	-	-	-	-	-
<i>F</i> <sub>peat CH<sub>4</sub></sub>	-	-	2.00	--	-	-	-	-	-	-	-
<i>F</i> <sub>methanotrophy</sub>	-	-	-0.92	*	-	-	-	-	-	-	-
<i>F</i> <sub>soil N<sub>2</sub>O</sub>	-	-	-	-	925	*	-	-	-	-	-
<i>F</i> <sub>soil &amp; biomass</sub>	-3,345	*	1.69	--	925	*	-3,046	**	110%	-2%	-8%
<i>F</i> <sub>grazing</sub>	484	*	-	-	-	-	484	*	-	-	-
<i>F</i> <sub>product oxidation</sub>	1,267	**	-	-	-	-	1,267	**	-	-	-
<i>F</i> <sub>weathering</sub>	-42	*	-	-	-	-	-42	*	-	-	-
<i>F</i> <sub>geo</sub>	-	-	2.50	-	-	-	68	-	-	-	-
<i>F</i> <sub>fire</sub>	31	*	0.08	*	3.0	*	34	*	91%	6%	2%
<i>F</i> <sub>IW</sub>	191	*	4.10	*	17	-	306	*	62%	36%	2%
<i>F</i> <sub>CWa</sub>	25	*	0.01	-	4.8	*	27	*	94%	1%	5%
<i>F</i> <sub>CWL</sub>	-15	-	0.01	-	-0.2	--	-15	-	101%	-2%	0%
Total	-1,403	*	8.40	-	949	*	-917	-	153%	-25%	-28%

Note. We assign different levels of confidence to our estimates: very high: ±10% (\*\*\*), high: ±25% (\*\*), moderate: ±50% (\*), low: ±100% (-), and very low (--). <sup>a</sup>The global warming potential at the 100-year horizon (GWP<sub>100</sub>) is calculated based on IPCC AR6.

### 2.1.2.3. Land N<sub>2</sub>O budget

$$F_{\text{land N}_2\text{O}} = F_{\text{soil N}_2\text{O}} + F_{\text{fire}} + F_{\text{IW}} + F_{\text{Cwa}} + F_{\text{CWL}} \quad (5)$$

For the land N<sub>2</sub>O budget (*F*<sub>land N<sub>2</sub>O</sub>), direct soil N<sub>2</sub>O emissions (*F*<sub>soil N<sub>2</sub>O</sub>) are the main flux between terrestrial ecosystems and the atmosphere (Equation 5). For a more detailed budget analysis, we split *F*<sub>soil N<sub>2</sub>O</sub> into a natural flux component *F*<sub>soil N<sub>2</sub>O,nat</sub>, and anthropogenic flux components related to management practices such as fertilizer and manure applications and residue management (*F*<sub>soil N<sub>2</sub>O,man</sub>), as well as indirect emissions related to atmospheric deposition of reactive N (*F*<sub>soil N<sub>2</sub>O,Ndep</sub>), which were further split into emissions from agricultural (*F*<sub>soil N<sub>2</sub>O,Ndep,agri</sub>) and other soils (*F*<sub>soil N<sub>2</sub>O,Ndep,other</sub>). With that last mentioned distinction, we account for the fact that the inventory-based assessments of EDGAR and GAINS only report *F*<sub>soil N<sub>2</sub>O,Ndep,agri</sub>. In general, inventory-based assessments such as EDGAR, UNFCCC, and FAO (see Table 1) cover only emissions from managed lands. Therefore, for *F*<sub>soil N<sub>2</sub>O</sub> and *F*<sub>soil N<sub>2</sub>O,nat</sub>, we resorted to DGVM simulation results as synthesized by the Nitrogen Model Intercomparison Project (NMIP, Tian et al., 2019). For the estimation of N<sub>2</sub>O emissions due to atmospheric N deposition on all soils, and on non-agricultural soils in particular, we use simulations results from the DGVM O-CN (Zaehle and Friend, 2010) as they were prepared for the second phase of NMIP, and come up with

an alternative data-driven estimate using gridded data of atmospheric N deposition from the European Monitoring and Evaluation Program (EMEP) and an emission factor of 1% following the guidance of IPCC (2019). From all these specific data sources for the land N<sub>2</sub>O budgets, we could derive flux estimates for the last three decades. The individual estimates used for the 2010s' budget are listed in Table S5 in Supporting Information S2. Those used for all three decades are listed in Table S6 in Supporting Information S2.

### 2.1.3. Total GHG Emissions

Finally, we express the budget of GHG emissions and removals in CO<sub>2</sub> equivalents (CO<sub>2</sub>-eq.) using global warming potential at a 100-year time horizon (GWP100), combining flux components from the CO<sub>2</sub>, CH<sub>4</sub>, and N<sub>2</sub>O budgets (Sections 2.1.1 and 2.1.2) and using the conversion factors of 27 kgCO<sub>2</sub>-eq./kg CH<sub>4</sub> and 273 kg CO<sub>2</sub>-eq./kg N<sub>2</sub>O proposed by the 6th assessment report (AR6) of the IPCC (IPCC, 2021, Table 7.15). Only for  $F_{\text{energy}}$  and  $F_{\text{IPPU}}$ , we used the factor of 29.8 kgCO<sub>2</sub>-eq./kg CH<sub>4</sub> proposed by the same source for fossil CH<sub>4</sub> emissions. For the direct anthropogenic emission fluxes  $F_{\text{energy}}$ ,  $F_{\text{IPPU}}$ ,  $F_{\text{waste}}$ , and  $F_{\text{agri}}$ , we simply summed up the estimated CO<sub>2</sub> equivalents for the individual GHGs. For the land GHG budget ( $F_{\text{GHG, land}}$ ), we did the same for  $F_{\text{fire}}$ ,  $F_{\text{IW}}$ ,  $F_{\text{Cwa}}$ , and  $F_{\text{CWL}}$  (Equation 6). Then, we combined the major terrestrial vegetation and soil GHG emissions and sinks ( $F_{\text{biomass \& soil}}$ ), which include GPP and  $\text{Re}_{\text{terr}}$  for CO<sub>2</sub>,  $F_{\text{peat CH}_4}$ ,  $F_{\text{methanotrophy}}$  and  $F_{\text{LULUCF}}$  for CH<sub>4</sub>, and  $F_{\text{soil N}_2\text{O}}$  for N<sub>2</sub>O (Equation 7). Finally, we obtained  $F_{\text{land GHG}}$  by additionally accounting for  $F_{\text{geo}}$  for CH<sub>4</sub> as well as  $F_{\text{weathering}}$  and  $F_{\text{product oxidation}}$  for CO<sub>2</sub> (Equation 6).

$$F_{\text{land GHG}} = F_{\text{fire}} + F_{\text{IW}} + F_{\text{Cwa}} + F_{\text{CWL}} + F_{\text{biomass \& soil}} + F_{\text{geo}} + F_{\text{weathering}} + F_{\text{product oxidation}} + F_{\text{grazing}} \quad (6)$$

$$F_{\text{biomass \& soil}} = \text{GPP} + \text{Re}_{\text{terr}} + F_{\text{peat CH}_4} + F_{\text{methanotrophy}} + F_{\text{LULUCF}} + F_{\text{soil N}_2\text{O}} \quad (7)$$

## 2.2. GHG Budgets From Top-Down Estimates

For each of the three GHGs, we use both global and coarsely resolved ( $\geq 1^\circ$ ) inversions as well as regional inversions for Europe at a higher spatial resolution ( $0.5^\circ$ ). Note that the regional inversions do not cover all of our RECCAP2 domain, but are bounded between  $15^\circ\text{E}$ – $35^\circ\text{W}$  and  $33^\circ\text{N}$ – $73^\circ\text{N}$ , which does not reach the far eastern and western extents of the domain (therefore missing the eastern parts of Ukraine, and most of Greenland and Iceland). However, the excluded area represents less than 4% of the total land area and its contribution to the GHG budgets is likely low compared to the general uncertainties related to atmospheric-inversion estimates (estimates range over a factor of 2 and more). More importantly, regional inversions may be expected to better resolve spatial patterns in GHG sources/sinks at the continental scale than global inversions (see Monteil et al., 2020; Petrescu et al., 2023). Therefore, we use these regional inversions for our analysis of spatial patterns in GHG sources and sinks across Europe (Section 3). For our TD CO<sub>2</sub> budget, we use seven global atmospheric inversions based on six inversion models (CAM5, CTE, Jena CarboScope, UoE, NISMOM-CO<sub>2</sub>, CMS-Flux) adjusted for fossil fuel emissions that were used for the Global Carbon Budget 2021 (Friedlingstein et al., 2022; see this ref. and appendix A4.2 in McGrath et al., 2023 for details). In addition, we use four regional inversions. Three of them (Jena CarboScope Regional, PYVAR-CHIMERE, LUMIA) were used for the VERIFY European budget (McGrath et al., 2023; see this ref. for details on the inversion configurations). The fourth one is a new CIF-CHIMERE inversion, whose configuration is very close to that of the CIF-CHIMERE inversion documented in McGrath et al. (2023), but corrects errors and relies on a prior knowledge of the terrestrial ecosystem fluxes from an ORCHIDEE-MICT (Guimberteau et al., 2018) simulation forced with the ERA5 reanalysis meteorological data. While all of these inversions allow us to derive a TD budget representative for the decade 2010–2019, three of the global inversions further allow us to compare TD budgets for the last three decades. For the CH<sub>4</sub> budget, we use the global inversions that were produced for the global methane budget GMB2020 (Saunio et al., 2020). That ensemble comprises 22 inversions, and covers the period 2000–2017, thus allowing us to derive TD budgets for the last two decades, though the second decade not being fully covered. Further, that ensemble is split into inversions based on ground based mole fraction measurements (XCH<sub>4</sub>, 11 SURF inversions) and inversions based on satellite-based observations of atmospheric XCH<sub>4</sub> (11 GOSAT inversions). In addition, we use three regional inversions (CTE-CH<sub>4</sub>, FLEXKF, FLEXINVERT) that have been prepared and used for the VERIFY European budget (Petrescu et al., 2023). These estimates cover the full period 2010–2019. For the N<sub>2</sub>O budget, we use five global inversions that were produced and used for the global N<sub>2</sub>O budget GN<sub>2</sub>OB2020 (Tian et al., 2020). Those inversions only cover the years 2000–2016, again allowing us to derive TD budgets for the last two decades,

though the more recent decade not being fully covered. Finally, we include one regional inversion (FLEX-INVERT) that was prepared and used for the VERIFY European budget (Petrescu et al., 2023) in our TD budget for 2010–2019.

### 2.3. Land C Budget

For the assessment of the land C budget, we slightly adapted the accounting scheme proposed by Ciais et al. (2022) (Figure 2). This scheme defines the net ecosystem exchange of C ( $NEE_C$ ) as the sum of all C exchange fluxes between land, inland water, and coastal ecosystems or pools of biological products and the atmosphere, all in units of mass of C (Equation 8). These flux components correspond to flux components of the land  $CO_2$  and  $CH_4$  budgets, while we consider exchange fluxes of volatile organic C and C monoxide to be negligible. Note that we did not include  $F_{LULUCF}$ , which represents a difference between GPP and  $RE_{terr}$  over land affected by land use change and land management. This flux is thus assumed to be implicitly included in our estimates of GPP,  $Re_{terr}$  and  $F_{fire}$  (in combination with changes by natural drivers) and the oxidation of agricultural and forestry products and grazing fluxes. Thus, to avoid double counting, we omitted  $F_{LULUCF}$  from our budget. Nevertheless, we use estimates of  $F_{LULUCF}$ , and more specifically of land use change emissions ( $F_{LUC}$ ) for comparison and discussion (Section 4). The  $F_{LUC}$  estimates are derived from two different bookkeeping models: the model by Houghton and Nassikas (2017) (hereafter H & N) and the Bookkeeping of Land Use Emissions model (BLUE, Hansis et al., 2015). We use estimates from H & N as prepared for the Global Carbon Budget 2020 (Friedlingstein et al., 2020), which used land use data from FAO (FAOSTAT, <https://www.fao.org/faostat/en/#data>, last accessed 2023-06-28). For BLUE, we used data from Ganzenmüller et al. (2022), which applied that model to two different land use data sets: LUH2 (Hurtt et al., 2020) and HILDA+ (Winkler et al., 2021). Note that the bookkeeping model estimates of  $F_{LUC}$  only target changes in C stocks due to land use change and harvest, while ignoring forest demography. This may lead to a smaller estimated C sink compared to  $F_{LULUCF}$  from inventories, which also account for the latter (Grassi et al., 2023).

$$NEE_C = F_{geo} + F_{weathering} + F_{IW} + F_{Cwa} + F_{CWL} + GPP + Re_{terr} + F_{fires} + F_{peat\ CH_4} + F_{methanotrophy} + F_{grazing} + F_{crop\ use} + F_{wood\ decay} + F_{wood\ burning} + F_{peat\ use} \quad (8)$$

$$\Delta C_{land} = -NEE_C - F_{river\ export} - F_{crop\ trade} - F_{wood\ trade} - F_{peat\ trade} \quad (9)$$

For the land C storage budget ( $\Delta C_{land}$ ) of Europe, we further take into account lateral net exports of C from the RECCAP2 region Europe through river transfers ( $F_{river\ exports}$ ) and the net trade of crop, wood, and peat products ( $F_{crop\ trade}$ ,  $F_{wood\ trade}$ , and  $F_{peat\ trade}$ , respectively) (Equation 9).  $F_{crop\ trade}$  and  $F_{wood\ trade}$  are derived from the corresponding FAO databases of product flows per country and year (FAOSTAT, <https://www.fao.org/faostat/en/#data>, last accessed 2023-06-28) using conversion factors representing dry mass content of harvested products and C content of dry mass. For  $F_{wood\ trade}$ , we used the conversion factors proposed by IPCC (2019). For  $F_{crop\ trade}$ , we build on the conversion factors proposed by Ciais et al. (2008) (see Table S7 in Supporting Information S2). The FAOSTAT data gives annual amounts of imports and exports to and from each country of our study domain, however, without detailing the origin of imports and the destiny of exports. Aggregating to the European scale, we report only net-exports in which trade fluxes between the countries of our study domain balance each other out.  $F_{peat\ trade}$  was derived from Hirschler & Oldenburg (2022) (see Table 1). For  $F_{crop\ trade}$  and  $F_{wood\ trade}$ , we could directly derive estimates for each of the last three decades. For  $F_{peat\ trade}$ , we had to assume that the inventory-based estimate Hirschler & Oldenburg (2022) for the 2010s is also a good estimate for the two preceding decades. As  $F_{peat\ trade}$  is a very small flux compared to  $F_{crop\ trade}$  and  $F_{wood\ trade}$ , we assume a limited impact of this assumption in the overall uncertainties of our C budget.

Then, we estimate the stock changes in the three categories of biological products:  $\Delta C_{wood}$ ,  $\Delta C_{crop}$ , and  $\Delta C_{peat}$ . These C stock changes are calculated as the budget of harvest, use, decay and/or burning of the products, and the net-export of the products out of Europe (Equations 10–12). For crop and wood products, the harvest fluxes ( $F_{crop\ harvest}$  and  $F_{wood\ harvest}$ , respectively) are derived from the FAOSTAT databases and conversion factors just as the corresponding trade fluxes. For crop products, we assume that there is no change in product stocks at annual time-scales ( $\Delta C_{crop} = 0$ ), and the C flux to the atmosphere, which is related to consumption of crop products ( $F_{crop\ use}$ ), equals the difference between  $F_{crop\ harvest}$  and  $F_{crop\ trade}$ . For wood products, we use the Tier 2 approach proposed by IPCC (2019), assuming that all fuel wood is burned within 1 year ( $F_{wood\ burn}$ ) and

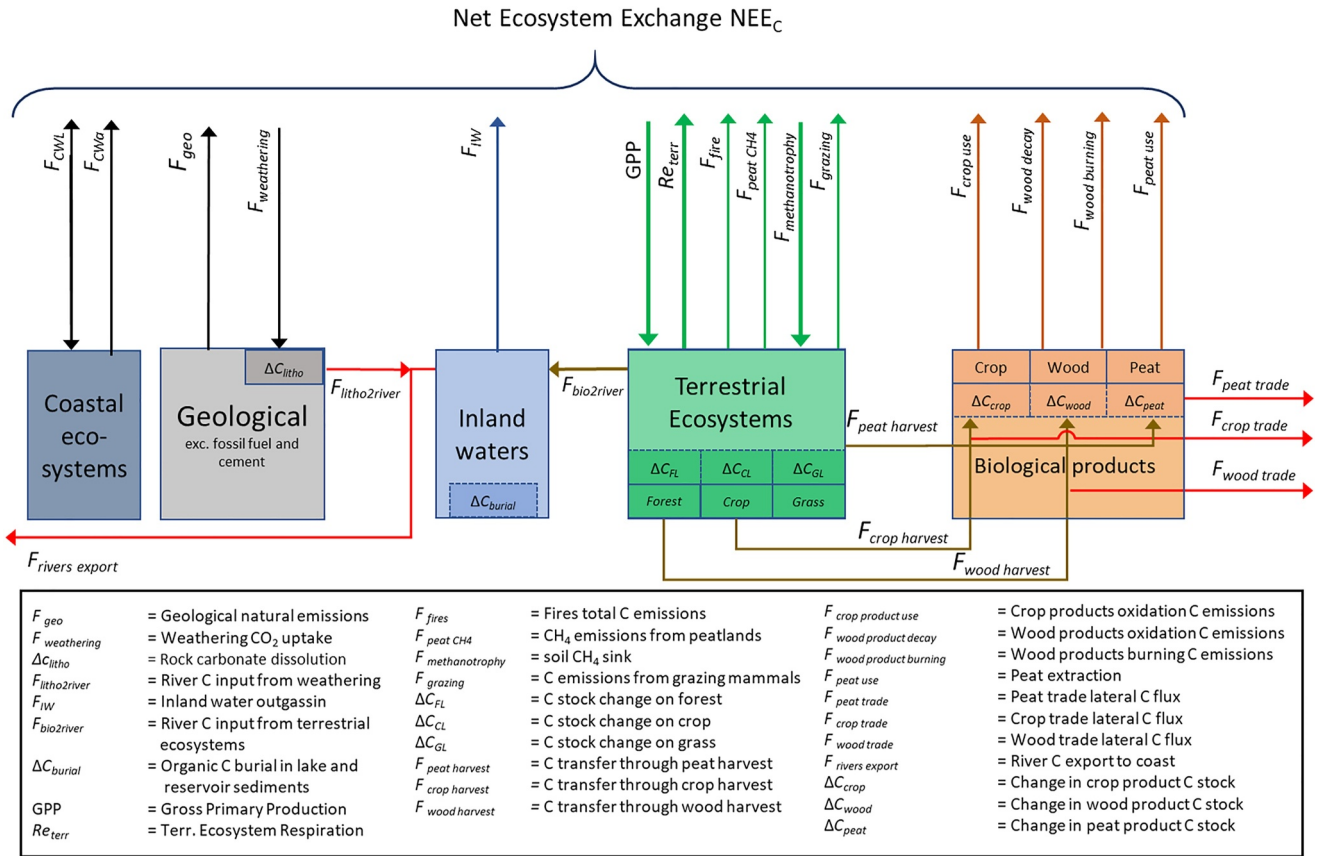


Figure 2. Detailed RECCAP2 accounting framework for the land C budget (adapted from Ciais et al. (2022)).

estimating oxidation of all other wood products ( $F_{wood\ decay}$ ) based on first order decay functions with product-specific half-lives (IPCC, 2019).

$$\Delta C_{wood} = F_{wood\ harvest} - F_{wood\ decay} - F_{wood\ burning} - F_{wood\ trade} \quad (10)$$

$$\Delta C_{crop} = F_{crop\ harvest} - F_{crop\ use} - F_{crop\ trade} \quad (11)$$

$$\Delta C_{peat} = F_{peat\ harvest} - F_{peat\ use} - F_{peat\ trade} \quad (12)$$

In addition, we use alternative estimates of  $F_{crop\ harvest}$ ,  $F_{wood\ harvest}$ ,  $F_{wood\ decay}$ ,  $F_{wood\ burn}$ , and  $F_{crop\ use}$  from an updated version (v4) of the spatialized product presented in Byrne et al. (2023) after the ideas of Ciais et al. (2022) and Deng et al. (2022). These annual maps are also based on trade statistics from the Food and Agriculture Organization of the United Nations (FAO; <http://www.fao.org/faostat/en/#data>, last access: 15 August 2023) and on energy statistics from the International Energy Agency (IEA; <https://wds.iea.org/wds/>, last access: 15 August 2023) that have been converted to carbon equivalent and disaggregated with high-resolution proxy data (satellite-derived NPP, population or livestock maps, etc.). For all fluxes included in the C stock budgets of wood and crop products, we derived annual fluxes, which we averaged over each of the last three decades.  $\Delta C_{peat}$  is calculated from the average annual flux of peat harvest ( $F_{peat\ harvest}$ ), consumption ( $F_{peat\ use}$ ) and trade fluxes ( $F_{peat\ trade}$ ) (Equation 12) reported in Hirschler and Osterburg (2022). As mentioned before, we only have fluxes as representative for the 2010s, which we had to use as well as first-order estimates for the preceding two decades.

$F_{river\ export}$  is taken from spatially explicit estimates published by Zscheischler et al. (2017) after the predictive models of Hartmann et al. (2009) and Mayorga et al. (2010). In our accounting framework,  $F_{river\ export}$  is fed by inputs from the lithosphere ( $F_{litho2river}$ ) and the biosphere ( $F_{bio2river}$ ) (Equation 13).

$$F_{\text{river export}} = F_{\text{litho2river}} + F_{\text{bio2river}} - F_{\text{IW}} - \Delta C_{\text{burial}} \quad (13)$$

$F_{\text{litho2river}}$  represents inputs in the form of carbonate alkalinity, which we assume to be non-reactive during transport. This flux incorporates both the weathering  $\text{CO}_2$  sink  $F_{\text{weathering}}$  as well as inputs from dissolving lithogenic carbonates, which we treat as change in lithospheric C stocks ( $\Delta C_{\text{litho}}$ ). Both  $F_{\text{weathering}}$  and  $\Delta C_{\text{litho}}$  are taken from the same spatial data set by Zscheischler et al. (2017). In contrast,  $F_{\text{bio2river}}$  represents organic carbon and  $\text{CO}_2$  inputs from the biosphere, which feed the evasion of  $\text{CO}_2$  and  $\text{CH}_4$  from inland waters to the atmosphere ( $F_{\text{IW}}$ ) as well as the burial of C in aquatic sediments ( $\Delta C_{\text{burial}}$ ) (Equation 13). However, only one part of  $F_{\text{bio2river}}$  is evading or buried, and the remaining fraction is exported to the coast (as part of  $F_{\text{river export}}$ ). At decadal time scales, we assume that change in the C stock of the inland water compartment is equal to the C burial rates  $\Delta C_{\text{burial}}$ , for which we have estimates of average annual fluxes that were statistically upscaled from observations (Mendonça et al., 2017). Based on the independent estimates of the other flux components,  $F_{\text{bio2river}}$  is estimated based on mass budget closure (Equation 13). Note further that all flux estimates used in this equation are climatologies of average annual fluxes, which we assume to be representative for the last three decades, excluding any trends over this timeframe.

For at least the most recent decade of the 2010s, we provide an alternative estimate of  $\Delta C_{\text{land}}$  based on the stock changes in different C pools (Equation 14). In addition to  $\Delta C_{\text{burial}}$ ,  $\Delta C_{\text{litho}}$ , and the C stock changes of the product pools ( $\Delta C_{\text{wood}}$ ,  $\Delta C_{\text{crop}}$ ,  $\Delta C_{\text{peat}}$ ) treated above, this approach required independent estimates of biospheric C stock changes in forest, grass- and cropland ( $\Delta C_{\text{FL}}$ ,  $\Delta C_{\text{GL}}$ ,  $\Delta C_{\text{CL}}$ ).

$$\Delta C_{\text{land}} = \Delta C_{\text{litho}} + \Delta C_{\text{burial}} + \Delta C_{\text{FL}} + \Delta C_{\text{GL}} + \Delta C_{\text{CL}} + \Delta C_{\text{wood}} + \Delta C_{\text{crop}} + \Delta C_{\text{peat}} \quad (14)$$

For  $\Delta C_{\text{FL}}$ , we use the estimates from the European Forest Information SCENario Model (EFISCEN) that cover C stock changes in biomass, deadwood, litter and soil C pools (Nabuurs et al., 2018; Petrescu et al., 2020; Petz et al., 2016). EFISCEN uses national forest inventory data on forest age structure and tree species composition and detailed information on management practices to project forest productivity and C stocks. Note that DGVMs represent forest structure and management practices rather rudimentarily, which is an important shortcoming and the main reason we prefer EFISCEN over TRENDY simulations. For  $\Delta C_{\text{GL}}$  and  $\Delta C_{\text{CL}}$ , we assume that the relevant stock changes at the decadal time-scale only concern the soil C stocks. The UNFCCC gives inventory-based estimates of  $\Delta C_{\text{GL}}$  and  $\Delta C_{\text{CL}}$  in general, but also separates grasslands on mineral versus organic soils. From the FAO (Tier 1), we have inventory-based  $\Delta C_{\text{GL}}$  and  $\Delta C_{\text{CL}}$  estimates for organic soils only.

#### 2.4. Analyses of Spatio-Temporal Patterns in GHG Budgets From Regional Inversions

The analysis of spatio-temporal variability in GHG budgets from regional inversions was based on the annual net land flux for each GHG as well as for fossil  $\text{CO}_2$  emissions. The long-term trend was estimated on a pixel-by-pixel basis through a linear least squares regression for the period reported. We also analyzed continental and regional scale interannual variability (IAV) based on spatially aggregated detrended fluxes for each GHG separately, as well as the IAV of the GHG net flux expressed in  $\text{CO}_2$  equivalent using GWP20 and GWP100.

To better understand IAV in GHG budgets, we followed the approach of Bastos et al. (2016) to assess anomalies in the annual budget of each GHG for specific combinations of phases of the North Atlantic Oscillation and the East Atlantic pattern. For this, we used the NAO and EA teleconnection indices calculated by NOAA CPC and available since 1950 at [https://ftp.cpc.ncep.noaa.gov/wd52dg/data/indices/tele\\_index.nh](https://ftp.cpc.ncep.noaa.gov/wd52dg/data/indices/tele_index.nh) (last access May 2021). We then calculated the boreal winter (December–February) mean values for each index over the period 1950–2020. Given the non-stationarity of the teleconnection indices and short periods covered by our observational data, it is likely for results to be sensitive to the period considered (Li et al., 2022). For comparability of our results with those of Bastos et al. (2016), who analyzed only  $\text{CO}_2$  and only global inversions, we used the upper (lower) terciles of the reference period in Bastos et al. (2016), that is, 1982–2013 to then define positive (negative) phases of NAO and EA over the common period of 1990–2020.

We then estimate the mean GHG anomalies across all years that correspond to each NAO-EA phase combination (NAO + -EA+, NAO + EA-, NAO-EA+, NAO-EA-) for each GHG individually and also for the combined GWP20 and GWP100. Finally, we analyze the corresponding anomalies in temperature and precipitation. For this, we rely on temperature at 2 m above ground and total precipitation from the ERA5 reanalysis (Hersbach

et al., 2020) selected for the period 1990–2020. The data were deseasonalized, and the mean annual anomalies were calculated for the years corresponding to each NAO and EA phase combination.

## 2.5. Analyzing Spatial Patterns of the European Land C Sink

Trends in C sink strength for seven different products from Sections 2.2 and 2.3 (global inversions; regional inversions; TRENDYv10; FLUXCOM; VPRM; EFISCEN-Space; L-VOD) were determined by linear regression of the annual fluxes across the years 2010–2019 for each pixel. In order to provide possible explanations for the observed trends in sink strength, we additionally examine trends in both climate variables and land use, both of which are potentially important drivers of large-scale spatial variation. For the meteorological variables, the trends in annual mean air temperature, total precipitation, and mean vapor pressure deficit (VPD) from 2010 to 2019 were calculated both using all 12 months in the year and using only the months of the growing season (May–August). The values were aggregated from the 0.125° CRUERA data set as described by McGrath et al. (2023), created from re-aligning ERA5-Land re-analysis with monthly 0.5-degree CRU observations. The VPD was calculated as described by Sedano and Randerson (2014) from the saturated vapor pressure of water and the relative humidity in the CRUERA data set. Trends in CO<sub>2</sub> land use emissions were calculated using the BLUE model with the Hilda + land use/land cover map (Ganzenmüller et al., 2022). For visual comparison and interpretation, all results were aggregated to a spatial resolution of 1.0°.

## 2.6. Impact of Forest Disturbances on Biomass Carbon Stocks

### 2.6.1. Quantification of Losses and Gains at Decadal Scale

We used the disturbance map of Senf & Seidl (2021a) based on analysis of changes in Landsat reflectances time series. The detection algorithm flags forested pixels (at 30 m) with a year of disturbance (1986–2020) and a severity index between 0 and 1, with 1 being the most severe type (assumed to be a stand replacing event). The disturbance type is unattributed, and it is not distinguished between anthropogenic and natural disturbances. A 30 m pixel is flagged only once during the entire period based on the most severe disturbance; therefore, disturbance severities across Europe are probably underestimated. Using manually interpreted reference plots, the mean absolute error in the timing of the disturbance was estimated at ±3 years. Here, we aggregated this disturbance map to 90 m to match the above-ground biomass (AGB) maps, and defined undisturbed forests at 90 m as forests that have not been disturbed from 1986 to 2020.

The AGB maps developed by CCI-ESA (version 3) for the years 2010, 2017, and 2018 (Santoro & Cartus, 2021) were derived from different satellites, leading to potential local biases that need to be corrected before the analysis. The original projection EPSG:4326 (global) has a resolution of 100 m at the equator, and the maps have been re-projected in EPSG:3035 (90 m). The potential above-ground biomass (AGB\*) is the maximum reachable AGB for a forest long after a stand-replacing disturbance. For each map (2010, 2017, and 2018), AGB\* was estimated by calculating the 95% quantile of undisturbed forests (based on the disturbance map) at an 18 km resolution (to capture a sufficient number of undisturbed forests at 30 m), and then it was disaggregated back to 90 m to match the original resolution. Assuming that AGB\* is similar between AGB maps, the biases between maps have then been corrected locally using a linear correction function (Equations 15–17), with  $AGB_i^{raw}$  being the raw AGB data for each year  $i$ , and  $\alpha_i$  being the matrix of correction factors. Across the European continent,  $\alpha_{2010} = 1.01 \pm 0.06$  (mean ± 1 SD),  $\alpha_{2017} = 1.00 \pm 0.07$  and  $\alpha_{2018} = 0.99 \pm 0.08$ , indicating that there is no systematic bias between maps at the European scale.

$$AGB_i = \alpha_i AGB_i^{raw} \quad (15)$$

$$\alpha_i = \frac{AGB^*}{AGB_i^*} \quad (16)$$

$$AGB^* = \frac{AGB_{2010}^* + AGB_{2017}^* + AGB_{2018}^*}{3} \quad (17)$$

For disturbed pixels (at 90 m) in a given local area (at 18 km) and a given decade  $T$  (1990–2000 for example), the loss of biomass (expressed in MtC/year) during the year of disturbance is approximated by Equation 18, where  $x$  is a pixel disturbed (90 m) during the period  $T$ ,  $A$  the total area disturbed,  $U(x)$  is the mean AGB of undisturbed

neighbors at 18 km and  $s(x)$  is the severity of the disturbance (aggregated from 30 to 90 m). The factor 0.5 corresponds to the conversion from dry biomass to carbon stocks. The undisturbed neighbor AGB is used here because the AGB of the pixels impacted by the disturbance is unknown. The gain of biomass of these disturbed forests from the decade  $T$  to present time (2017–2018) is calculated according to Equation 19.

$$AGB_{\text{loss}} = \frac{A}{2} \sum_x (s(x) \times U(x)) \quad (18)$$

$$AGB_{\text{gain}} = \frac{A}{2} \sum_x AGB_i(x) \quad (19)$$

The analysis has been conducted separately for four major European biogeographical regions approximated with the country borders: Mediterranean (Spain, Portugal, Italy, Greece, Croatia, Slovenia), Continental (Romania, Bulgaria, Ukraine, Belarus, Czechia, Poland, Hungary, Slovakia), Atlantic (France, Ireland, United Kingdom, Belgium, Netherlands, Germany, Austria, Switzerland) and Boreal (Norway, Finland, Sweden, Denmark, Estonia, Lithuania, Latvia). Uncertainties for the sources and sinks have been estimated using the absolute difference between the 2017 and 2018 maps.

### 2.6.2. Disentangling the Effect of Natural Disturbances

Natural disturbances—large pulses of tree mortality that originate from abiotic and biotic factors such as fires, strong winds, or insect outbreaks—represent serious peril for maintaining healthy and productive forests (Anderegg et al., 2020; MacDowell et al., 2020). Recent studies have shown an increase in forest vulnerability to such disturbances at the European level (Forzieri et al., 2021), consistent with the observed widespread decline in forest resilience (Forzieri et al., 2022; Smith et al., 2022) and the reported intensification of forest damage associated with climate-driven events (Patacca et al., 2023). Emerging signs of C sink saturation and sink decline in European forest biomass have been associated with such an increased disturbance regime (Korosuo et al., 2023; Nabuurs et al., 2013), which is expected to be further exacerbated by climate change (Anderegg et al., 2022; Seidl et al., 2014).

Quantifying the contribution of natural disturbances and associated temporal variations is therefore crucial to properly evaluate their effect on the C budget. To this aim, we complement the analyses described in the previous section with an assessment of the biomass losses due to fires, windthrown events and insect outbreaks documented in the Database on Forest Disturbances in Europe (DFDE). The DFDE reports forest damages in terms of timber volume loss aggregated at the country level associated with single disturbance events occurring over the period 1950–2019 (Patacca et al., 2023; Schelhaas et al., 2003) and retrieved from a literature search.

We provide a synthesis of the natural disturbances documented at the European scale in the DFDE in terms of relative importance of each single agent type and in terms of temporal trends over the observational period (Patacca et al., 2023). We point out that spatial extents and temporal coverage of DFDE differ slightly from those utilized as reference in RECCAP2. However, we believe that aggregated estimates can be considered a reasonably good approximation for the scope of this assessment (Section 8.2).

## 3. Bottom-Up Greenhouse Gas Budgets of Europe

This section deals with the BU budget of the three GHGs, first presented individually (Sections 3.1–3.3, respectively) and then grouping all GHGs using the global warming potential of  $\text{CH}_4$  and  $\text{N}_2\text{O}$  at 100 years horizon (Section 3.4). The fluxes of our BU budget are presented in Figure 1. For the most recent decade of the 2010s, we listed our best estimates for these fluxes and our assessment of the level of confidence in these numbers in Table 2. We compare our BU estimates of the GHG budgets against atmospheric inversions, the value ranges of which are listed in Table 3. In addition, we reconstruct the development of GHG budgets over the last three decades, that is, the 1990s, the 2000s, and the 2010s, based on a subset of data sources that cover that time frame as completely and as consistently as possible. For a detailed list of fluxes taken from different sources, we refer the interested reader to Tables S1–S6 in Supporting Information S2.

**Table 3**  
*Comparison of Our Bottom-Up Land GHG Budgets Against Top-Down Estimates From Atmospheric Inversions*

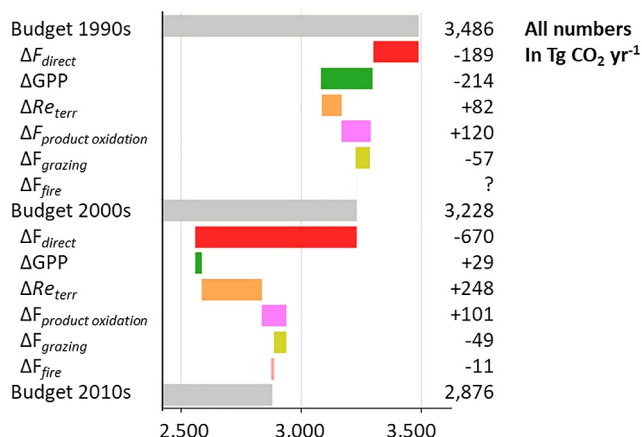
Part of GHG budget assessed	Method of assessment	Estimated flux in Tg CO <sub>2</sub> yr <sup>-1</sup> , Tg CH <sub>4</sub> yr <sup>-1</sup> , or Gg N <sub>2</sub> O yr <sup>-1</sup>		
		Best estimate	Lower estimate	Upper estimate
<b>CO<sub>2</sub> budget</b>				
$F_{\text{land CO}_2}$	Bottom up, Equation 2	-1,403		
	Global inversions	-958	-1478	185
	Regional inversions	-743	-1013	-593
<b>CH<sub>4</sub> budget</b>				
$F_{\text{total CH}_4}$	Bottom up	32		
	Global inversions, surface observations	32	22	39
	Global inversions, satellite based	28	25	37
	Regional inversions	36	33	44
$F_{\text{land CH}_4} - (F_{\text{fire}} + F_{\text{geo}})$	Bottom up	6		
	Regional inversion (CTECH4)	4		
$F_{\text{peat CH}_4}$	Bottom up	2.0	0.6	3.3
	Global inversions, surface observations	2.0	1.7	8.4
	Global inversions, satellite based	2.1	1.7	4.9
<b>N<sub>2</sub>O budget</b>				
$F_{\text{total N}_2\text{O}}$	Bottom up	1,274		
	Global inversions	1,472	682	1,594
	Regional inversion (Flexinvert)	1,331		

### 3.1. CO<sub>2</sub>

Direct anthropogenic emissions, which do not include  $F_{\text{LULUCF}}$  nor  $F_{\text{LUC}}$  in our assessment, dominate the CO<sub>2</sub> budget, and amount to an average flux of 4.1 Pg CO<sub>2</sub> yr<sup>-1</sup> over the period 2010–2019 (Table 2). The largest contribution (~90%) of direct anthropogenic emissions is attributed to  $F_{\text{energy}}$ . Another 8% is attributed to  $F_{\text{IPPU}}$ . Contributions from  $F_{\text{agri}}$  and  $F_{\text{waste}}$  are minor. Apart from the waste sector, we have a high level of confidence in these estimates of direct anthropogenic CO<sub>2</sub> emissions.

For the land CO<sub>2</sub> budget, our BU estimate gives a net sink of an average 1.4 Pg CO<sub>2</sub> yr<sup>-1</sup> over the period 2010–2019 (Figure S2 in Supporting Information S1), which counterbalances about one third of the direct anthropogenic emissions (Table 2). We assign a moderate level of confidence (±50%) based on expert judgment to our estimate of this land sink. Our BU estimate is in the range of global atmospheric inversions but gives a stronger sink than any of the regional inversions considered here (Table 3). The land CO<sub>2</sub> budget is dominated by the imbalance between gross primary production (GPP) and net ecosystem respiration of terrestrial ecosystems ( $\text{Re}_{\text{terr}}$ ), which amounts to about 3.3 Pg CO<sub>2</sub> yr<sup>-1</sup>. While we have a high level of confidence (i.e., ±25%) in GPP and  $\text{Re}_{\text{terr}}$  estimates, the balance between both fluxes is more uncertain. Nevertheless, we still assigned a moderate level of confidence (±50%) to the estimated difference  $\text{GPP} - \text{Re}_{\text{terr}}$ . This imbalance between both fluxes is largely due to the anthropogenic appropriation of biomass through the harvest and use of wood and crop products, which does not feed into the ecosystem respiration (see Ciaia et al., 2021). This appropriated biomass is returned to the atmosphere through the oxidation of the products, which we estimate at ~1.3 Pg CO<sub>2</sub> yr<sup>-1</sup>. Note that this flux accounts for the imports and exports of products as well as a Tier 2 assessment of stock changes. We assign a high level of confidence to that estimate (±25%). For a more detailed description of this flux, see Section 5. Another ~0.5 Pg CO<sub>2</sub> yr<sup>-1</sup> is returned from biomass to the atmosphere through grazing by livestock. A still sizable source of CO<sub>2</sub> is inland water emissions of roughly 0.2 Pg CO<sub>2</sub> yr<sup>-1</sup>. Emissions from coastal waters and wildfires are additional, minor land sources of CO<sub>2</sub> to the atmosphere. Rock weathering and coastal wetlands are minor sinks of CO<sub>2</sub>.





**Figure 3.** Evolution of the European CO<sub>2</sub> budget over the last three decades. Note that there is no estimate for  $F_{fire}$  in the 1990s.

concerns  $F_{IW}$ ,  $F_{Cwa}$ ,  $F_{CWL}$ , and  $F_{weathering}$ . In addition, we had to assume that  $F_{fire}$  did not change between the 1990s and the 2000s. In this analysis, we put the four direct anthropogenic emissions  $F_{energy}$ ,  $F_{IPPU}$ ,  $F_{waste}$  and  $F_{agri}$  together as  $F_{direct}$ . Detailed information on decadal changes in each of these fluxes is given in Table S2 in Supporting Information S2.

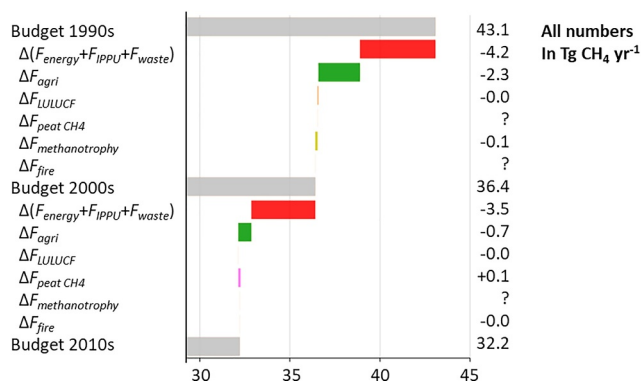
We see from Figure 3 that the overall net source has notably decreased from the 1990s to the 2000s and further to the 2010s. For the 2000s, our estimate of 3,228 Tg CO<sub>2</sub> yr<sup>-1</sup> is quite close to the estimate by Luysaert et al. (2012) of ~3,270 Tg CO<sub>2</sub> yr<sup>-1</sup> for RECCAP1. However, as RECCAP1 excluded Ukraine, Belarus, and the Republic of Moldova, a direct comparison is difficult. From the 1990s to the 2000s, the reduction in the net source of 258 Tg CO<sub>2</sub> yr<sup>-1</sup> was largely due to reductions in  $F_{direct}$ . However, 69 Tg CO<sub>2</sub> yr<sup>-1</sup> are still due to an increase in the land CO<sub>2</sub> sink. Between these two decades, we find an important increase in average GPP, which is only partly offset by an increase in  $Re_{terr}$ . We further find an increase in  $F_{product\ oxidation}$  and a decrease in  $F_{grazing}$ . The sum of changes in these fluxes gives an overall increase in oxidation of anthropogenically appropriated biomass of 64 Tg CO<sub>2</sub> yr<sup>-1</sup> within Europe, which offsets another fraction of the increase in GPP although it may include imported biomass from other RECCAP2 regions.

From the 2000s to the 2010s, the reduction in  $F_{direct}$  was about 3.5 times as strong as between the 1990s and 2000s. A similar trend was found for EU27+UK by the VERIFY synthesis (McGrath et al., 2023; Petrescu et al., 2021a) that shows a significant decrease in net-CO<sub>2</sub> emissions driven by decreased fossil fuel emissions ( $F_{energy} + F_{IPPU}$ ) that sets in around 2005 and continues until the end of our RECCAP2 period. However, this reduction in direct anthropogenic emissions was partly offset by a strong reduction in the land CO<sub>2</sub> sink of 318 Tg CO<sub>2</sub> yr<sup>-1</sup> (Figure 3). From the 2000s to the 2010s, even if average GPP slightly decreased, it was accompanied by a strong increase in  $Re_{terr}$  that was three times higher than that between the 1990s and the 2000s. Changes in  $F_{grazing}$  and  $F_{product\ oxidation}$  are comparable to those between the 1990s and the 2000s, with a similar increase in emissions from anthropogenically appropriated biomass back to the atmosphere of 52 Tg CO<sub>2</sub> yr<sup>-1</sup>. Being generally a minor flux in the European CO<sub>2</sub> budget (Table 3, Table S2 in Supporting Information S2), also changes in  $F_{fire}$  have only a small influence on decadal trends in the CO<sub>2</sub> budget (Figure 3).

Overall, according to our BU assessment, the strength of the land CO<sub>2</sub> sink has decreased from 1.5 Pg CO<sub>2</sub> yr<sup>-1</sup> in the 1990s to 1.3 Pg CO<sub>2</sub> yr<sup>-1</sup> in the 2010s (Table S2 in Supporting Information S2). This is comparable to the TD estimates from global inversions that give a decrease from 1.3 (0.3–1.5) Pg CO<sub>2</sub> yr<sup>-1</sup> to 1.0 (0.0–1.5) Pg CO<sub>2</sub> yr<sup>-1</sup>, respectively (ensemble median and range, Table S2 in Supporting Information S2). For the 2000s, however, our BU estimate diverges substantially from global inversions, with 1.6 Pg CO<sub>2</sub> yr<sup>-1</sup> versus 0.9 (0.1–1.2) Pg CO<sub>2</sub> yr<sup>-1</sup>, respectively (Table S2 in Supporting Information S2). Thus, while TD assessments show the weakest land CO<sub>2</sub> sink for the 2000s, our BU assessment identifies the 2000s as the decade with the strongest land CO<sub>2</sub> sink.

Overall, our BU CO<sub>2</sub> budget including direct anthropogenic emissions and the land CO<sub>2</sub> budget gives a net source of ~2.7 Pg CO<sub>2</sub> yr<sup>-1</sup> for the 2010s. Using the smaller selection of data sources of the different flux components that were available for the last three decades, the estimated net source for the 2010s was slightly higher with ~2.9 Pg CO<sub>2</sub> yr<sup>-1</sup> (Figure 3). This follows differences in GPP. For a consistent analysis over these three decades, GPP and  $Re_{terr}$  are taken solely from the FLUXCOM ERA5 data set. Although the FLUXCOM ERA5 values for GPP are close to the median values derived from all together five estimates, and for  $Re_{terr}$  even identical to the three estimates for the 2010s (Table S1 in Supporting Information S2), the absolute difference is significant in relation to the CO<sub>2</sub> budget where GPP and  $Re_{terr}$  are the dominant fluxes that balance each other out to a large degree.

Figure 3 gives the total CO<sub>2</sub> budget for the last three decades as well as changes in certain fluxes that explain the differences between these decadal budgets. Note that not all fluxes used in the budgets are included in this figure, as for some of these fluxes, we only have estimates of average annual fluxes that we have to assume to remain constant across the three decades. That



**Figure 4.** Evolution of the European CH<sub>4</sub> budget over the last three decades. Note that there is no estimate for  $F_{\text{fire}}$  in the 1990s.

### 3.2. CH<sub>4</sub>

For the European CH<sub>4</sub> budget 2010–2019, our BU estimates give an average net emission of  $\sim 32 \text{ Tg CH}_4 \text{ yr}^{-1}$ . We assign a moderate level of confidence (up to  $\pm 50\%$ ) to this estimate. This BU estimate lies within the range of TD estimates from the two global inversion ensembles used in GMB2020 by Saunio et al. (2020), of which one is based on surface observations of atmospheric CH<sub>4</sub> concentrations ( $22\text{--}39 \text{ Tg CH}_4 \text{ yr}^{-1}$ , median of  $32 \text{ Tg CH}_4 \text{ yr}^{-1}$ ) and one based on satellite observations ( $25\text{--}37 \text{ Tg CH}_4 \text{ yr}^{-1}$ , median of  $28 \text{ Tg CH}_4 \text{ yr}^{-1}$ , Table 3). In contrast, our BU estimate lies on the far lower end of TD estimates from regional inversions ( $33\text{--}44 \text{ Tg CH}_4 \text{ yr}^{-1}$ , Table 3).

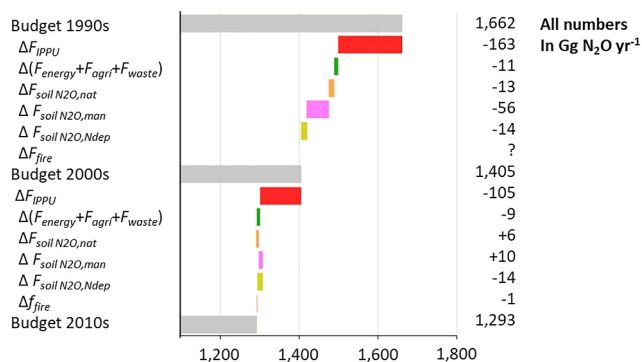
About three quarters of European CH<sub>4</sub> emissions, that is,  $\sim 24 \text{ Tg CH}_4 \text{ yr}^{-1}$ , can be attributed to  $F_{\text{direct}}$ , that is, the sum of direct anthropogenic emissions  $F_{\text{energy}}$ ,  $F_{\text{IPPU}}$ ,  $F_{\text{waste}}$ , and  $F_{\text{agri}}$ . With  $\sim 11 \text{ Tg CH}_4 \text{ yr}^{-1}$ , the agricultural sector nearly contributes half of the direct emissions. With 6 to 7  $\text{Tg CH}_4 \text{ yr}^{-1}$ , the energy and the waste sector are similarly less strong emitters, while contri-

butions of the industrial production and product use sector are minor. For the comparison of BU and TD estimates, we have to keep in mind that the BU estimates include  $F_{\text{direct}}$  emissions derived from country totals of inventories, which include offshore emissions from within the economic zones of European countries, and in the case of UNFCCC inventories, also overseas territories (see Section 2.1.1). For the TD estimates, in contrast, we used a land mask to constrain all sources and sinks, incl.  $F_{\text{direct}}$ , to the land surface of our RECCAP2 region, as far as this is possible considering the coarse resolution of the TD data. While overseas territories play a negligible role (see Section 2.1.1), the contribution of  $F_{\text{energy}}$  in the offshore part of the economic zones of continental Europe may be more important. Quantification of this contribution is, however, beyond the scope of this study.

About one quarter of CH<sub>4</sub> emissions is attributed to natural sources. In contrast to  $F_{\text{direct}}$ , which is estimated largely from inventory data, we assign a low level of confidence to our BU estimate of the land CH<sub>4</sub> budget. The two largest sources in our land CH<sub>4</sub> budget are inland waters and geological emissions with 4.1 and 2.5  $\text{Tg CH}_4 \text{ yr}^{-1}$  (Table 2, Figure S3 in Supporting Information S1). For inland water emissions, we assigned a moderate level of confidence ( $\pm 50\%$ ). In contrast, we assign a very low level of confidence to geological emissions. Note that our flux estimate is based on the global but spatialized estimate by Etiope et al. (2019), which is currently disputed. The study by Hmiel et al. (2020) suggests that global geological CH<sub>4</sub> emissions are about one order of magnitude smaller than those estimated by Etiope et al. (2019). Peatland emissions are very likely sizable but also very poorly constrained (range of 0.6–3.3  $\text{Tg CH}_4 \text{ yr}^{-1}$ , Table S3 in Supporting Information S2). Emissions from fires, coastal waters and coastal wetlands do not play a significant role in the land CH<sub>4</sub> budget of Europe. The regional inversion CTE-CH<sub>4</sub> gives an estimate for the land CH<sub>4</sub> budget excluding geological and fire emissions. This TD estimate of a net-source of 4.2  $\text{Tg CH}_4 \text{ yr}^{-1}$  is lower but still comparable to our corresponding BU estimate of 5.1  $\text{Tg CH}_4 \text{ yr}^{-1}$ . This suggests that our bottom up estimate of land CH<sub>4</sub> sources is overestimated, which may in part be due to our estimate of geological emissions.

When comparing the CH<sub>4</sub> budgets for the 1990s, 2000s, and 2010s, the BU estimates show a strong decrease in the overall net sources (Figure 4). Note that we have split changes in  $F_{\text{direct}}$  into changes in  $F_{\text{agri}}$  as the single largest contributor and the sum of changes in the remaining flux components  $F_{\text{energy}}$ ,  $F_{\text{IPPU}}$ , and  $F_{\text{waste}}$ . From the 1990s to the 2010s, the net source decreased by about one quarter, mainly due to reductions in  $F_{\text{energy}}$  and  $F_{\text{waste}}$ . Changes in natural sinks and sources do not appear to be important for the overall CH<sub>4</sub> budget. Note however that for  $F_{\text{IW}}$  as the largest natural source, no assessment of long-term trends exists.

Our CH<sub>4</sub> net emission estimate of 36  $\text{Tg CH}_4 \text{ yr}^{-1}$  for the 2000s is higher than the RECCAP1 estimate of 28  $\text{Tg CH}_4 \text{ yr}^{-1}$  by Luyssaert et al. (2012) for the period 2001–2005. However, direct comparison is difficult as the RECCAP1 analysis excluded the Eastern European countries of Rep. of Moldova, Ukraine and Belarus. For EU27+UK, a detailed inventory - based analysis of trends in direct CH<sub>4</sub> emissions from the period 2000–2009 to the RECCAP2 period 2010–2019 was given by Petrescu et al. (2023). They found a decrease in direct emissions by 16.5%, mainly due to reductions in  $F_{\text{waste}}$  ( $-10.1\%$ ) and  $F_{\text{energy}}$  ( $-4.4\%$ ). This is comparable to the relative reduction in  $F_{\text{direct}}$  by 15% from the 2000s to the 2010s identified in our study (see Table S4 in Supporting Information S2). The decrease in  $F_{\text{energy}}$  in Europe can be explained by strong reductions in coal emissions, followed by reductions in oil and gas emissions (Stavert et al., 2022). The strong decrease in  $F_{\text{waste}}$  follows



**Figure 5.** Evolution of the European N<sub>2</sub>O budget over the last three decades. Note that there is no estimate for  $F_{fire}$  in the 1990s.

legislative changes in the EU that started with the so called “Land fill directive” in 1999 that made gas control obligatory on landfills by 2009 (Petrescu et al., 2023; Sauniois et al., 2020). However, from the global inversions, we do not see a trend from the 2000s–2010s, with TD estimates of a net source of 32 (23–42) Tg CH<sub>4</sub> yr<sup>-1</sup> versus 32 (22–39) Tg CH<sub>4</sub> yr<sup>-1</sup>, respectively (median and range, Table S4 in Supporting Information S2). Similarly, Petrescu et al. (2023) were not able to confirm the trends from their BU assessment through TD estimates.

### 3.3. N<sub>2</sub>O

For the European N<sub>2</sub>O budget 2010–2019, our BU estimates give an average total emission of ~1.3 Tg N<sub>2</sub>O yr<sup>-1</sup>. We assigned a moderate level (±50%) of confidence to this estimate. Our BU estimate is within the range of TD estimates from global inversions used by Tian et al. (2020) (0.7–1.6 Tg N<sub>2</sub>O yr<sup>-1</sup>, median of 1.5 Tg N<sub>2</sub>O yr<sup>-1</sup>), and very close to the regional TD estimate

from Flexinvert that was used by Petrescu et al. (2023) (1.3 Tg N<sub>2</sub>O yr<sup>-1</sup>, Table 3). In our bottom-up estimate, we attribute only about one quarter of emissions to  $F_{direct}$ , to which all four flux components, that is,  $F_{energy}$ ,  $F_{IPPU}$ ,  $F_{waste}$ , and  $F_{agri}$ , contribute substantially. Note that for  $F_{agri}$ , we only include emissions from manure management and biomass burning. Emissions due to fertilizer and manure application as well as residue management are put together as the soil management flux  $F_{soil\ N_2O,man}$  that is a component of the soil emission flux  $F_{soil\ N_2O}$ , and thus of the land N<sub>2</sub>O budget, which we keep separate from  $F_{direct}$ .

From the different inventories we use for our budget, we get quite similar estimates for  $F_{energy}$  and  $F_{agri}$ . However, since the inventories partly use similar activity data and emission factors, we assume only a moderate level of certainty. For the estimate of  $F_{IPPU}$ , we are less confident because the inventory based estimates considered in our study range from 58 Gg N<sub>2</sub>O yr<sup>-1</sup> (UNFCCC) to 210 Gg N<sub>2</sub>O yr<sup>-1</sup> (EDGAR) (see Table S5 in Supporting Information S2). Here, we assign a very low level of confidence. Similarly, we assign a low level of confidence to  $F_{waste}$  for which estimates range from 42 Gg N<sub>2</sub>O yr<sup>-1</sup> (UNFCCC) to 76 Gg N<sub>2</sub>O yr<sup>-1</sup> (GAINS).

The land N<sub>2</sub>O budget, which accounts for three quarters of the total emissions, is dominated by soil N<sub>2</sub>O emissions ( $F_{N_2O,soil}$ , about 97% of the land N<sub>2</sub>O budget, see Figure S4 in Supporting Information S1). We are confident that the real value for  $F_{N_2O,soil}$  lies within ±50% (“moderate” level of confidence) of our estimate of ~0.93 Tg N<sub>2</sub>O yr<sup>-1</sup>. Moreover, 0.68 Tg N<sub>2</sub>O yr<sup>-1</sup> of  $F_{N_2O,soil}$  can be attributed to  $F_{soil\ N_2O,man}$ , while atmospheric deposition of reactive N ( $F_{soil\ N_2O,Ndep}$ ) is responsible for another 0.07 Tg N<sub>2</sub>O yr<sup>-1</sup> of soil indirect emissions, and the remaining 0.17 Tg N<sub>2</sub>O yr<sup>-1</sup> can be attributed to natural background emissions  $F_{N_2O,soil,nat}$  (Table S5 in Supporting Information S2). The remaining emissions in the land N<sub>2</sub>O budget stem mainly from inland and coastal waters (Table 2). Note further that these fluxes are not fully natural. In Europe, about two thirds of inland water emissions can be attributed to anthropogenic N inputs from fertilizer, manure and sewage water (Petrescu et al., 2023 based on Yao et al., 2020).

Figure 5 shows the evolution of decadal N<sub>2</sub>O budgets since the 1990s, including the responsible flux changes. From the 1990s to the 2010s, total emissions of N<sub>2</sub>O have decreased by about one fifth, mainly due to reductions in  $F_{IPPU}$ . From the 2000s to the 2010s, the decrease in our BU emissions is supported by a similar decrease in TD budgets from 1.6 (0.9–1.7) to 1.5 (0.6–1.6) Tg N<sub>2</sub>O yr<sup>-1</sup>, respectively, derived from global inversions (median and range; see Table S6 in Supporting Information S2). This decrease in net emissions is largely due to the reduction in  $F_{IPPU}$ . In contrast,  $F_{energy}$ ,  $F_{waste}$ , and  $F_{agri}$  remained relatively constant. As mentioned before, we see a huge spread in different estimates of  $F_{IPPU}$ . However, we see a strong decline in  $F_{IPPU}$  over the three decades from all three inventories we used for this flux (UNFCCC, EDGAR, GAINS), with a decline that ranges from 141 Gg N<sub>2</sub>O yr<sup>-1</sup> (EDGAR) to 339 Gg N<sub>2</sub>O yr<sup>-1</sup> (GAINS). Interestingly, for the 2000s, the spread between these three inventory-based estimates is quite low, with estimates ranging from 210 to 226 Gg N<sub>2</sub>O yr<sup>-1</sup> only (Table S6 in Supporting Information S2). For the 1990s and the 2010s there is a much more pronounced spread between the different data sources that explains the difference in flux changes over the three decades between the different estimates. Despite the large uncertainties related to  $F_{IPPU}$ , we can conclude that reductions in this flux are the most important driver behind the reduction in total N<sub>2</sub>O emissions. Note that  $F_{IPPU}$  is mainly associated with the production of nitric acid (mainly for fertilizer production) and adipic acid (mainly for nylon production). The

strong decrease in  $F_{\text{IPPU}}$  is due to the installation of efficient abatement technology, first in the adipic acid producing facilities (late 1990s/early 2000s) and then also in nitric acid producing facilities (Petrescu et al., 2023).

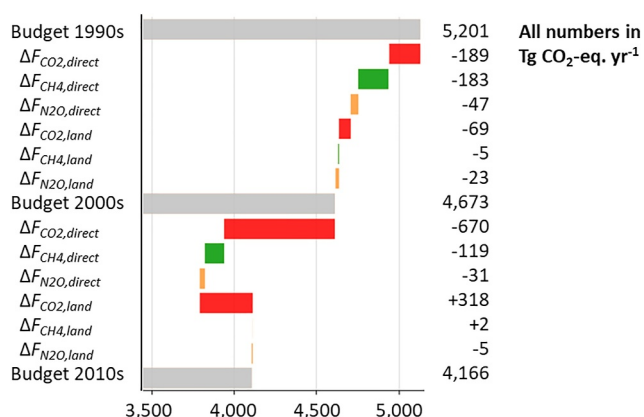
From the 1990s to the 2000s, there appears to be a notable reduction in  $F_{\text{soil N}_2\text{O,man}}$ , followed by a slight increase to the 2010s. Note that both EDGAR and FAO agree on this trend. For  $F_{\text{soil N}_2\text{O,Ndep}}$ , we derived a continuously decreasing trend from 99 Gg  $\text{N}_2\text{O yr}^{-1}$  in the 1990s to 71 Gg  $\text{N}_2\text{O yr}^{-1}$  in the 2010s based on EMEP data, the only data source that covers all soils. Comparing EMEP estimates for agricultural soils only ( $F_{\text{soil N}_2\text{O,Ndep,agri}}$ ), we see very similar trends and flux sizes from GAINS and EDGAR (see Table S6 in Supporting Information S2). In contrast, simulations with O-CN give  $F_{\text{soil N}_2\text{O,Ndep}}$  that would increase from 106 Gg  $\text{N}_2\text{O yr}^{-1}$  in the 1990s to 135 Gg  $\text{N}_2\text{O yr}^{-1}$  in the 2010s. This may be explained by the fact that with the model OC-N,  $F_{\text{soil N}_2\text{O,Ndep}}$  is calculated as the difference between simulations with and without atmospheric deposition of N, and thus accounts for indirect effects on  $\text{N}_2\text{O}$  emissions through fertilizing effects and accumulation of N in biomass, litter and soil organic matter. Depending on the residence time in these organic N pools, a historically increased N-deposition may have a certain legacy effect on  $\text{N}_2\text{O}$  emissions. In contrast, the EF-based methods account only for  $\text{N}_2\text{O}$  emissions from direct (de-)nitrification of deposited reactive N itself, and thus only accounts for the instantaneous effect of deposition on  $\text{N}_2\text{O}$  emissions. Overall, for  $F_{\text{N}_2\text{O,soil}}$ , that is, the sum of  $F_{\text{soil N}_2\text{O,man}}$ ,  $F_{\text{soil N}_2\text{O,Ndep}}$  and the natural background flux  $F_{\text{N}_2\text{O,soil,nat}}$ , and largest source of  $\text{N}_2\text{O}$ , our BU assessment gives a slight decrease from the 1990s–2000s, but there is no notable trend between the 2000s and the 2010s. That agrees with Tian et al. (2020), who did not find a notable trend in soil  $\text{N}_2\text{O}$  emissions for Europe over the last two decades. The decrease from the 1990s to the 2000s may be explained by the EU nitrate directive, which led to a decrease in manure and fertilizer application during the 2000s, which may have led to a subsequent decrease in  $\text{N}_2\text{O}$  emissions (Velthof et al., 2014).

### 3.4. All GHGs

When we combine the three GHGs for the decade of the 2010s, we obtain a total  $\text{CO}_2$ -equivalent emission of 4.87 Pg  $\text{CO}_2\text{-eq. yr}^{-1}$  for direct anthropogenic emissions. For the land budget, we obtain a net sink of  $-0.92$  Pg  $\text{CO}_2\text{-eq. yr}^{-1}$ . However, while we have a high level of confidence in the estimated direct emissions, our level of confidence in the land budget is rather low (Table 2).  $F_{\text{energy}}$  contributes  $\sim 80\%$  to direct anthropogenic emissions.  $\text{CO}_2$  dominates the  $\text{CO}_2$ -eq. emissions of both  $F_{\text{energy}}$  and  $F_{\text{IPPU}}$  ( $>90\%$ , Table 2). In contrast,  $\text{CH}_4$  dominates the  $\text{CO}_2$ -eq. emissions of  $F_{\text{waste}}$  and  $F_{\text{agri}}$  ( $\sim 90\%$  in each case).

The land GHG budget is dominated by the strong land  $\text{CO}_2$  sink, of which only one third is counterbalanced by net  $\text{CH}_4$  and  $\text{N}_2\text{O}$  emissions. Also, Luyssaert et al. (2012) had found the European land budget to be a net-sink of GHGs. In contrast, Tian et al. (2016) found the European land budget to be a net-source based on a BU assessment, while a TD assessment showed the budgets to be close to neutral with a huge range of uncertainties. As the most important flux components, the net-exchange between plant biomass, vegetation and atmosphere ( $F_{\text{soil} + \text{biomass}}$ ), as well as the oxidation of harvested products ( $F_{\text{product oxidation}}$ ) are dominated by  $\text{CO}_2$ . However, as these fluxes partly balance each other, the overall dominance of  $\text{CO}_2$  in the land GHG budget diminished. As a component of the final net land GHG sink of  $-0.92$  Pg  $\text{CO}_2\text{-eq. yr}^{-1}$ , the inland water emissions of 0.31 Pg  $\text{CO}_2\text{-eq. yr}^{-1}$  become an important flux component. While  $\sim 62\%$  of  $F_{\text{IW}}$  is attributed to  $\text{CO}_2$ ,  $\text{CH}_4$  has a sizable contribution of 36%, which demonstrates the significant role of this GHG in the land budget. The contribution of  $\text{N}_2\text{O}$  in  $F_{\text{IW}}$  is nearly negligible. Moreover, the weight of  $\text{N}_2\text{O}$  emissions in the land GHG budget is largely due to soil emissions, of which the major proportion represents anthropogenic perturbations through management and atmospheric deposition of reactive nitrogen (see Section 3.3). As found in Section 3.2, our bottom-up estimate of land  $\text{CH}_4$  emissions is likely too high, which means that the net GHG sink could be slightly higher. If we follow the findings by Hmiel et al. (2020) and assume  $F_{\text{geo}}$  to be one order of magnitude lower, the net land GHG sink could increase to  $-0.98$  Pg  $\text{CO}_2\text{-eq. yr}^{-1}$ .

Figure 6 shows the evolution of the European GHG budget over the last three decades, summing up direct emissions and land budgets of  $\text{CO}_2$ ,  $\text{CH}_4$ , and  $\text{N}_2\text{O}$ , and expressing their sum using AR6 global warming potential at the 100-year horizon. The figure further lists how changes in direct emissions versus changes in the land budgets of the three GHGs contributed to the changes in the GHG budgets between the three decades. Note that for the last decade, the net-emissions here are slightly higher than reported in Table 2, mainly following the lower land  $\text{CO}_2$  sink resulting from a narrower selection of data sets covering better the three decades (see Section 2.1.2). From the 1990s to the 2010s, net emissions decreased by nearly one fourth. From the 1990' to 2000s,



**Figure 6.** Evolution of the European greenhouse gas budget over the last three decades, reported as global warming potential in CO<sub>2</sub> equivalents at 100-year horizon.

this decrease amounted to  $\sim 0.5$  Pg CO<sub>2</sub>-eq. yr<sup>-1</sup>, of which about two thirds were due to reductions in direct emissions of CH<sub>4</sub> and CO<sub>2</sub>. From the 2000s to the 2010s, net emissions decreased by another  $\sim 0.5$  Pg CO<sub>2</sub>-eq. yr<sup>-1</sup>, which was mainly due to net decrease in direct CO<sub>2</sub> emissions of similar size. From the 1990s to the 2000s, the strength in the land CO<sub>2</sub> sink slightly increased, whilst it decreased from the 2000s to the 2010s, largely off-setting the effect of reduced direct emissions of the other two GHGs CH<sub>4</sub> and N<sub>2</sub>O. Changes in the land budgets of CH<sub>4</sub> and N<sub>2</sub>O are small compared with those in other sectors.

## 4. Land Carbon Budget

### 4.1. Land Carbon Budget of the Period 2010–2019

We describe the flux-based C budget of Europe following an adaptation of the scheme proposed by Ciais et al. (2022), which is depicted in Figure 2. The C budget includes CO<sub>2</sub> and CH<sub>4</sub> fluxes from the land GHG budgets in C units (Figure 1), but in addition also changes in C stocks in the biosphere and of

biological products, and lateral exchange fluxes between different C stocks and across the boundaries of our study region. Table 4 lists the estimates of the different fluxes and stock changes derived from different data sets. Flux names highlighted by an “\*” indicate estimates which we finally used in our budget. Other fluxes are listed for comparison. Figure 7 displays the European carbon budget based on the best estimates of the different fluxes. An estimate of the budget based on independent estimates of stock changes is given for comparison.

In our land C budget, we distinguish four compartments that are in exchange with the atmosphere and with each other: the geological compartment, inland waters, terrestrial ecosystems, coastal ecosystems and the biological product pools (Figure 2, Table 4). Terrestrial ecosystems are in the center of the land C budget, with GPP and Re<sub>terr</sub> being the most important exchange fluxes with the atmosphere. We have calculated the best estimates of GPP and Re<sub>terr</sub> for our budget as the median values from five and three estimates, respectively, avoiding estimates from land surface models. With the exception of the GLASS estimates of GPP, the individual estimates for each of these two fluxes are very close, and we have a high level of confidence in both GPP and Re<sub>terr</sub>. In absolute terms, these best estimates are in the lower value range of the corresponding flux estimates simulated by the land surface models of the TRENDY v10 ensemble (Table 4). A general overestimation of both fluxes by DGVMs can be explained by the poor representation of perturbation, anthropogenic appropriation of biomass, and lateral export fluxes (Ciais et al., 2021)—the reason for which we avoid using these data.

The difference between GPP and Re<sub>terr</sub> would result in a net uptake of 0.9 Pg C yr<sup>-1</sup> by terrestrial ecosystems from the atmosphere. Other exchange fluxes between terrestrial ecosystems and the atmosphere, that is,  $F_{\text{fire}}$ ,  $F_{\text{peat CH}_4}$  and  $F_{\text{methanotrophy}}$ , are of minor importance. The accumulation of C in the biosphere is however diminished to  $\sim 0.4$  Pg C yr<sup>-1</sup> by emissions from grazing livestock ( $F_{\text{grazing}}$ ), from harvested wood ( $F_{\text{wood harvest}}$ ), crop ( $F_{\text{crop harvest}}$ ) and peat ( $F_{\text{peat harvest}}$ ) products. Another  $\sim 0.1$  Pg C yr<sup>-1</sup> are exported from soils to the inland water network ( $F_{\text{bio2river}}$ ).

Note that we assume that our estimates of GPP and Re<sub>terr</sub> implicitly include the land use change flux  $F_{\text{LUC}}$ , which we thus did not add explicitly to our C budget. Nevertheless, we list various estimates of  $F_{\text{LUC}}$  for comparison and discussion. We find strong differences between the two bookkeeping models HN and BLUE, but also between the two estimates based on BLUE using different land cover data as input (Table 4). Between the lowest and highest estimates, there is a factor of 3.5 difference. Therefore, for our best estimate of  $F_{\text{LUC}}$ , which is the median of the three estimates, we assigned only a low level of confidence.

For  $F_{\text{grazing}}$ , we only have the estimates obtained by Chang et al. (2021) using the land surface model ORCHIDEE. However, as the grazing flux in the simulations is scaled to inventory data on livestock density, we assigned a moderate level of confidence to this flux estimate. While we have a high level of confidence in the estimates of  $F_{\text{crop harvest}}$ ,  $F_{\text{wood harvest}}$ ,  $F_{\text{peat harvest}}$ , which are all based on inventory data, we have a low level of confidence in  $F_{\text{bio2river}}$ , because it is only based on a mass budget of fluxes from or to the inland water compartment (Equation 13). For  $F_{\text{crop harvest}}$  and  $F_{\text{wood harvest}}$ , our estimates agree well with those from Byrne et al. (2023), which can be easily explained by the fact that both are based on the same FAOSTAT data.

**Table 4**  
Flux Estimates ( $Tg\ C\ yr^{-1}$ ) for the European Land C Budget 2010–2019 (\* Behind Flux Name Indicates Estimates Used in Budget)

Flux	Estimated flux in $Tg\ C\ yr^{-1}$			Source
	Best estimate	Range	Conf.	
<b>Geological</b>				
$F_{geo}^*$	1.9		--	Etiopé et al. (2019)
$F_{weathering}^*$	-11.3		*	Zscheichler et al. (2017)
$F_{litho2river}^*$	18.6		*	Zscheichler et al. (2017)
$\Delta C_{litho}^*$	7.3		*	Zscheichler et al. (2017)
<b>Inland waters</b>				
$F_{river\ export, OC}$	12.5		**	Zscheichler et al. (2017)
$F_{river\ export}^*$	31.1		**	Zscheichler et al. (2017)
$F_{IW}^*$	55.2		*	Lauerwald et al. (2023)
$\Delta C_{burial}^*$	-4.4		-	Mendonça et al. (2017)
$F_{bio2river}^*$	90.6		-	Equation 13
<b>Terrestrial Ecosystems</b>				
GPP	-5,596			BESS
GPP	-6,478			GLASS
GPP	-5,144			Madani and Parazoo (2020)
GPP	-5,478			FLUXCOM RS v006
GPP	-5,437			FLUXCOM ERA
GPP*	-5,478		**	Median of above
GPP	-6,634	-8945; -4697		TRENDY v10
$Ra^*$	2,900		**	GLASS
$Ra$	3,126	1711; 5072		TRENDY v10
NPP	3,579			GLASS
NPP	3,318			MODIS
NPP	3,470	2462; 4814		TRENDY v10
$Rh^*$	1,947		-	Yao et al. (2021)
$Rh$	2,897	2078; 4292		TRENDY v10
$Re_{terr}$	4,566			FLUXCOM RS v006
$Re_{terr}$	4,565			FLUXCOM ERA
$Re_{terr}$	4,846			GLASS $Ra$ + Yao et al. $Rh$
$Re_{terr}^*$	4,566		**	Median of above
$Re_{terr}$	5,940	3789; 8423		TRENDY v10
$F_{LUC}$	-156.4			HN
$F_{LUC}$	-44.2			BLUE HILDA+
$F_{LUC}$	-65.4			BLUE LUH2
$F_{LUC}^*$	-65.4		--	Best estimate
$F_{fire}$	8.2			GFAS
$F_{fire}$	11.0			GFED
$F_{fire}^*$	9.6		*	Median of above
$F_{peat\ CH_4}^*$	1.5	0.4; 2.5	--	GMB2020, BU models
$F_{methanotrophy}^*$	0.7		*	MeMo

**Table 4**  
*Continued*

Flux	Estimated flux in Tg C yr <sup>-1</sup>			Source
	Best estimate	Range	Conf.	
$F_{\text{grazing}}^*$	132		*	Chang et al. (2021)
<b>Terrestrial Ecosystems</b>				
$\Delta C_{\text{FL}}$	-130			EFISCEN
$\Delta C_{\text{FL}}$	-133			FAO Tier 1
$\Delta C_{\text{FL}}^*$	-131		*	Median of above
$\Delta C_{\text{CL}}^*$	22		-	UNFCCC
$\Delta C_{\text{CL,organic soils}}$	14.7			UNFCCC
$\Delta C_{\text{CL,mineral soils}}$	7.9			UNFCCC
$\Delta C_{\text{CL,organic soils}}$	26.3			FAO Tier 1
$\Delta C_{\text{GL}}^*$	10		-	UNFCCC
$\Delta C_{\text{GL,organic soils}}$	14			UNFCCC
$\Delta C_{\text{GL,mineral soils}}$	-2			UNFCCC
$\Delta C_{\text{GL,organic soils}}$	1.4			FAO Tier 1
<b>Coastal Ecosystems</b>				
$F_{\text{Cwa}}^*$	6.9		*	Rosentreter et al. (2023)
$F_{\text{CWL}}^*$	-4.2		-	Rosentreter et al. (2023)
<b>Biological products</b>				
$F_{\text{crop harvest}}^*$	-224		**	FAO
$F_{\text{crop harvest}}$	-256			Byrne et al. (2023)
$F_{\text{wood harvest}}^*$	-142		**	FAO
$F_{\text{wood harvest}}$	-140			Byrne et al. (2023)
$F_{\text{peat harvest}}^*$	-10		**	Hirschler and Osterburg (2022)
$F_{\text{crop use}}^*$	207		*	based on FAO, Equation 11
$F_{\text{crop use}}$	314			Byrne et al. (2023)
$F_{\text{wood decay}}^*$	94		*	FAO
$F_{\text{wood burning}}^*$	34		*	FAO
$F_{\text{wood decay}}$	16			Byrne et al. (2023)
$F_{\text{wood burning}}$	63			Byrne et al. (2023)
$F_{\text{peat use}}^*$	9.7		**	Hirschler and Osterburg (2022)
$F_{\text{product oxidation}}^*$	346		*	Sum of our best estimates*
$F_{\text{crop trade}}^*$	17		**	FAO
$F_{\text{wood trade}}^*$	6		**	FAO
$F_{\text{peat trade}}^*$	-0.5		*	Hirschler and Osterburg (2022)
$\Delta C_{\text{crop products}}^*$	0.0		-	Assumption
$\Delta C_{\text{wood products}}^*$	-8.1		*	Equation 10
$\Delta C_{\text{peat products}}^*$	-0.8		*	Hirschler and Osterburg (2022)
<b>Budget summaries</b>				
NEEc*	-362		-	Equation 8
$\Delta C_{\text{land}}^*$	-309		-	Equation 9
$\Delta C_{\text{land}}$	-72		-	Equation 14
$\Delta C_{\text{FL}} + \Delta C_{\text{FL}} + \Delta C_{\text{GL}}$	-99		-	Our best estimates*

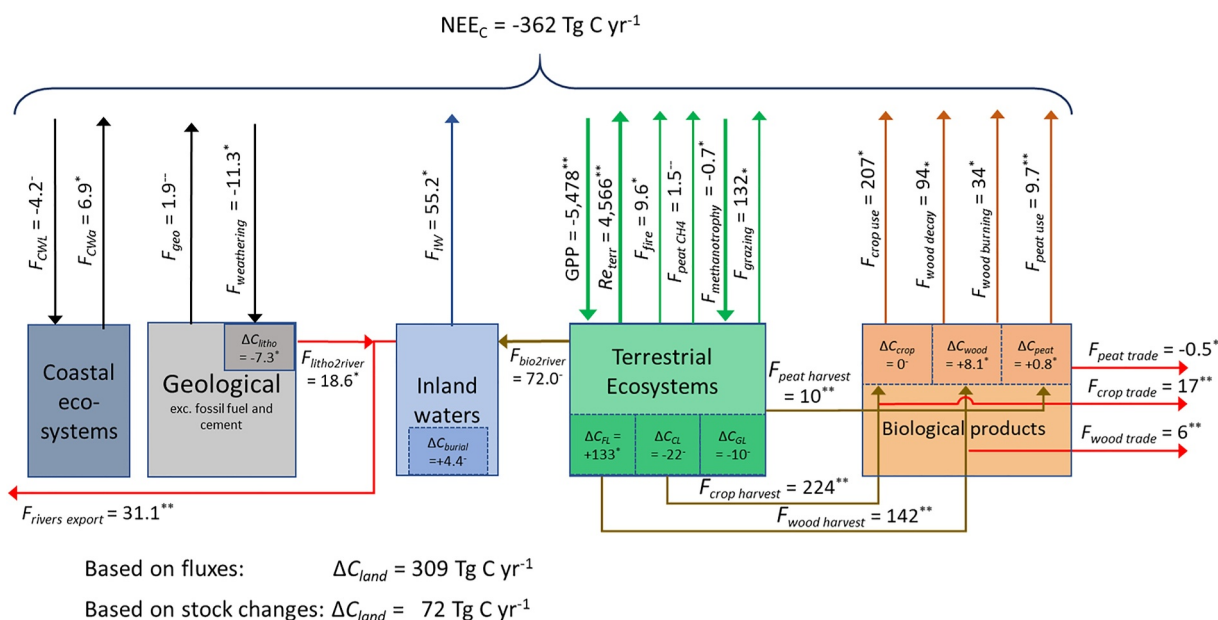
**Table 4**  
Continued

Flux	Estimated flux in Tg C yr <sup>-1</sup>			Source
	Best estimate	Range	Conf.	
$\Delta C_{FL} + \Delta C_{GL} + \Delta C_{GL}$	-103	-314; 8		TRENDY
$F_{LULUCF}$	-112			UNFCCC

Note. We assign different levels of confidence to our estimates: very high:  $\pm 10\%$  (\*\*\*), high:  $\pm 25\%$  (\*\*), moderate:  $\pm 50\%$  (\*), low:  $\pm 100\%$  (-), and very low (-).

The three harvest fluxes— $F_{crop\ harvest}$ ,  $F_{wood\ harvest}$ , and  $F_{peat\ harvest}$ —feed into the corresponding product pools, which themselves are a sizable source of C to the atmosphere of  $\sim 0.3$  Pg C yr<sup>-1</sup> through use, burning and decomposition of these products ( $F_{product\ oxidation}$ , as the sum of  $F_{crop\ use}$ ,  $F_{wood\ decay}$ ,  $F_{wood\ burning}$  and  $F_{peat\ use}$ ). Emissions from wood and crop products are dominant, with only minor contributions related to peat products. Europe is a net exporter of crop and wood products but a net importer of peat. However, these net trade fluxes are rather small, representing  $\leq 10\%$  of the corresponding harvest fluxes, and amount to a net-export of only 22 Tg C yr<sup>-1</sup>. In contrast, in RECCAP1, Luysaert et al. (2012) identified Europe as a net-importer of 19 Tg C yr<sup>-1</sup>. That discrepancy may partly be explained by the fact that for RECCAP2, we additionally include Moldova, Ukraine and Belarus, which, according to our calculations based on the FAOSTAT data, are a net-exporter of 16 Tg C yr<sup>-1</sup> linked to the trade of crop products. While changes in the crop product stock ( $\Delta C_{crop}$ ) are set to 0 Tg C yr<sup>-1</sup> per definition, we estimate an average increase in the European wood product C stock ( $\Delta C_{wood}$ ) of  $\sim 8$  Tg C yr<sup>-1</sup>. Note that for RECCAP1, Luysaert et al. (2012) estimated an increase in wood product C stocks of even 19 Tg C yr<sup>-1</sup> based on a different inventory data set (Eggers, 2002), and for the year 2000 only. For the peat product pool ( $\Delta C_{peat}$ ), we estimate an increase of 0.9 Tg C yr<sup>-1</sup> based on the inventory data from Hirschler and Osterburg (2022).

The net exchange of C between the geological compartment and the atmosphere is of minor importance in the land C budget. In addition, the dissolution of carbonate minerals ( $\Delta C_{litho}$ ) is of minor importance compared to other C stock changes in the land C budget. The exports of C from the geological compartment to the inland water compartment of 19 Tg C yr<sup>-1</sup> add to  $F_{bio2river}$  of 72 Tg C yr<sup>-1</sup>. Of the total C input to inland waters ( $F_{litho2river} + F_{bio2river}$ ) of 91 Tg C yr<sup>-1</sup>, only about one third is actually exported to the sea. The C burial in



**Figure 7.** European carbon budget over the period 2010–2019. The numbers represent the best estimates of average annual fluxes in Tg C yr<sup>-1</sup>. We assign different levels of confidence to our estimates: very high:  $\pm 10\%$  (\*\*\*), high:  $\pm 25\%$  (\*\*), moderate:  $\pm 50\%$  (\*), low:  $\pm 100\%$  (-), and very low (-).



sediments ( $\Delta C_{\text{burial}}$ ) is a minor contribution to the land C stock change ( $\Delta C_{\text{land}}$ ). The emissions of inland waters to the atmosphere of  $55 \text{ Tg C yr}^{-1}$  may appear small compared to the exchange fluxes between terrestrial ecosystems and the atmosphere, but are still important for the  $NEE_C$ , that is, the balance of all vertical exchange fluxes in the land C budget. Coastal ecosystems in Europe add a small net source of C to the atmosphere, as emissions from estuaries ( $F_{\text{Cwa}}$ ) of  $6.9 \text{ Tg C yr}^{-1}$  are only partly counterbalanced by a net-uptake in coastal wetlands ( $F_{\text{CWL}}$ ) of  $4.2 \text{ Tg C yr}^{-1}$ .

Based on budget closure, we estimate  $NEE_C$  at  $-0.4 \text{ Pg C yr}^{-1}$  during 2010–2019, and we assign a low level of confidence to this estimate. The low level of confidence reflects the fact that  $NEE_C$  accumulates the uncertainties of the different component fluxes, while these fluxes balance each other out to a large degree, resulting in an uncertainty that is large relative to the calculated flux balance. Nevertheless,  $NEE_C$  is dominated by the land  $\text{CO}_2$  budget, for which we found good agreement between our BU estimate and different TD estimates (Section 3.1), which is thus in support of our assessment of  $NEE_C$ . When we finally assess the net C stock change in the land C budget by including lateral net exports through trade and river transport (Equation 9), we obtain a flux-derived increase in  $\Delta C_{\text{land}}$  of  $0.3 \text{ Pg C yr}^{-1}$ . As an alternative result from the calculation of  $\Delta C_{\text{land}}$  as the sum of all C stock changes in the land C budget (Equation 14), we obtain a much lower increase in  $\Delta C_{\text{land}}$  of only  $0.1 \text{ Pg C yr}^{-1}$ .

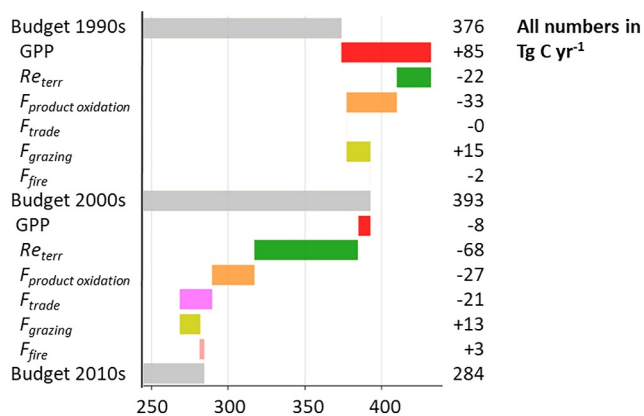
For this alternative result, we used independent estimates of terrestrial ecosystem C stock changes that give a net C sink for forests ( $\Delta C_{\text{FL}}$ ) of about  $130 \text{ Tg C yr}^{-1}$ , and net sources from grass- ( $\Delta C_{\text{GL}}$ ) and croplands ( $\Delta C_{\text{CL}}$ ) of  $22$  and  $10 \text{ Tg C yr}^{-1}$ , respectively. While we have a moderate level of confidence in  $\Delta C_{\text{FL}}$ , in particular as the two independent estimates by EFISCEN and FAO agree well (see Table 4), our confidence in  $\Delta C_{\text{GL}}$  and  $\Delta C_{\text{CL}}$  is low. For both  $\Delta C_{\text{GL}}$  and  $\Delta C_{\text{CL}}$ , we used the estimates from the national inventories (UNFCCC). Based on the LUCAS database of repeated measurements of topsoil organic C stocks, De Rosa et al. (2024) have recently estimated a net-loss of topsoil organic C of only  $7 \text{ Tg C yr}^{-1}$  on agricultural land (i.e.,  $\Delta C_{\text{GL}} + \Delta C_{\text{CL}}$ ) for the EU27+UK over the period 2009–2018. Although EU27+UK represents only a bit more than 80% of our RECCAP2 region, this latest study advocates for a more conservative estimate of soil C losses. Note finally that the national inventories split  $\Delta C_{\text{GL}}$  and  $\Delta C_{\text{CL}}$  further into estimates for mineral soils and organic soils (Table 4). Although organic soils represent only a very minor fraction of croplands and grasslands in Europe ( $\sim 3\%$  each), they make up a larger part of these emissions. From the FAO, we have Tier 1 estimates for emissions from organic soils, which is twice as high for croplands but only one tenth of what is estimated for grasslands based on the national inventories (Table 4). The estimates of total C losses from organic soils are very similar between UNFCCC and FAO,  $29$  and  $28 \text{ Tg C yr}^{-1}$ , respectively. However, while the NGHIGs from UNFCCC give a similar magnitude in losses from croplands versus grasslands, croplands are the dominant emitter in the FAO accounting for  $26 \text{ Tg C yr}^{-1}$ . This number is in turn still slightly lower than the C loss from organic cropland soils of  $33 \text{ Tg C yr}^{-1}$  estimated by Carlson et al. (2017) for Europe. These large discrepancies in different estimates show how poorly constrained these storage changes are, and are thus the main justification for the low level of confidence we have in this second estimate of  $\Delta C_{\text{land}}$ .

Note that for RECCAP1, Luyssaert et al. (2012) also calculated a lower land C sink based on inventory-based estimates of stock changes than based on flux estimates, with  $0.1 \pm 0.1$  and  $0.2 \pm 0.2 \text{ Pg C yr}^{-1}$ , respectively. These values are rather comparable to our corresponding estimates of  $0.1$  and  $0.3 \text{ Pg C yr}^{-1}$ , respectively. The potential bias due to different definitions of the spatial domain between RECCAP1 and RECCAP2 is significant. Given the huge uncertainties in estimated  $\Delta C_{\text{land}}$ , however, this comparison is rather encouraging.

The TRENDYv10 estimates of  $\Delta C_{\text{land}}$  give an ensemble median of  $0.1 \text{ Pg C yr}^{-1}$ , which is quite close to our inventory based assessment. However, individual simulations of  $\Delta C_{\text{land}}$  in TRENDYv10 range from  $\sim 0$  to  $0.3 \text{ Pg C yr}^{-1}$ , which reveals the high uncertainty of DGVM simulations.

#### 4.2. Evolution of the Carbon Budget Over the Last Three Decades

Figure 8 shows the evolution of the European C budget ( $\Delta C_{\text{land}}$ ) over the last three decades as well as the changes in different fluxes that are responsible for this evolution. Note that a series of C fluxes, although important for the land C budget as such, are not included in this figure as we assume them not to have changed over the last three decades. This concerns  $F_{\text{IW}}$ ,  $F_{\text{river export}}$ ,  $F_{\text{geo}}$ ,  $F_{\text{weathering}}$ ,  $F_{\text{Cwa}}$ , and  $F_{\text{CWL}}$ . A detailed list of all fluxes averaged for the three decades can be found in Table S8 in Supporting Information S2.



**Figure 8.** Evolution of the European carbon budget over the last three decades based on flux estimates (Equation 9). Note that there is no estimate for  $F_{\text{fire}}$  in the 1990s.

$\Delta C_{\text{land}}$  increases slightly from the 1990s to the 2000s, before it decreases substantially to the 2010s. From the 1990s to the 2000s, an increase in GPP is more or less counterbalanced by increases in  $Re_{\text{terr}}$  and  $F_{\text{product oxidation}}$ , while a decrease in  $F_{\text{grazing}}$  still permits for a slight increase in  $\Delta C_{\text{land}}$ . Changes in  $F_{\text{trade}}$  are negligible between these two decades. From the 2000s to the 2010s,  $Re_{\text{terr}}$  increased substantially while GPP even slightly decreased, which appears to be the main reason for the comparatively large drop in  $\Delta C_{\text{land}}$ . In contrast, changes in  $F_{\text{product oxidation}}$  and  $F_{\text{grazing}}$  seem to continue in about the same magnitude as between the 1990s and 2000s, and changes in  $F_{\text{trade}}$  and  $F_{\text{fire}}$  have only a minor effect on  $\Delta C_{\text{land}}$ .

Interestingly,  $F_{\text{LULUCF}}$  from UNFCCC inventories shows a similar trend, but the implied increase in biosphere C stocks is less pronounced and generally at a lower magnitude. According to these inventories,  $F_{\text{LULUCF}}$  increased from  $-119 \text{ Tg C yr}^{-1}$  in the 1990s to  $-125 \text{ Tg C yr}^{-1}$  in the 2000s, before it fell to its lowest value of  $-112 \text{ Tg C yr}^{-1}$  (Table S7 in Supporting Information S2, negative values indicate a sink). Note that trends in these inventories are largely driven by land use data. We can thus assume changes in land use to be

an important driver behind the low  $F_{\text{LULUCF}}$  in the 2010s. The three BK model estimates of  $F_{\text{LULUCF}}$  considered in this study consistently represent this flux as a net C sink during the 1990s, 2000s, and 2010s of  $81 (43\text{--}150) \text{ Tg C yr}^{-1}$ ,  $82 (72\text{--}160) \text{ Tg C yr}^{-1}$ , and  $65 (44\text{--}156) \text{ Tg C yr}^{-1}$ , respectively (median and range of the three estimates, Table S8 in Supporting Information S2). Most importantly, all three estimates of  $F_{\text{LULUCF}}$  indicate the lowest sink for the 2010s, which is consistent with our BU assessment.

From the ensemble medians (range) of TRENDYv10, we find an increase in  $\Delta C_{\text{land}}$  from  $78 (-183 \text{ to } +228) \text{ Tg C yr}^{-1}$  in the 1990s to  $106 (-240 \text{ to } +294) \text{ Tg C yr}^{-1}$  in the 2000s, but no further increase in the 2010s where  $\Delta C_{\text{land}}$  is simulated at  $103 (8\text{--}314) \text{ Tg C yr}^{-1}$ . However, the range in the model results, from net-sources to net-sinks of C, reflects the high level of uncertainties associated with this trend, which can thus be used neither to support nor to refute the trend in our BU assessment.

## 5. Spatio-Temporal Patterns in GHG Budgets From Regional Inversions

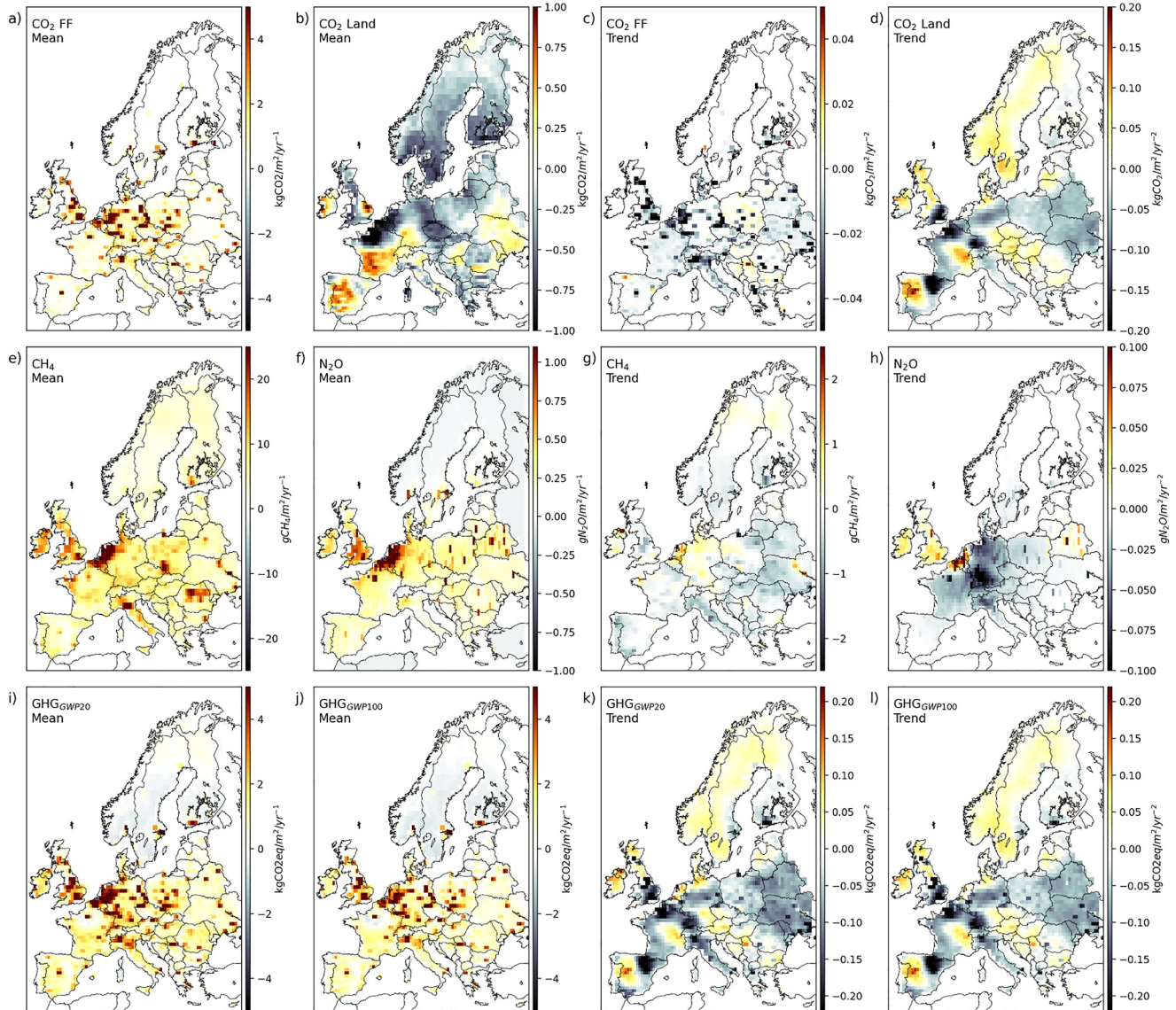
In this section, we analyze spatiotemporal patterns of fossil  $\text{CO}_2$  emissions and land  $\text{CO}_2$ ,  $\text{CH}_4$ ,  $\text{N}_2\text{O}$  fluxes over the period 2010–2019, including local hotspots and areas with large temporal trends, based on the mean of regional inversions re-gridded to  $1^\circ$ .

### 5.1. Fossil $\text{CO}_2$ Emissions

The spatial distribution and trend of fossil  $\text{CO}_2$  emissions prescribed to regional inversions (i.e., not optimized) are shown in Figures 9a and 9c. These priors were derived from EDGAR v4.3, BP statistics, and satellite measurements of atmospheric concentration of  $\text{NO}_2$  as an important co-emittant of  $\text{CO}_2$  in fossil fuel combustion, while the spatial disaggregation is entirely based on EDGAR v4.3 and is representative for the year 2010 (see McGrath et al., 2023 for details). Emissions are concentrated over densely populated areas in the UK, Benelux, and Italy's Po Valley with emission rates higher than  $6 \text{ kgCO}_2 \text{ m}^{-2} \text{ yr}^{-1}$  over  $1^\circ$  grid cells, and in megacities and point sources such as power plants and industrial sites. In total, 80% of emissions are located over 23% of the land area when spatial resolution is smoothed to  $1^\circ$ , as shown in Figures 9a and 9c.

Following the numbers assembled by the Global Carbon Atlas (<https://globalcarbonatlas.org/>, accessed on 2024-01-02) based on Friedlingstein et al. (2022), fossil  $\text{CO}_2$  emissions have been going down in Europe since 1990, with an average rate of decrease of  $-1.5\% \text{ yr}^{-1}$ . Emission reduction rates differ between countries with the largest reduction rates being in the UK ( $-2.8\% \text{ yr}^{-1}$ ), Italy ( $-2.2\% \text{ yr}^{-1}$ ), intermediate values in France ( $-1.6\% \text{ yr}^{-1}$ ) and Germany ( $-1.5\% \text{ yr}^{-1}$ ), Spain ( $-1.1\% \text{ yr}^{-1}$ ) and in former eastern bloc countries excluding Poland ( $-1.2\% \text{ yr}^{-1}$ ). In Poland, emissions decreased only by  $-0.2\% \text{ yr}^{-1}$ . Note however that the map of emission trends in Figure 9c has grid cells with increasing emissions, highlighting that some sectors have continued to increase emissions.

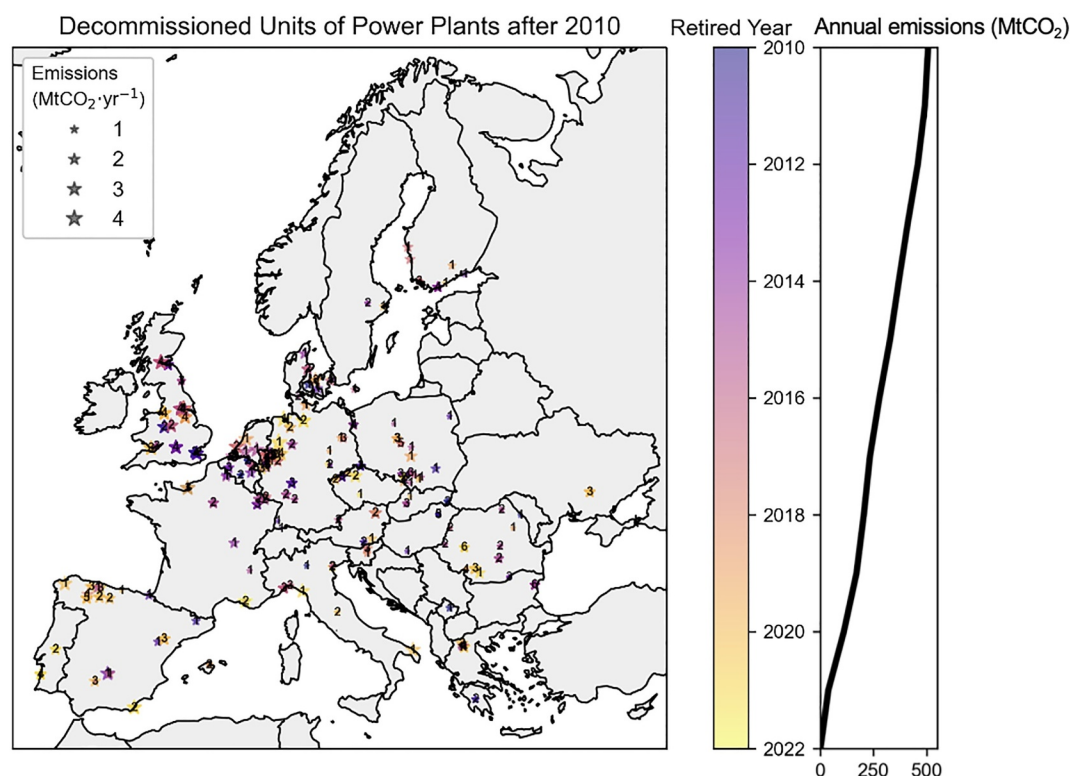
Since 1990, fossil  $\text{CO}_2$  emissions have been going down, with an average rate of decrease of  $-1.1\% \text{ yr}^{-1}$  in the EU28 (UK27+UK) and  $-1.5\% \text{ yr}^{-1}$  in Europe (excluding Russia). Coal emissions showed the fastest decrease by



**Figure 9.** Spatial patterns in GHG budgets from regional inversions for the period 2010–2019: prescribed fossil CO<sub>2</sub> emissions (a, c), land CO<sub>2</sub> fluxes (b, d), CH<sub>4</sub> emissions (e, g), N<sub>2</sub>O emissions (f, h), and net GHG balance combining the three GHGs at a 20 years (i, k) and 100 years (j, l) horizon. Left two columns are the means, right two columns are the trends.

$-3.2\% \text{ yr}^{-1}$  in the EU28 and  $-2.6\% \text{ yr}^{-1}$  in Europe. Emissions from oil burning experienced a smaller decrease ( $-0.8\% \text{ yr}^{-1}$  in EU28) while those from natural gas decreased to a minimum in 2015 and then increased again, resulting in an average trend of  $-0.9\% \text{ yr}^{-1}$  during 2010–2019. Emission reduction rates differ between countries; the largest reduction rates are found in the UK ( $-2.8\% \text{ yr}^{-1}$ ), Italy ( $-2.2\% \text{ yr}^{-1}$ ), intermediate values in France ( $-1.6\% \text{ yr}^{-1}$ ) and Germany ( $-1.5\% \text{ yr}^{-1}$ ), Spain ( $-1.1\% \text{ yr}^{-1}$ ) and in former Eastern bloc countries excluding Poland ( $-1.2\% \text{ yr}^{-1}$ ). In Poland, emissions decreased only by  $-0.2\% \text{ yr}^{-1}$ . In total, 90% of the EU28 emission's reduction originated from the five largest economies (Germany, France, UK, Italy, Spain, Poland), which altogether represent 80% of the mean EU28 emission. Note however that the map of emission trends in Figure 9c has grid cells with increasing emissions as some sectors have continued to increase emissions.

Note that the spatial activity data for the year  $\sim 2015$  used for the GRIDFed emission map underlying the trend patterns in Figure 9c are not updated each year, so that the annual national fossil CO<sub>2</sub> emissions reduction are spatially distributed in proportion to emissions per each grid cell. Therefore, the grid cells containing coal plants that closed during the period do not show up with a huge local reduction of emission in Figure 9c. Typically, a



**Figure 10.** Location of the coal power plants that closed in Europe between 2010 and 2022. The magnitude of the emission prior closure is indicated by the size of each star symbol and the year of closure by the color palette. The right hand plot shows the reduction of corresponding CO<sub>2</sub> emissions since 2010 with a total reduction of 500 MtCO<sub>2</sub> by 2022.

large plant (~1,000 MW) emits 5 Mt CO<sub>2</sub> yr<sup>-1</sup>, equivalent to the emissions from a 300,000 people city in Europe (Moran et al., 2022). In 2016, only the UK, Belgium and Sweden announced a phase out of coal in power generation for 2030, whereas in 2022, more than 12 countries committed to it and 10 others phased out coal. It is therefore important for the fossil emission map prescribed to inversions to be up to date for the location of disappearing (or appearing) point sources, as shown in Figure 10. Because emissions of power plants which do not exist anymore were wrongly prescribed to atmospheric transport models, all regional inversions likely compensated by adding an increasing land CO<sub>2</sub> sink around decommissioned plants, which biases the patterns of their land CO<sub>2</sub> sink and its trends, making a comparison to bottom-up estimates challenging. This artificial trend of wrongly assigned increasing land sink can be seen clearly in Figure 9, where the three regions of strongest increase in land sink are located just downwind of power plants which closed (North-Eastern Spain for plants that closed upwind in Asturias, Western Germany for plants that closed in East of France, and in Belgium and South Western UK for plants that closed in Southern UK, Belgium and Germany close to the Belgian border, as shown in Figure 10).

## 5.2. Land CO<sub>2</sub> Budget

Figure 9b shows the mean annual net CO<sub>2</sub> land flux excluding fossil CO<sub>2</sub> emissions, as estimated by the mean of regional inversions. The range of the corresponding sinks and sources (negative and positive values) at 1° spatial resolution is three times smaller than that of fossil CO<sub>2</sub> emissions. According to the mean of regional inversions, most European countries are net CO<sub>2</sub> sinks except Spain, southern UK, southern France and Ukraine. The trend of the land CO<sub>2</sub> sink shows patterns different from the mean value. We verified that the trend of inversions is not given by the trend of their prior land flux. The trend of the prior shows a decreasing CO<sub>2</sub> sink (Figure S5 in Supporting Information S1) where the trend of inversions shows regions with strong increases (North of France, North of Spain). However, there are also large areas where both priors and inversions show strong decreases of the land CO<sub>2</sub> sink (in UK, from Southern Germany to Czech Republic, and in Scandinavia). Interestingly, regions that are weak sinks in the mean flux of inversions (Northern Spain in Figure 9) show the largest sink increase over

time. There is no evidence for “favorable” trends in climate driving increased plant growth or for shifts in land use (such as decreased harvest) in these two regions. The trend of weakening CO<sub>2</sub> sinks in Scandinavia is possibly linked to changes in forest management and the cutting of old forests (Ahlström et al., 2022). On the other hand, Poland and Eastern European countries show a strong CO<sub>2</sub> sink that intensifies over time, which may be explained by a substantial increase in forest biomass (Winkler et al., 2023).

### 5.3. CH<sub>4</sub> Emissions

The CH<sub>4</sub> emissions from the mean of regional inversions shown in Figure 9 include anthropogenic and natural emissions. Fossil fuel extraction in Europe is limited mainly to gas extraction in the Netherlands, the North Sea (offshore), and Romania as well as coal mining in Poland. CH<sub>4</sub> emissions are more diffuse but present high values in agricultural and populated areas (landfills) and in coal mining basins (e.g., the Silesia region of Poland). There are few hotspot regions of CH<sub>4</sub> emissions with emission rates exceeding 0.01 kg CH<sub>4</sub> m<sup>-2</sup> yr<sup>-1</sup>, namely in the UK, Benelux and Western Germany, Southern Poland and Italy's Po Valley. These high emission rates are mainly associated with CH<sub>4</sub> emissions from agricultural activities (e.g., cattle farming (enteric fermentation) and rice cultivation). According to UNFCCC (2022) official inventories submissions, these regions/countries are in the top 10 of the CH<sub>4</sub> agricultural emitters, responsible for 70% of the total CH<sub>4</sub> emissions in the EU27+UK. Following the same sources, the emission rates in Belarus and Ukraine are lower on average than in EU27+UK. Note that the regional inversions are constrained by atmospheric observations over Western Europe but not over Eastern Europe where their solution is close to the prior inventory (Petrescu et al., 2023). This may further explain why with regard to average emissions, global inversions tend to be better in agreement with bottom-up estimates than the regional inversions (see Table 4).

Deng et al. (2022) used global CH<sub>4</sub> inversions from Sauniois et al. (2020) updated until 2017, which have a coarser spatial resolution than the three regional inversions used in this study. They found a consistent decreasing trend in inventories and inversions for the EU27 over the period 2000–2017, including both GOSAT-based and surface station-based inversions. Here, from regional inversions limited to a shorter period in 2010–2019, the spatial distribution of the CH<sub>4</sub> emissions trend suggests large decreases in Belarus and Ukraine, no strong increase in Poland (unlike in the prior, see Figure S5 in Supporting Information S1) and an increase in Benelux countries, Germany, Ireland, Western France and Scandinavia. The trend of CH<sub>4</sub> emissions from regional inversions is therefore different from the trend of the prior (EDGARv4.2), which shows a small decrease across all European countries and large increases in Ireland and Poland (Figure S5e in Supporting Information S1).

### 5.4. N<sub>2</sub>O Emissions

Anthropogenic and natural N<sub>2</sub>O emissions from inversions include industrial emissions (point sources) from the production of chemicals and other emissions (diffuse) mainly from agriculture. The map of N<sub>2</sub>O emissions optimized by regional inversions shown in Figure 9f shows diffuse emissions with a rate of less than 0.002 kg N<sub>2</sub>O m<sup>-2</sup> yr<sup>-1</sup>, representing direct and indirect emissions from fertilized croplands and pastures. There are also hotspots of emissions corresponding to industrial emitters and high emission rates from intensive agriculture over the Benelux (0.005 kg N<sub>2</sub>O m<sup>-2</sup> yr<sup>-1</sup>, see de Vries et al., 2021). The trend of N<sub>2</sub>O emissions optimized by inversions (Figure 9h) is slightly negative for all diffuse emissions in Germany and France, consistent with reduced nitrogen fertilizers applications (following the Nitrate Directive of the EEC, 1991), whereas prior emissions used by inversions had no trend (Figure S5d in Supporting Information S1). On the other hand, point sources show positive or negative trends. Much of the IPPU emissions from nitric acid plants were cut in a similar manner around 2010 with the introduction of the European Emission Trading System that made it economically interesting for companies to apply emission abatement technologies (catalytic reduction of N<sub>2</sub>O in the flue gas) to reduce their emissions (Petrescu et al., 2023). Belgium and the Netherlands indicate a strong increase in N<sub>2</sub>O emissions (Figure 9h).

## 6. Interannual Variability of European GHG Budgets

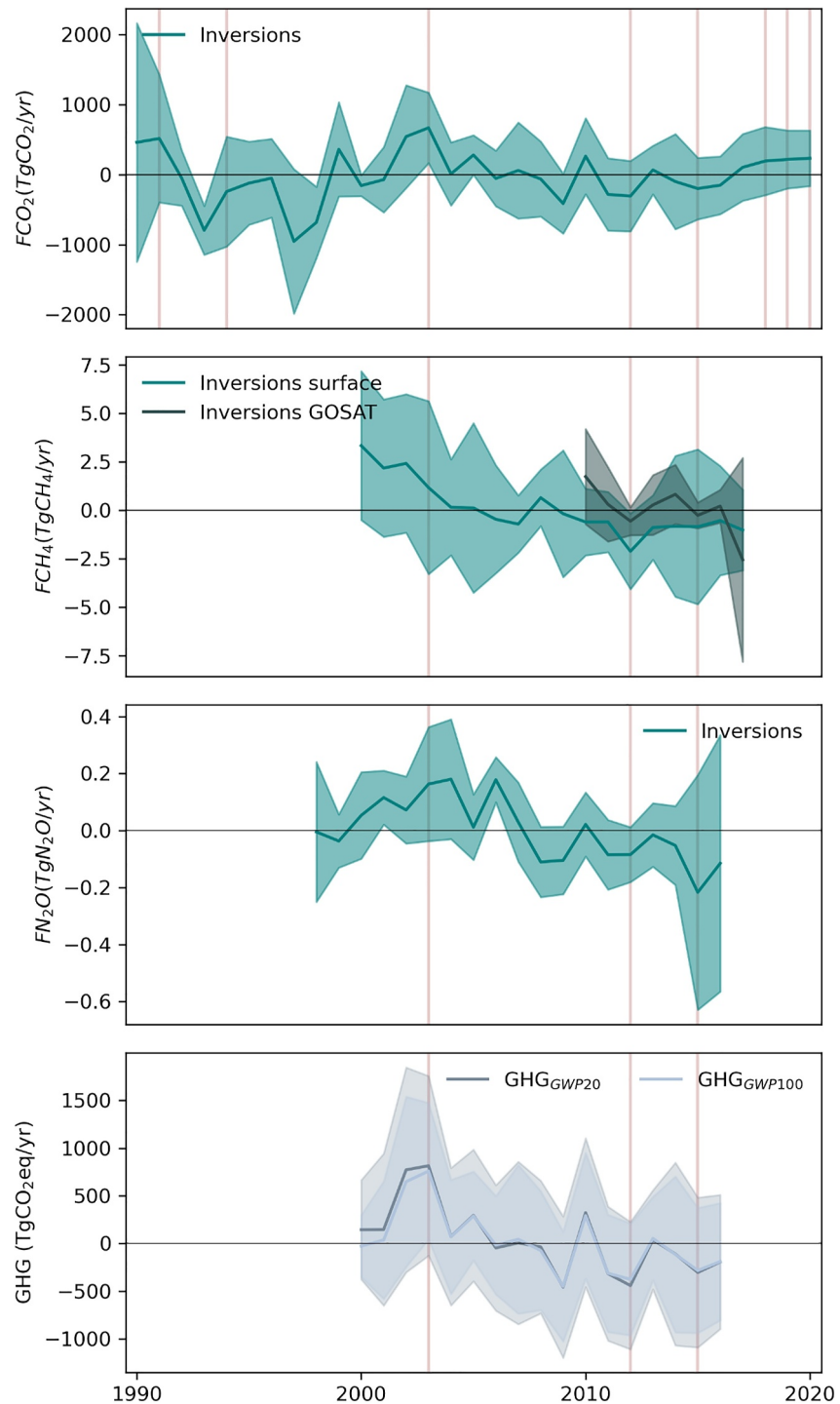
Quantifying interannual variability (IAV) and identifying its drivers is important to gain an understanding of the processes controlling variations in sources and sinks of GHGs, but also to appropriately separate long-term trends (human-driven) from short-lived variations due to natural climate variability. Variability in the European CO<sub>2</sub> sink has been previously analyzed, including the main drivers of long-term IAV in sources and sinks of CO<sub>2</sub>

(Bastos et al., 2016; Ciais, Wattenbach, et al., 2010; Ciais, Soussana, et al., 2010; Luysaert et al., 2010), seasonal compensation effects (Buermann et al., 2018) and the impacts of extreme events on annual carbon budgets (Bastos et al., 2014, 2020; Ciais et al., 2005). For CH<sub>4</sub> and N<sub>2</sub>O, little is known about the magnitude and spatio-temporal distribution of IAV in the European region. It is also unclear how IAV in each of the three GHGs relates to variability in the overall global warming potential (GWP). Depending on the main drivers of variability in each GHG, anomalies may reinforce each other in a particular year (if climatic conditions lead to anomalies of the same sign in all three GHGs) or counterbalance each other partly (if the same climatic conditions lead to anomalies of opposite signs among the GHGs). In this section, we compare the magnitude and spatial distribution of IAV in net CO<sub>2</sub>, CH<sub>4</sub>, and N<sub>2</sub>O emissions and their combined GWP at the 20- and 100-year time horizons (GWP<sub>20</sub> and GWP<sub>100</sub>, respectively). We then analyze how two important modes of climate variability influencing European climate affect anomalies in the three GHGs separately, as well as their combined GWP.

Figure 11 shows the regionally integrated annual anomalies of CO<sub>2</sub>, CH<sub>4</sub>, and N<sub>2</sub>O and the respective aggregated GWP<sub>20</sub> and GWP<sub>100</sub> anomalies from the global atmospheric inversions. For CH<sub>4</sub>, we separately show the in situ and satellite based inversions, due to their different temporal coverage. Both CH<sub>4</sub> and N<sub>2</sub>O show a decreasing trend, while CO<sub>2</sub> shows multi-annual variations with a predominant sink in the 1990s and predominant source fluxes in the 2000s. Hot and dry years are generally associated with source anomalies, except 2012 and 2015, when drought conditions were more localized and mostly located over southern Europe. The 2003 drought and the 2018–2020 extreme summers were associated with strong CO<sub>2</sub> sources. 2003 is also associated with large CH<sub>4</sub> and N<sub>2</sub>O sources, so that 2003 is the year with the highest associated GWP, and 2010 shows a peak in emissions following a downward trend (bottom panel). It should be noted that the spread of the inversions is generally larger than the anomalies themselves for all three GHGs, which indicates a reduced ability to constrain annual anomalies at the continental scale.

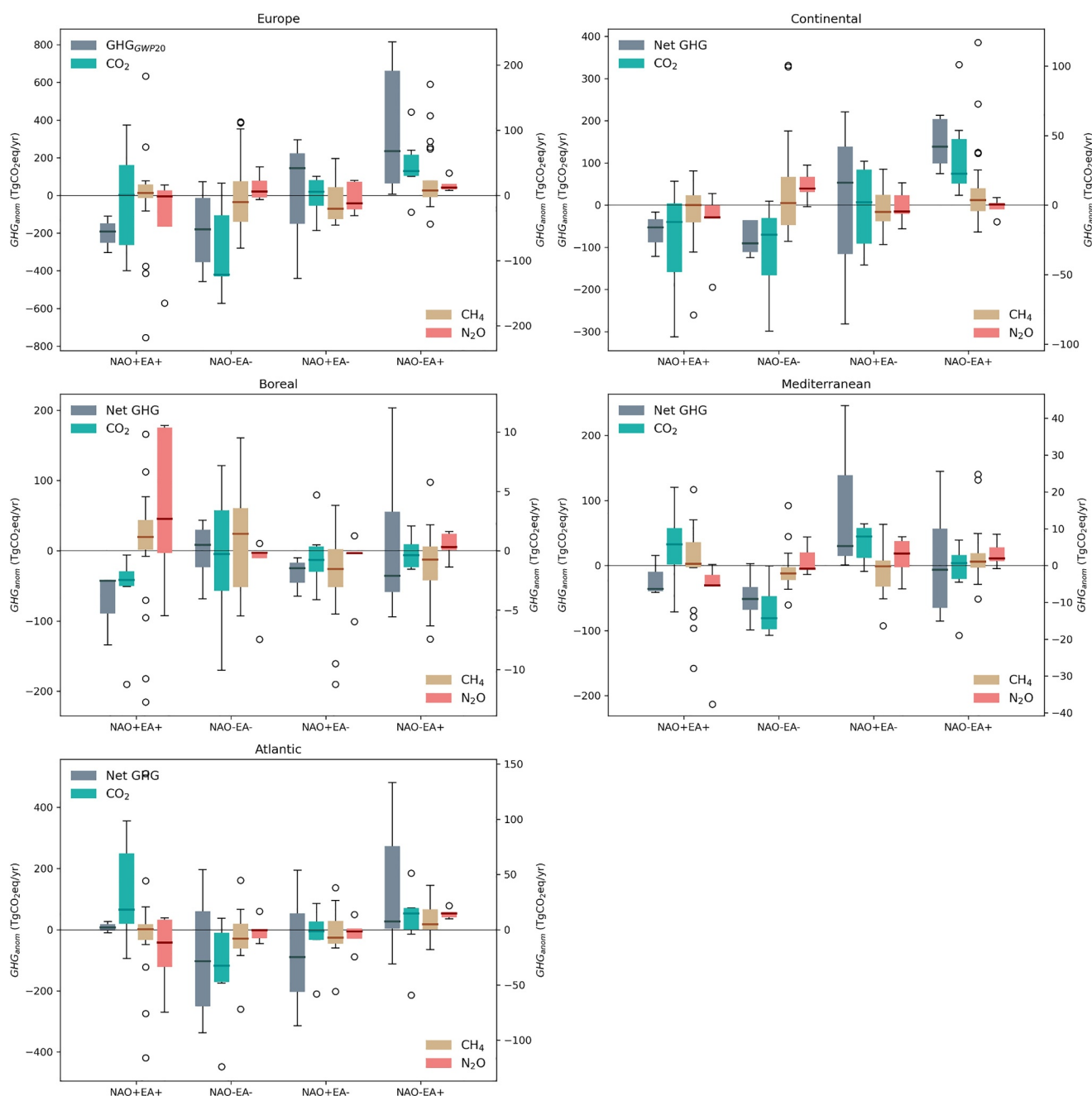
In Figure 12, we evaluate how anomalies in the three GHGs vary with two important modes of large-scale atmospheric circulation influencing European climate: the North Atlantic Oscillation (NAO) and the East-Atlantic (EA) Pattern. We analyze how far anomalies in each GHG and GWP of all three GHGs combined are related to possible NAO/EA combinations—at the European scale, and for four major climate regions within Europe: Atlantic, Continental, Boreal, and Mediterranean. At the European scale, we find that both combinations of NAO/EA in-phase (NAO+EA+ and NAO-EA-) are associated with below-average GWP (GHG<sub>GWP20</sub>). In the case of NAO+EA+, this is because of a combination of below-average values of CO<sub>2</sub> and N<sub>2</sub>O, but this is likely driven by outlier values, as the median anomalies for both gasses are close to zero. For NAO-EA-, CO<sub>2</sub> anomalies are predominantly negative, consistent with the results in Bastos et al. (2016), along with generally negative CH<sub>4</sub> anomalies, which are however associated with a large spread among inversions. Because the impacts of NAO and EA are regionally different, we need to analyze the regional dependence of GHG anomalies on climate drivers for each NAO/EA phase. During NAO + EA+, GHG sink anomalies are found for all regions except the Atlantic sector, but this is due to different combinations of anomalies in the three GHGs and of climate conditions: below-average GHG emissions in Continental and Boreal regions are mainly associated with below-average CO<sub>2</sub> anomalies driven by warmer than average conditions and close to normal—but slightly negative—precipitation anomalies (Figure S6 in Supporting Information S1). In the Atlantic section, warmer and drier conditions during NAO+EA+ are associated with a positive CO<sub>2</sub> anomaly, which is partly offset by a negative N<sub>2</sub>O anomaly, consistent with below average precipitation. For NAO-EA-, the European GHG sink is dominated by negative GHG<sub>GWP20</sub> anomalies in Continental and Mediterranean regions, mostly associated with below-average CO<sub>2</sub> emissions in both regions and additionally with negative CH<sub>4</sub> anomalies in the Mediterranean. In the Boreal section, negative CO<sub>2</sub> anomalies are linked to below average temperature and precipitation, consistent with results in Bastos et al. (2016) who showed that increased snow cover in winter due to cold winters and later soil-moisture availability led to increased summer GPP, while predominantly cooler temperatures kept Re<sub>terr</sub> anomalies low. The above-average N<sub>2</sub>O emissions in this region might be associated with the higher soil moisture during summer in this region (see Bastos et al. (2016) for seasonal climate anomalies). The negative anomalies in GHG<sub>GWP20</sub> in the Mediterranean are also likely explained by differences in the seasonal climate anomalies, with the increased CO<sub>2</sub> sink associated with higher soil-moisture availability during winter and early spring, when vegetation activity is at its peak in this region.

For the anti-phase combinations, GHG<sub>GWP20</sub> shows a clear source anomaly for NAO-EA+ and close to neutral but predominantly source anomaly for NAO+EA-, with both phase combinations showing a very large spread (Figure 12). The clear GHG<sub>GWP20</sub> source anomaly in NAO-EA+ results from positive anomalies in the three



**Figure 11.** Time-series of annual anomalies of the three GHGs - CO<sub>2</sub>, CH<sub>4</sub>, and N<sub>2</sub>O, from top to the third panel, and the respective aggregated GWP<sub>20</sub> and GWP<sub>100</sub> anomalies. The vertical red lines indicate years associated with hot and/or drought events.

GHGs at the European scale, while NAO + EA- shows close to neutral anomalies for all three GHGs, although slightly positive for CO<sub>2</sub> and slightly negative for CH<sub>4</sub> and N<sub>2</sub>O. The continental scale neutral balance for NAO + EA- is explained by offsetting effects between the Boreal and Mediterranean sectors, the first showing a sink anomaly associated with below-average CO<sub>2</sub> and CH<sub>4</sub> along with close to normal but tendentially warmer



**Figure 12.** Anomalies in annual CO<sub>2</sub>, CH<sub>4</sub>, and N<sub>2</sub>O fluxes and combined GWP<sub>20</sub> during the four combined phases of two main atmospheric circulation patterns influencing European climate: the North Atlantic Oscillation (NAO) and the East Atlantic Pattern (EA). The boxplots show the spread across the inversions for the mean of each phase combination. For each individual GHG, the anomalies are calculated for the available time-series length for each GHG, while for the GWP, the data are limited to the period 2000–2016, so that only two years are considered for the two in-phase composites (NAO + EA+ and NAO-EA-).

and slightly wetter than average conditions (Figure S6 in Supporting Information S1). Bastos et al. (2016) showed that the warm conditions for this phase occurred predominantly in winter and spring, so that the CO<sub>2</sub> sink might be associated with the earlier onset of the growing season. The positive GHG<sub>GWP20</sub> anomalies during NAO + EA- in the Mediterranean are associated with CO<sub>2</sub> source anomalies due to lower than average temperatures (especially in winter, the peak of the growing season, see Bastos et al. (2016)) and a N<sub>2</sub>O source anomaly likely explained by wetter than average conditions during this phase. Finally, the source anomaly at the European scale during NAO-EA+ is mostly explained by positive anomalies in CO<sub>2</sub> and CH<sub>4</sub> in the Continental region, associated with cooler



than average and much wetter conditions, and by positive anomalies in all three GHGs in the Atlantic region, associated with warmer and wetter conditions during this phase.

## 7. Processes and Drivers of Long-Term Trends in the European Carbon Budget

Figure 13 gives a consensus view of the trends of net carbon fluxes and stocks in Europe over the past decade. Negative values indicate an increasing sink or a decreasing source. The various products (TD global inversions, BU data driven models, BU process-based models) show good agreement on trends in northern Spain (region A) and Romania (region C), with a strengthening sink in both places. On the other hand, the Czech Republic (region B) leans more toward a weakening sink. These observations are confirmed by the frequency distributions of the number of products indicating a positive trend in the region when compared against the frequency distribution for all of Europe (right panel, Figure 13). Noticeable lack of agreement between the products is seen in the United Kingdom, the Balkans, Finland and Eastern Europe. The remaining areas show a mix of strengthening and weakening of the sink with agreement between at least five out of the seven products. The distribution across Europe is roughly Gaussian centered at three data sets showing a positive trend (four data sets showing a negative trend), while the distributions of each region are clearly skewed, even if region A is perhaps only offset by one data set. Due to vastly different magnitudes in the trends between different products (two orders of magnitude in extreme cases), we limit our discussion to the sign of the trend.

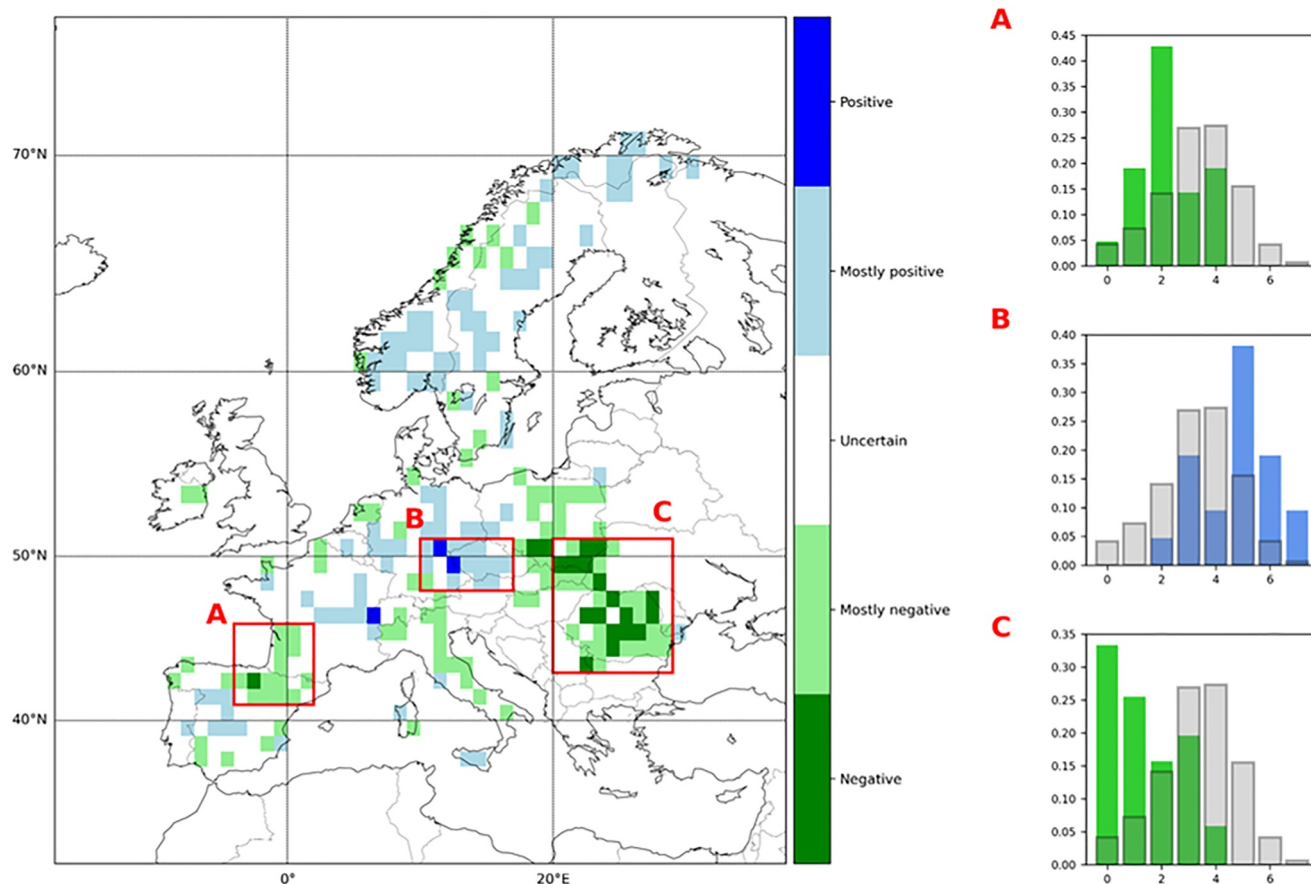
Figure 14 shows trends for regions A, B, and C for potential environmental drivers of the trends in sink strength observed in Figure 13 (reproduced in the left column in Figure 14). “ELUC” indicates total land use change emissions ( $F_{LUC}$ ) from 2010 to 2019 (sum of sink and source terms), while “sink” refers to abandonment of agricultural land and “source” refers to conversion from forest to pasture and cropland, and wood harvest. The different regions show agreement with different drivers, and indeed, depending on the region,  $F_{LUC}$  is driven by different processes: the sink dominates in Romania, while the source term dominates in northern Spain. Broadly increasing temperatures and vapor pressure deficit (VPD) may drive weakening sinks in the Czech Republic and strengthening sinks in Romania, although the spatial patterns appear to resemble more strongly those from land use change.

Land use trends are also shown in Figure 15 using a related approach by directly looking at the land-use and land-cover maps from Hilda+. Hilda+ consists of annual gross changes between urban, cropland, pasture/rangeland, forest, unmanaged grass/shrubland, and sparse/no vegetation areas (Winkler et al., 2021). The increasing sink strength in Romania corresponds to increasing sink due to cropland abandonment in the BLUE-Hilda+ results (region C, bottom right, Figure 14), while the fraction of cropland abandoned is much weaker than in surrounding regions in the pure Hilda+ maps (Figure 15). On the other hand, the increasing change in harvested forest area in the original Hilda+ data set over the Czech Republic corresponds nicely to the increasing emissions from BLUE-Hilda+ for the same region, suggesting that harvest may be driving observed trends in that region.

## 8. Contribution of Recent Forest Disturbances on the European Forest Carbon Balance

### 8.1. Losses and Gains Over the Last Three Decades

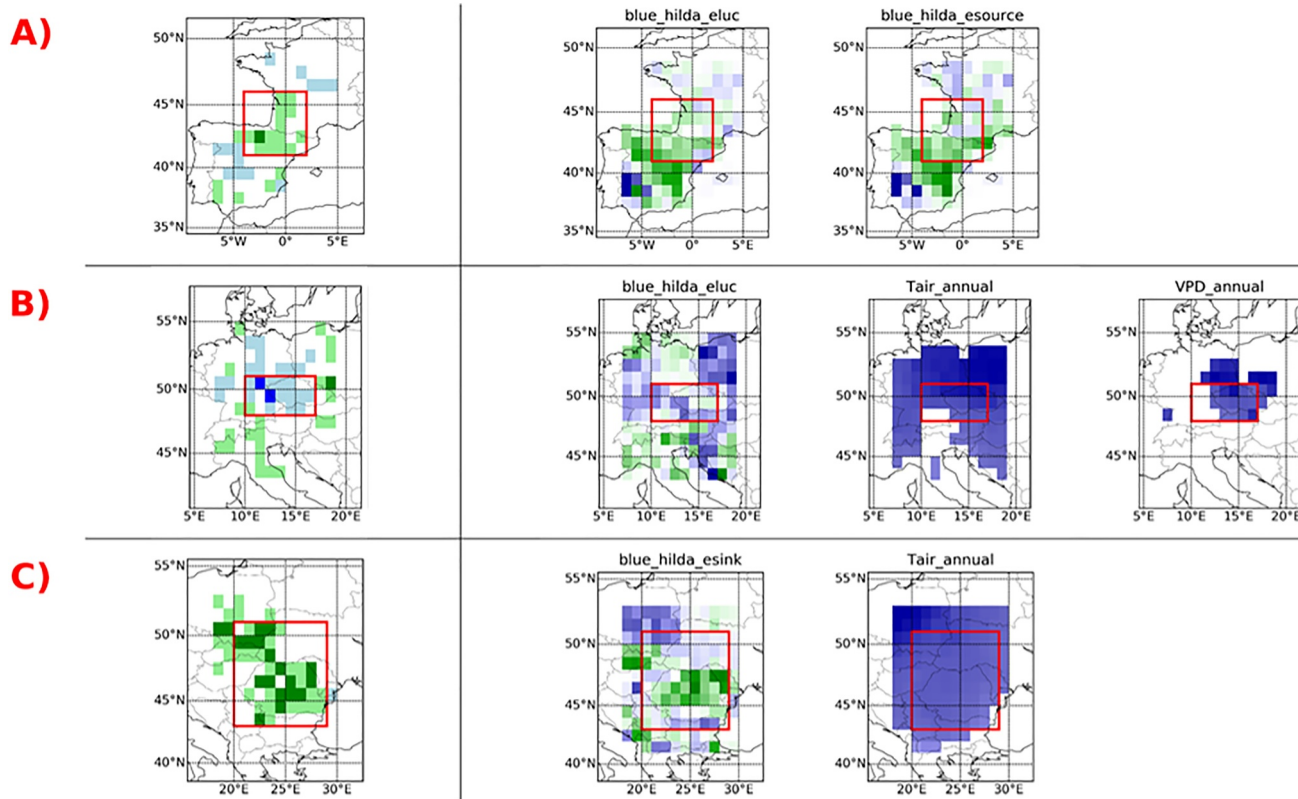
European forests experience various types of disturbances (mainly harvests, followed by storms, wildfires and insect outbreaks) that damage forests, resulting in a loss of productivity and biomass carbon stocks over the short term (Seidl et al., 2014). Several years after a disturbance event, however, a recovery has been observed, such as an increase in forest diversity and C stocks (Senf et al., 2019). To evaluate the net impact of forest disturbances on the European carbon budget, we analyzed carbon losses and recovery gains across four regions (Atlantic, Boreal, Mediterranean, and Continental) during three time periods (1990–1999, 2000–2009, and 2010–2018). Note that this analysis is only a partial C budget from disturbances, which includes the losses and gains from disturbances that occurred during each decade. Disturbances from previous decades contribute to additional recovery gains which are not accounted for. We utilized two data sets: (a) the European disturbance map from Senf & Seidl (2021a, 2021b, 2021c) based on Landsat data and (b) the CCI-ESA Above Ground Biomass data for 2010, 2017, and 2018, corrected for possible biases due to the use of different sensors between 2010 and other epochs based on the assumption that the biomass of undisturbed forest plots was constant (see Section 2.6.1). Estimates of carbon budget changes based on the above-mentioned products integrate the effects of both human- and natural-induced disturbances on forests.



**Figure 13.** Significant trends in carbon stocks and net fluxes for the period 2010–2019 as indicated by agreement among seven different products: EFISCEN, L-VOD, FLUXCOM, global inversions, regional inversions, TRENDY, and VPRM. “Positive” and “Negative” indicate unanimous agreement, while “Mostly” indicates that five out of seven products have this sign. The sign convention is such that negative values of the annual values indicate a sink into the land surface, while a positive value indicates a source to the atmosphere; negative trends thus indicate strengthening sinks. The three highlighted regions are A: [40°N, 45°N, 5°W, 3°E], B: [48°N, 51°N, 10°E, 17°E], and C: [43°N, 51°N, 20°E, 30°E] moving from west to east, roughly corresponding to northern Spain, the Czech Republic, and Romania, respectively. The right panels show the frequency distribution of pixels with the number of data sets showing a positive trend (increasing emissions or weakening sink), with gray bars showing the distribution for all pixels across Europe and green/blue showing just the pixels in that region.

The data in Figure 16 shows the location of disturbances and the average fraction of disturbed forests per decade. The data set from Senf & Seidl (2021a, 2021b, 2021c) only indicates the year of the most severe disturbance within the last 30 years, implying that a forest that experienced multiple disturbances since 1990 is considered as disturbed only once, which underestimates the disturbed fraction. The data in Figure 16 show that forests in boreal countries experienced more disturbances than in other regions due to intensive forest management practices (Ceccherini et al., 2020). The fraction of disturbed forests increased over time in Europe, the Atlantic and Mediterranean regions, reaching peaks of disturbed areas during the period 2000–2010. This increase may reflect the increasing frequency and intensity of natural disturbances, discussed in more detail later on, but could also be related to increasing harvested areas in some regions. However, the partition between harvests and natural disturbance is a sensitive topic, as inconsistencies have emerged between ground-based and remote-sensing attributions of disturbance type (Breidenbach et al., 2022; Ceccherini et al., 2020, 2021; Palahi et al., 2021; Wernick et al., 2021).

Table 5 presents the gains and losses of biomass carbon due to disturbances in the four regions of Figure 16. The largest carbon losses are observed in the Boreal region, followed by the Continental, Atlantic, and Mediterranean regions. On average, disturbances caused a cumulative loss of 690 TgC from 1990 to 2018, which represents 24% of the cumulative forest biomass carbon sink estimated from national inventories (Grassi et al., 2022). Decadal carbon gains associated with recovery from disturbances that occurred during the same decade are smaller than the losses. This implies that regrowing forests cannot fully compensate for the carbon losses due to disturbances

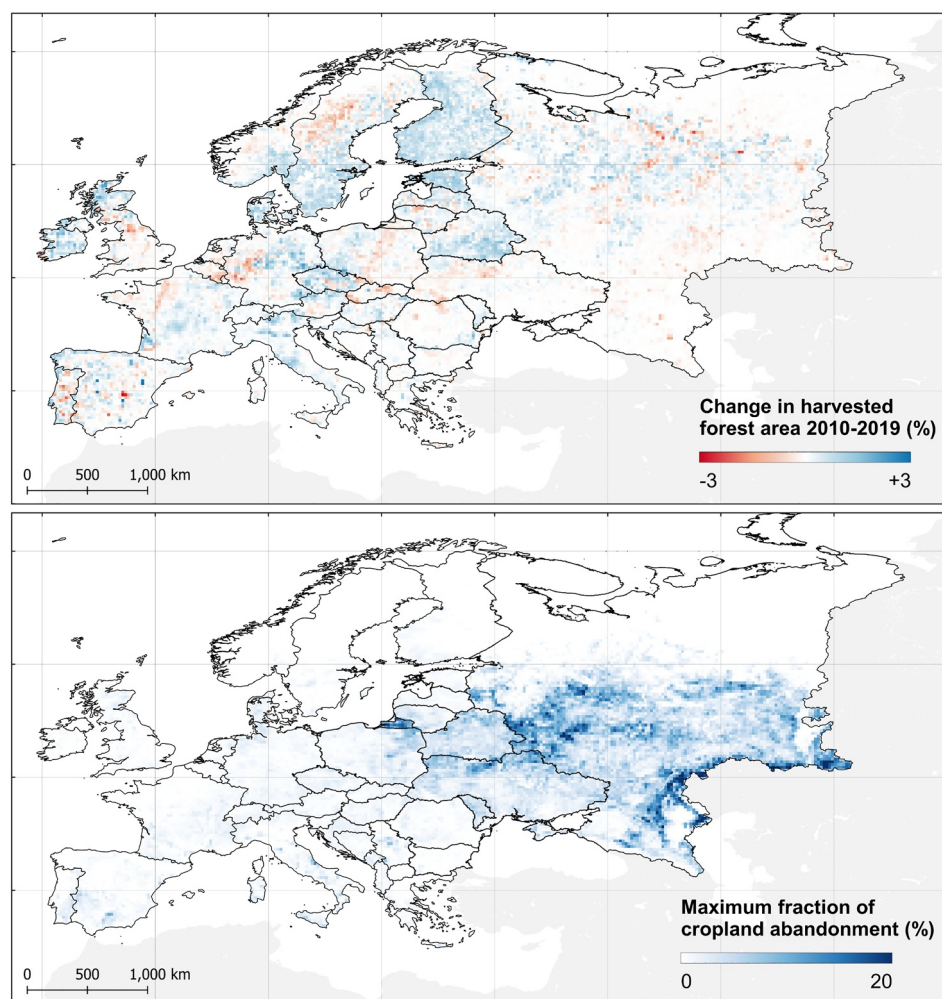


**Figure 14.** Comparison of data set agreement from Figure 13 with 2010–2019 trends in various meteorological and land use drivers for three distinct regions. Results have been aggregated to 1.0° spatial resolution for easier analysis. Meteorological variables (T and VPD) show pixels for which trends are statistically significant ( $P < 0.05$ ). The drivers shown on the right for each region are those for which the spatial patterns are closest to the observed agreement on the left. Blue indicates positive trends, that is, increasing emissions/weakening sink, increasing temperature, and increasing VPD.

during the same decade, which is consistent with a previous study (Nabuurs et al., 2013). This finding is also in line with recovery biomass curves in Europe, which show typical recovery times of 30 years (Senf & Seidl, 2021a, 2021b, 2021c GEB). However, gains continue to accrue after the decade when disturbances occur. The regions with the largest net carbon losses (i.e., losses exceeding gains) on a decadal window are ranked as follows: Boreal, Mediterranean, Continental, and Atlantic. Increasing disturbances observed in the last decade have led to higher losses in all the regions, so that the balance between losses and gains has become more negative in recent years.

## 8.2. Contribution of Natural Disturbances

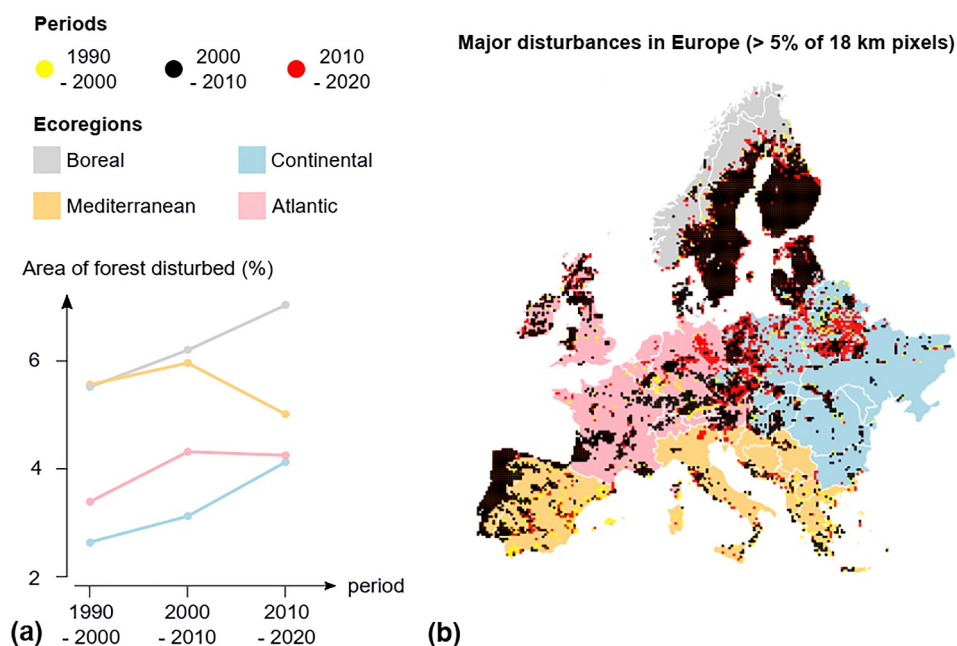
We complemented the aforementioned analyses of the role of disturbances within each decade on the C budgets with an assessment of the impact of major natural disturbances, including fires, windthrows and insect outbreaks, based on the DFDE database (Patacca et al., 2023). Windthrows provide the largest contribution to the overall damage induced by natural agents in European forests, causing an average of 24 Mm<sup>3</sup> (~5.5 Tg C yr<sup>-1</sup>) annually, corresponding to 46% of the total timber volume disturbed over the 1950–2019 period. Northern and Western European regions are more prominently exposed to strong wind gusts typically associated with areas of deep low atmospheric pressure (Roberts et al., 2014). Windthrows, being an extreme event strongly dependent on exceptional weather conditions, show high interannual variability dominated by individual extreme events such as the storms Vivian and Wiebke in 1990, Lothar and Martin in 1999, Gudrun in 2005, Kyrill in 2007, Klaus in 2009, and Xynthia in 2010. Despite the high stochasticity, wind disturbances experienced a significant positive trend at the European scale, with 310,000 m<sup>3</sup> timber volume lost more per year. Such an estimate agrees with independent assessments based on satellite retrievals (Senf & Seidl, 2021a, 2021b, 2021c).



**Figure 15.** Change in harvested forest area between 2010 and 2019 (top) and maximum fraction of cropland abandonment (bottom) from the Hilda + land use/land cover data set. The spatial resolution is 0.25°.

Fire is the second most important natural disturbance in Europe's forests, with an annual average biomass loss of 12.5 Mm<sup>3</sup> (~2.9 Tg C yr<sup>-1</sup>), corresponding to 24% of the total timber volume damage over the study period. Severe aridity conditions typical of Southern European regions—affecting both triggering and susceptibility mechanisms—make these areas in particular subject to such disturbance (Littell et al., 2009). Fire impact has increased significantly between 1950 and 2019 at the European level, with 99,609 m<sup>3</sup> timber volume lost per year and a sharper trend between 1970 and 1990. Large peaks of strong individual disturbance years are evident from the 1990 onward and are plausibly associated with severe droughts which have triggered extreme fire years (Senf et al., 2020).

The timber volume damaged by bark beetles accounts for 8.9 Mm<sup>3</sup> (~2.0 Tg C yr<sup>-1</sup>), which corresponds to 17% of the total volume disturbed between 1950 and 2019. The magnitude of bark beetle disturbance shows a significant increase over the observational period with a trend of 182,897 of m<sup>3</sup> timber volume lost per year. A substantial higher damage rate manifested from 2000 onwards. This is consistent with the abrupt increase in vulnerability of forests to insect outbreaks observed for warming levels that occurred around year 2000 at the European scale and documented in previous studies (Forzieri et al., 2021). Such pronounced increases in temperature have likely reduced plant defense mechanisms by ultimately favoring triggering processes and making forests more vulnerable to insect attacks. This seems confirmed by independent evidence documenting the recent rise in infestations of bark beetles responsible for massive and destructive attacks on coniferous forests in many northern and eastern European regions (Biedermann et al., 2019).



**Figure 16.** Area disturbed in Europe for four ecoregions (Atlantic, Mediterranean, Boreal, and Continental) and three periods (1990–2000, 2000–2010, and 2010–2020) based on the disturbance map of Senf & Seidl (2021a, 2021b, 2021c). Panel (a) shows the spatial mean of the percentage of disturbed forest, and panel (b) shows the major disturbances which have occurred in Europe (forested pixels of 18 km disturbed by more than 5%).

**Table 5**

*Gains and Losses of Carbon Due To Disturbances for Three Different Periods (1990–1999, 2000–2009, 2010–2018) Across Four Different Ecoregions (Atlantic, Mediterranean, Boreal, and Continental) Based on the AGB Maps 2017 and 2018 (Mean Values)<sup>a</sup>*

Period	Gain of C [Tg C yr <sup>-1</sup> ]	Loss of C	Net budget
<b>Atlantic</b>			
1990–1999	8.70 ± 0.10	-8.26 ± 0.06	+0.44 ± 0.12
2000–2009	8.53 ± 0.11	-13.96 ± 0.12	-5.43 ± 0.18
2010–2018	5.38 ± 0.75	-9.94 ± 0.06	-4.56 ± 0.71
<b>Mediterranean</b>			
1990–1999	0.02 ± 0.40	-6.71 ± 0.16	-6.69 ± 0.44
2000–2009	-0.93 ± 0.47	-8.15 ± 0.20	-9.08 ± 0.53
2010–2018	-0.59 ± 0.84	-7.12 ± 0.14	-7.71 ± 0.83
<b>Boreal</b>			
1990–1999	21.58 ± 0.34	-23.78 ± 0.25	-2.20 ± 0.46
2000–2009	15.03 ± 0.29	-25.71 ± 0.25	-10.68 ± 0.41
2010–2018	13.14 ± 1.84	-25.27 ± 0.22	-12.13 ± 1.77
<b>Continental</b>			
1990–1999	11.49 ± 0.42	-12.41 ± 0.22	-0.92 ± 0.50
2000–2009	10.75 ± 0.42	-16.30 ± 0.26	-5.55 ± 0.53
2010–2018	11.05 ± 0.40	-18.79 ± 0.26	-7.73 ± 0.52

<sup>a</sup>Uncertainties for the sources and sinks represent the absolute difference between the 2017 and 2018 maps. Uncertainties for the net budget have been obtained using a bootstrapping method ( $n = 10^5$ ).

We highlight that estimates of biomass losses based on DFDE should be viewed with caution as they are subject to multiple sources of potential biases. The DFDE database is based on damage data statistics reported at a country scale and collected by literature search and is therefore built on the contribution of data retrieved from different actors and through different acquisition methods. Despite the relevance of these issues, there is still a substantial lack of systematic monitoring systems of forest disturbances at the European level (McDowell et al., 2011). Recent joint efforts across European research institutions and forestry services have contributed to the collection of harmonized databases of spatially explicit records of windthrows (Forzieri et al., 2020) and pest outbreaks (Forzieri et al., 2023) at the Pan-European scale. These products have paved the way for the future development of novel methodologies for forest disturbance detection and attribution, which could provide enhanced estimates of the impact of forest disturbances on the land carbon budget.

## 9. Conclusion

Our BU estimate of the European GHG budget for the decade 2010–2019 gives net emissions of 3.9 Pg CO<sub>2</sub>-eq. yr<sup>-1</sup> (100 years horizon). These net emissions are mainly driven by direct anthropogenic emissions of 4.9 Pg CO<sub>2</sub>-eq. yr<sup>-1</sup>, to which CO<sub>2</sub> emissions from fossil fuel combustion (Energy + IPPU sector) contribute about 85%. The land GHG budget gives a net-sink of 0.9 Pg CO<sub>2</sub>-eq. yr<sup>-1</sup>, mainly driven by the land CO<sub>2</sub> sink of 1.4 Pg CO<sub>2</sub>-eq. yr<sup>-1</sup>, which is only partially offset by net-emissions of CH<sub>4</sub> and N<sub>2</sub>O. Our BU CH<sub>4</sub> and N<sub>2</sub>O budgets agree well with regional and global inversions. In contrast, our BU estimate of the land CO<sub>2</sub> sink is at the higher end of the range of global inversions, and substantially higher than that estimated by regional inversions.

Over the decades of the 1990s, 2000s, and 2010s, our BU estimates give decreasing average net-GHG emissions (anthropogenic emissions + land budget) of 5.1, 4.6, and 3.9 Pg CO<sub>2</sub>-eq. yr<sup>-1</sup>, respectively. This decrease in net-emissions is mainly driven by decreases in direct anthropogenic emissions of CO<sub>2</sub> and CH<sub>4</sub>, and in particular by a reduction in fossil fuel emissions. From the 2000s to the 2010s, the reduction in fossil fuel CO<sub>2</sub> emissions was particularly strong (by 0.7 Pg CO<sub>2</sub> yr<sup>-1</sup>) but partly counterbalanced by a substantial weakening of the land CO<sub>2</sub> sink (by 0.2 Pg CO<sub>2</sub> yr<sup>-1</sup>). N<sub>2</sub>O contributes less to the overall GHG budgets but also shows a pronounced decrease in total emissions, largely due to reduced emissions from the IPPU sector, for which however large uncertainties persist.

Global inversions, which cover the last two (CH<sub>4</sub>, N<sub>2</sub>O, but only until 2016) or three (CO<sub>2</sub>) decades, confirm the decreasing trend in CH<sub>4</sub> and N<sub>2</sub>O emissions. For the land CO<sub>2</sub> budget, the trend is less clear, but a pronounced interannual variability is visible. The drought in 2003 and the hot summers of 2018 and 2020, associated with unprecedented disturbances, are likely responsible for the weakened land CO<sub>2</sub> sink visible for these years. The drought year of 2003 also shows the highest net-GHG emissions in terms of the combined global warming potential of the three GHGs.

Regional inversions permit us to identify large scale spatial patterns in GHG emissions over Europe. For CO<sub>2</sub>, direct anthropogenic emissions (mainly fossil fuel emissions) show many local hotspots linked to large cities, power plants and industrial complexes. For the land CO<sub>2</sub> budget, regional inversions reveal sinks mainly in the northern half of Europe, whereas southern France and the Iberian Peninsula appear as large CO<sub>2</sub> sources. CH<sub>4</sub> and N<sub>2</sub>O emissions stem largely from diffusive sources on agricultural land (fertilizer- and manure-driven N<sub>2</sub>O emissions from soils, and CH<sub>4</sub> emissions from ruminant livestock). Belgium, the Netherlands and southern UK appear as large areas of intense emissions of both GHGs.

Our BU C budget is based on the fluxes from the land budgets of CO<sub>2</sub> and CH<sub>4</sub>, and further includes estimates of lateral C net-exports through the trade of crop, wood, and peat products and the fluvial export of C to the sea. Alternatively, we constructed a C budget for the 2010s as a sum of individual estimates of changes in different C stocks, most importantly the biospheric C stocks of forest, grassland and cropland systems and the stock of harvested wood products.

For the 2010s, our flux-based estimate gives an average increase in the overall C stocks of 0.3 Pg C yr<sup>-1</sup>. The stock-based BU estimate is substantially lower with only 0.1 Pg C yr<sup>-1</sup>. However, we have to acknowledge that both estimates are associated with large uncertainties, larger in fact than the difference between both estimates. Nevertheless, our stock-based estimate is quite close to the UNFCCC estimate and the ensemble-median of the TRENDYv10 simulations. However, the range between individual TRENDYv10 simulations is also much larger than the difference between our flux-based and our stock-based estimates, highlighting that DGVMs are not an adequate tool to constrain the European C budget.

When comparing the flux-based BU estimates of C budgets for the last three decades, we find very much the same trend as for the land CO<sub>2</sub> budgets, which is largely driving C stock changes, while changes in CH<sub>4</sub> emissions and lateral C exports play a minor role. We find a substantial decrease of ~90 Tg C yr<sup>-1</sup> in the land C sink from the 2000s to the 2010s, which is dominated by increases in ecosystem respiration Re<sub>terr</sub> and emissions from the use, decay, or burning of biological products. At the same time, GPP also slightly decreased between these two decades. Note that changes in ecosystem respiration and GPP are based here on extrapolated flux tower measurements of the FLUXCOM data set. The TRENDYv10 ensemble does not reproduce the decrease in the land C sink nor the underlying trends in GPP and Re<sub>terr</sub>. In contrast, a slight decrease in the C budget is estimated by the UNFCCC national inventories, suggesting that changes in land management also play a role in decreased C sink strength.

We evaluated what is known about spatial patterns in the recent temporal trends in the land C sink strength by comparing different spatialized TD and BU estimates. On the TD side, this included the ensembles of regional and global inversions of the land CO<sub>2</sub> budget. On the BU side, we include inventory and remote sensing based estimates of changes in forest biomass, the FLUXCOM data set and the VRPM model, both of which represent spatial extrapolations of flux tower measurements, and the TRENDYv10 ensemble. While over large parts of Europe, these data sets disagree whether we have a strengthening or weakening of the land C sink, we found a general agreement for increasing sink strengths over larger areas in and north-west of Romania and in the northern part of Spain, as well as for a weakening of the sink strength over the Czech Republic. To a certain degree, these trends can be explained by changes in land use but extreme events and climate-driven disturbances are also likely to have played

an important role. We also find a certain degree of agreement on a decreasing land C sink over large parts of Scandinavia, which can be explained by an intensification of forest management.

We finally investigated the impact of disturbances on forest biomass stocks in Europe, including disturbances through management (wood harvest in particular) as well as natural disturbances. Naturally, these disturbances play the largest role in Scandinavia and the Baltic, where we find large, managed forest areas. In Europe, net-losses of forest biomass have increased since the 1990s. In the last decade, they amounted to about 32 Tg C yr<sup>-1</sup>, which equals one third to one tenth of our estimates of the European land C sink. Most of the net-losses are likely due to management practices, though natural disturbances may still play a non-negligible role. The most important form of natural disturbance of forest biomass loss in Europe is windthrow, followed by forest fires and bark beetle outbreaks. However, more research is required to quantitatively disentangle the effects of natural disturbance and management on the forest biomass C stocks.

Overall, our study provides the most up-to-date and comprehensive assessment of the European budget for CO<sub>2</sub>, CH<sub>4</sub>, and N<sub>2</sub>O for the past three decades, including their combined GWP, as well as their trends and interannual variability. We combine a wide range of TD and BU estimates to separate these budgets into their different components and to produce the best estimate of their budget for the 2010s decade. By comparing our estimates with those of UNFCCC reports, our study provides a key contribution to the evaluation of national reporting of GHG and C emissions on a continental scale. Moreover, our study helps to set the path toward an improved carbon monitoring framework at the European scale that can guide policy making.

#### Acknowledgments

R.L., P.C. and F.R. acknowledge funding from French state aid managed by ANR under the “Investissements d’avenir” programme (ANR-16-CONV-0003) and R.L. from EU’s Horizon Europe Research and Innovation Programme under Grant 101060423. A.B. was funded by the European Union (ERC StG, ForExD, Grant 101039567). Views and opinions expressed are however those of the authors only and do not necessarily reflect those of the European Union or the European Research Council. Neither the European Union nor the granting authority can be held responsible for them. AMRP, MJM, RMA, MJS, GJN, PC were supported by the European Commission, Horizon 2020 Framework Programme (VERIFY, Grant 776810), AMRP, MJM, RMA by Grant 958927 (CoCO2), AMRP by Grant 101081322 (AVENGERS) and RMA, PC and PP by Grant 101081395 (EYE-CLIMA). P.C. is partly supported by the European Space Agency Climate Change Initiative (ESA-CCI) Biomass project (ESA ESRIN/4000123662) and RECCAP2 project 1190 (ESA ESRIN/4000123002/18/I-NB). P.K.P. is partly supported by the Environmental Research and Technology Development Fund (JPMEERF21S20800) of the MOEJ and ERCA. G.F. was supported by the Horizon Europe Project ECO2ADAPT (Grant 101059498). MJS and GJN were partly funded by Ministry Agriculture, Nature Management and Food Quality in Netherlands and its Knowledge Bases programme. GJN acknowledges RESONATE project (H2020 Grant 101000574) and the Horizon Europe Project SUPERB (Grant 101036849) and FORWARDS (Grant 101084481). For the aggregated national forest inventory data behind the EFISCEN simulations MJS and GJN acknowledge the national forest inventories of 27 EU countries, CW was funded by the Natural Environment Research Council through its grants to the UK National Centre for Earth Observation (NCEO; NERC Grants NE/R016518/1 and NE/N018079/1). CTE2021 runs were supported by the HPC cluster Aether at the University of Bremen, financed by DFG within the scope of the Excellence Initiative. PR acknowledges funding from the FRS-FRNS PDR project T.0191.23 CH4-lakes.

#### Data Availability Statement

Data used for the RECCAP2 project are available from [MPI-BGC \(n.d.\)](#). Additional data used for our study was taken from: Jung et al. (2020) for gridded FLUXCOM data; Andrew (2020) for updated fossil fuel emission inventories; UNFCCC (n.d.) for national inventories collected by UNFCCC; FAO (n.d.) for the FAOSTAT database; Byrne et al. (2023) for gridded estimates of lateral carbon transfers; O’Sullivan (2022) for TREN-DYv10 simulations; McGrath et al. (2023) and Petrescu et al. (2023) for regional atmospheric inversions; Chang et al. (2021) for estimates of livestock grazing; Hirschler and Oldenburg (2022) for estimates of peat harvest, trade and use; Murguia-Flores et al. (2018) for MeMo simulation data; Gerbig and Koch (2021) for gridded VPRM simulation outputs; Ganzenmüller et al. (2022) for gridded BLUE simulation results; Winkler et al. (2021) for gridded HILDA+ land use and land use change data; Madani and Parazoo (2020), Zhao et al. (2005), and Jiang and Ryu (2016) for gridded estimates of terrestrial primary production; Yao et al. (2021) for gridded estimate of soil heterotrophic respiration; Mendonca et al. (2017) for regionalized estimates of lake carbon burial; Etiope et al. (2019) for spatially resolved estimates of geogenic methane emissions; Nabuurs et al. (2018) and Petrescu et al. (2020) for EFISCEN estimates of forest carbon stock changes; Fan et al. (2023) for the L-VOD based estimates of changes in above ground biomass; EMEP (n.d.) for EMEP data; Randerson et al. (2018) for GFEDv4 data; ECMWF (n.d.) for GFASv1.2 data.

#### References

- Ahlström, A., Canadell, J. G., & Metcalfe, D. B. (2022). Widespread unquantified conversion of old boreal forests to plantations. *Earth's Future*, 10(11), e2022EF003221. <https://doi.org/10.1029/2022EF003221>
- Anderegg, W. R. L., Trugman, A. T., Badgley, G., Anderson, C. M., Bartuska, A., Ciais, P., et al. (2020). Climate-driven risks to the climate mitigation potential of forests. *Science*, 368(6497), eaaz7005. <https://doi.org/10.1126/science.aaz7005>
- Anderegg, W. R. L., Wu, C., Acil, N., Carvalhais, N., Pugh, T. A. M., Sadler, J. P., & Seidl, R. (2022). A climate risk analysis of Earth’s forests in the 21st century. *Science*, 377(6610), 1099–1103. <https://doi.org/10.1126/science.abp9723>
- Andrew, R. M. (2020). A comparison of estimates of global carbon dioxide emissions from fossil carbon sources. *Earth System Science Data*, 12(2), 1437–1465. <https://doi.org/10.5194/essd-12-1437-2020>
- Bastos, A., Fu, Z., Ciais, P., Friedlingstein, P., Sitch, S., Pongratz, J., et al. (2020). Impacts of extreme summers on European ecosystems: A comparative analysis of 2003, 2010 and 2018: European extreme summers and the C-cycle. *Philosophical Transactions of the Royal Society B: Biological Sciences*, 375(1810), 20190507. <https://doi.org/10.1098/rstb.2019.0507>
- Bastos, A., Gouveia, C. M., Trigo, R. M., & Running, S. W. (2014). Analysing the spatio-temporal impacts of the 2003 and 2010 extreme heatwaves on plant productivity in Europe. *Biogeosciences*, 11(13), 3421–3435. <https://doi.org/10.5194/bg-11-3421-2014>
- Bastos, A., Janssens, I. A., Gouveia, C. M., Trigo, R. M., Ciais, P., Chevallier, F., et al. (2016). European land CO<sub>2</sub> sink influenced by NAO and East-Atlantic Pattern coupling. *Nature Communications*, 7(1), 10315. <https://doi.org/10.1038/ncomms10315>
- Battin, T. J., Lauerwald, R., Bernhardt, E. S., Bertuzzo, E., Gener, L. G., Hall, R. O., et al. (2023). River ecosystem metabolism and carbon biogeochemistry in a changing world. *Nature*, 613(7944), 449–459. <https://doi.org/10.1038/s41586-022-05500-8>
- Biedermann, P. H. W., Müller, J., Grégoire, J.-C., Gruppe, A., Hagge, J., Hammerbacher, A., et al. (2019). Bark beetle population dynamics in the anthropocene: Challenges and solutions. *Trends in Ecology & Evolution*, 34(10), 914–924. <https://doi.org/10.1016/j.tree.2019.06.002>

- Breidenbach, J., Ellison, D., Petersson, H., Korhonen, K. T., Henttonen, H. M., Wallerman, J., et al. (2022). Harvested area did not increase abruptly—How advancements in satellite-based mapping led to erroneous conclusions. *Annals of Forest Science*, 79(1), 2. <https://doi.org/10.1186/s13595-022-01120-4>
- Buermann, W., Forkel, M., O'Sullivan, M., Sitch, S., Friedlingstein, P., Haverd, V., et al. (2018). Widespread seasonal compensation effects of spring warming on northern plant productivity. *Nature*, 562(7725), 110–114. <https://doi.org/10.1038/s41586-018-0555-7>
- Byrne, B., Baker, D. F., Basu, S., Bertolacci, M., Bowman, K. W., Carroll, D., et al. (2023). National CO<sub>2</sub> budgets (2015–2020) inferred from atmospheric CO<sub>2</sub> observations in support of the global stocktake. *Earth System Science Data*, 15(2), 963–1004. <https://doi.org/10.5194/essd-15-963-2023>
- Canadell, J. G., Ciais, P., Gurney, K., Le Quéré, C., Piao, S., Raupach, M. R., & Sabine, C. L. (2011). An international effort to quantify regional carbon fluxes. *Eos, Transactions American Geophysical Union*, 92(10), 81–82. <https://doi.org/10.1029/2011EO100001>
- Carlson, K., Gerber, J., Mueller, N., Herrero, M., MacDonald, G. K., Brauman, K. A., et al. (2017). Greenhouse gas emissions intensity of global croplands. *Nature Climate Change*, 7(1), 63–68. <https://doi.org/10.1038/nclimate3158>
- Ceccherini, G., Duveiller, G., Grassi, G., Lemoine, G., Avitabile, V., Pilli, R., & Cescatti, A. (2020). Abrupt increase in harvested forest area over Europe after 2015. *Nature*, 583(7814), 72–77. <https://doi.org/10.1038/s41586-020-2438-y>
- Ceccherini, G., Duveiller, G., Grassi, G., Lemoine, G., Avitabile, V., Pilli, R., & Cescatti, A. (2021). Reply to Wernick, I. K. et al.; Palahí, M. et al. *Nature*, 592(7856), E18–E23. <https://doi.org/10.1038/s41586-021-03294-9>
- Chang, J., Ciais, P., Gasser, T., Smith, P., Herrero, M., Havlík, P., et al. (2021). Climate warming from managed grasslands cancels the cooling effect of carbon sinks in sparsely grazed and natural grasslands. *Nature Communications*, 12(1), 118. <https://doi.org/10.1038/s41467-020-20406-7>
- Ciais, P., Bastos, A., Chevallier, F., Lauerwald, R., Poulter, B., Canadell, J. G., et al. (2022). Definitions and methods to estimate regional land carbon fluxes for the second phase of the REgional Carbon Cycle Assessment and Processes Project (RECCAP-2). *Geoscientific Model Development*, 15(3), 1289–1316. <https://doi.org/10.5194/gmd-15-1289-2022>
- Ciais, P., Borges, A. V., Abril, G., Meybeck, M., Folberth, G., Hauglustaine, D., & Janssens, I. A. (2008). The impact of lateral carbon fluxes on the European carbon balance. *Biogeosciences*, 5(5), 1259–1271. <https://doi.org/10.5194/bg-5-1259-2008>
- Ciais, P., Reichstein, M., Viovy, N., Granier, A., Ogée, J., Allard, V., et al. (2005). Europe-wide reduction in primary productivity caused by the heat and drought in 2003. *Nature*, 437(7058), 529–533. <https://doi.org/10.1038/nature03972>
- Ciais, P., Soussana, J. F., Vuichard, N., Luysaert, S., Don, A., Janssens, I. A., et al. (2010). The greenhouse gas balance of European grasslands. *Biogeosciences Discussions*, 2010, 5997–6050. <https://doi.org/10.5194/bgd-7-5997-2010>
- Ciais, P., Wattenbach, M., Vuichard, N., Smith, P., Piao, S. L., Don, A., et al. (2010). The European carbon balance. Part 2: Croplands. *Global Change Biology*, 16(5), 1409–1428. <https://doi.org/10.1111/j.1365-2486.2009.02055.x>
- Ciais, P., Yao, Y., Gasser, T., Baccini, A., Wang, Y., Lauerwald, R., et al. (2021). Empirical estimates of regional carbon budgets imply reduced global soil heterotrophic respiration. *National Science Review*, 8(2). <https://doi.org/10.1093/nsr/nwaa145>
- Deng, Z., Ciais, P., Tzompa-Sosa, Z. A., Saunio, M., Qiu, C., Tan, C., et al. (2022). Comparing national greenhouse gas budgets reported in UNFCCC inventories against atmospheric inversions. *Earth System Science Data*, 14(4), 1639–1675. <https://doi.org/10.5194/essd-14-1639-2022>
- De Rosa, D., Ballabio, C., Lugato, E., Fasiolo, M., Jones, A., & Panagos, P. (2024). Soil organic carbon stocks in European croplands and grasslands: How much have we lost in the past decade? *Global Change Biology*, 30(1), e16992. <https://doi.org/10.1111/gcb.16992>
- de Vries, W., Schulte-Uebbing, L., Kros, H., Voogd, J. C., & Louwagie, G. (2021). Spatially explicit boundaries for agricultural nitrogen inputs in the European Union to meet air and water quality targets. *Science of the Total Environment*, 786, 147283. <https://doi.org/10.1016/j.scitotenv.2021.147283>
- ECMWF. (n.d.). Global Fire Assimilation System (GFAS) [Dataset]. *ECMWF*. Retrieved from <https://www.ecmwf.int/en/forecasts/dataset/global-fire-assimilation-system>
- Eggers, T. (2002). The impacts of manufacturing and utilisation of wood products on the European carbon budget Internal Report 9.
- EMEP. (n.d.). Daily N deposition data (from the co-operative programme for monitoring and evaluation of the long-range transmission of air pollutants in Europe—EMEP). Retrieved from [https://thredds.met.no/thredds/catalog/data/EMEP/2021\\_Reporting/catalog.html](https://thredds.met.no/thredds/catalog/data/EMEP/2021_Reporting/catalog.html)
- Étiépe, G., Ciotoli, G., Schwietzke, S., & Schoell, M. (2019). Gridded maps of geological methane emissions and their isotopic signature. *Earth System Science Data*, 11(1), 1–22. <https://doi.org/10.5194/essd-11-1-2019>
- European Communities Council. (1991). Council directive of the 12 December 1991 concerning the protection of water against pollution caused by nitrates from agricultural sources (91/676/EEC). *Official Journal of the European Communities*, No. L 375/1, 1991. Retrieved from <https://eur-lex.europa.eu/legal-content/EN/TXT/PDF/?uri=CELEX:31991L0676>
- Fan, L., Wigneron, J. P., Ciais, P., Chave, J., Brandt, M., Sitch, S., et al. (2023). Siberian carbon sink reduced by forest disturbances. *Nature Geoscience*, 16(1), 56–62. <https://doi.org/10.1038/s41561-022-01087-x>
- FAO. (n.d.). Food and agriculture data [Dataset]. *FAOSTAT*. Retrieved from [www.fao.org/faostat/#!/access/2024/06/03](http://www.fao.org/faostat/#!/access/2024/06/03)
- Forzieri, G., Dakos, V., McDowell, N. G., Ramdane, A., & Cescatti, A. (2022). Emerging signals of declining forest resilience under climate change. *Nature*, 608(7923), 534–539. <https://doi.org/10.1038/s41586-022-04959-9>
- Forzieri, G., Dutrieux, L. P., Elia, A., Eckhardt, B., Caudullo, G., Taboada, F. Á., et al. (2023). The database of European forest insect and disease disturbances: DEFID2. *Global Change Biology*, 29(21), 6040–6065. <https://doi.org/10.1111/gcb.16912>
- Forzieri, G., Girardello, M., Ceccherini, G., Spinoni, J., Feyen, L., Hartmann, H., et al. (2021). Emergent vulnerability to climate-driven disturbances in European forests. *Nature Communications*, 12(1), 1081. <https://doi.org/10.1038/s41467-021-21399-7>
- Forzieri, G., Pecchi, M., Girardello, M., Mauri, A., Klaus, M., Nikolov, C., et al. (2020). A spatially explicit database of wind disturbances in European forests over the period 2000–2018. *Earth System Science Data*, 12(1), 257–276. <https://doi.org/10.5194/essd-12-257-2020>
- Friedlingstein, P., Jones, M. W., O'Sullivan, M., Andrew, R. M., Bakker, D. C. E., Hauck, J., et al. (2022). Global carbon budget 2021. *Earth System Science Data*, 14(4), 1917–2005. <https://doi.org/10.5194/essd-14-1917-2022>
- Friedlingstein, P., O'Sullivan, M., Jones, M. W., Andrew, R. M., Hauck, J., Olsen, A., et al. (2020). Global carbon budget 2020. *Earth System Science Data*, 12(4), 3269–3340. <https://doi.org/10.5194/essd-12-3269-2020>
- Ganzenmüller, R., Bultan, S., Winkler, K., Fuchs, R., Zabel, F., & Pongratz, J. (2022). Land-use change emissions based on high-resolution activity data substantially lower than previously estimated. *Environmental Research Letters*, 17(6), 064050. <https://doi.org/10.1088/1748-9326/ac70d8>
- Gerbig, C., & Koch, F.-T. (2021). Biosphere-atmosphere exchange fluxes for CO<sub>2</sub> from the vegetation photosynthesis and respiration model VPRM for 2006–2021 2021. <https://doi.org/10.18160/VX78-HVA1>
- Grassi, G., Conchedda, G., Federici, S., Abad Viñas, R., Korosuo, A., Melo, J., et al. (2022). Carbon fluxes from land 2000–2020: Bringing clarity to countries' reporting. *Earth System Science Data*, 14(10), 4643–4666. <https://doi.org/10.5194/essd-14-4643-2022>



- Grassi, G., Schwingshackl, C., Gasser, T., Houghton, R. A., Sitch, S., Canadell, J. G., et al. (2023). Harmonising the land-use flux estimates of global models and national inventories for 2000–2020. *Earth System Science Data*, 15(3), 1093–1114. <https://doi.org/10.5194/essd-15-1093-2023>
- Guimberteau, M., Zhu, D., Maignan, F., Huang, Y., Yue, C., Dantec-Nédélec, S., et al. (2018). ORCHIDEE-MICT (v8.4.1), a land surface model for the high latitudes: Model description and validation. *Geoscientific Model Development*, 11(1), 121–163. <https://doi.org/10.5194/gmd-11-121-2018>
- Hansis, E., Davis, S. J., & Pongratz, J. (2015). Relevance of methodological choices for accounting of land use change carbon fluxes. *Global Biogeochemical Cycles*, 29(8), 1230–1246. <https://doi.org/10.1002/2014GB004997>
- Hartmann, J., Jansen, N., Dürr, H. H., Kempe, S., & Köhler, P. (2009). Global CO<sub>2</sub>-consumption by chemical weathering: What is the contribution of highly active weathering regions? *Global and Planetary Change*, 69(4), 185–194. <https://doi.org/10.1016/j.gloplacha.2009.07.007>
- Hersbach, H., Bell, B., Berrisford, P., Hirahara, S., Horányi, A., Muñoz-Sabater, J., et al. (2020). The ERA5 global reanalysis. *Quarterly Journal of the Royal Meteorological Society*, 146(730), 1999–2049. <https://doi.org/10.1002/qj.3803>
- Hirschler, O., & Osterburg, B. (2022). Peat extraction, trade and use in Europe: A material flow analysis. *Mires & Peat*, 28, 24–27. <https://doi.org/10.19189/MaP.2021.SNPG.StA.2315>
- Hmiel, B., Petrenko, V. V., Dyonisius, M. N., Buizert, C., Smith, A. M., Place, P. F., et al. (2020). Preindustrial <sup>14</sup>CH<sub>4</sub> indicates greater anthropogenic fossil CH<sub>4</sub> emissions. *Nature*, 578(7795), 409–412. <https://doi.org/10.1038/s41586-020-1991-8>
- Houghton, R. A., & Nassikas, A. A. (2017). Global and regional fluxes of carbon from land use and land cover change 1850–2015. *Global Biogeochemical Cycles*, 31(3), 456–472. <https://doi.org/10.1002/2016GB005546>
- Hurttt, G. C., Chini, L., Sahajpal, R., Frohking, S., Bodirsky, B. L., Calvin, K., et al. (2020). Harmonization of global land use change and management for the period 850–2100 (LUH2) for CMIP6. *Geoscientific Model Development*, 13(11), 5425–5464. <https://doi.org/10.5194/gmd-13-5425-2020>
- IPCC. (2006). 2006 IPCC guidelines for national greenhouse gas inventories. Retrieved from <https://www.ipcc-nggip.iges.or.jp/public/2006gl/>
- IPCC. (2019). 2019 refinement to the 2006 IPCC guidelines for national greenhouse gas inventories. Retrieved from <https://www.ipcc-nggip.iges.or.jp/public/2019rf/index.html>
- IPCC. (2021). In V. Masson-Delmotte, P. Zhai, A. Pirani, S. L. Connors, C. Péan, S. Berger, et al. (Eds.), *Climate Change 2021: The Physical Science Basis. Contribution of Working Group I to the Sixth Assessment Report of the Intergovernmental Panel on Climate Change*. Cambridge University Press. <https://doi.org/10.1017/9781009157896>
- Jiang, C., & Ryu, Y. (2016). Multi-scale evaluation of global gross primary productivity and evapotranspiration products derived from Breathing Earth System Simulator (BESS). *Remote Sensing of Environment*, 186, 528–547. <https://doi.org/10.1016/j.rse.2016.08.030>
- Jung, M., Schwalm, C., Migliavacca, M., Walther, S., Camps-Valls, G., Koiraala, S., et al. (2020). Scaling carbon fluxes from eddy covariance sites to globe: Synthesis and evaluation of the FLUXCOM approach. *Biogeosciences*, 17(5), 1343–1365. <https://doi.org/10.5194/bg-17-1343-2020>
- Kaiser, J. W., Heil, A., Andreae, M. O., Benedetti, A., Chubarova, N., Jones, L., et al. (2012). Biomass burning emissions estimated with a global fire assimilation system based on observed fire radiative power. *Biogeosciences*, 9(1), 527–554. <https://doi.org/10.5194/bg-9-527-2012>
- Korosuo, A., Pilli, R., Abad Viñas, R., Blujdea, V. N. B., Colditz, R. R., Fiorese, G., et al. (2023). The role of forests in the EU climate policy: Are we on the right track? *Carbon Balance and Management*, 18(1), 15. <https://doi.org/10.1186/s13021-023-00234-0>
- Lauerwald, R., Allen, G. H., Deemer, B. R., Liu, S., Maavara, T., Raymond, P., et al. (2023). Inland water greenhouse gas budgets for RECCAP2: 2. Regionalization and homogenization of estimates. *Global Biogeochemical Cycles*, 37(5). <https://doi.org/10.1029/2022GB007658>
- Li, N., Sippel, S., Winkler, A. J., Mahecha, M. D., Reichstein, M., & Bastos, A. (2022). Interannual global carbon cycle variations linked to atmospheric circulation variability. *Earth System Dynamics*, 13(4), 1505–1533. <https://doi.org/10.5194/esd-13-1505-2022>
- Littell, J. S., McKenzie, D., Peterson, D. L., & Westerling, A. L. (2009). Climate and wildfire area burned in western U.S. ecoregions, 1916–2003. *Ecological Applications*, 19(4), 1003–1021. <https://doi.org/10.1890/07-1183.1>
- Luyssaert, S., Abril, G., Andres, R., Bastviken, D., Bellassen, V., Bergamaschi, P., et al. (2012). The European land and inland water CO<sub>2</sub>, CO, CH<sub>4</sub> and N<sub>2</sub>O balance between 2001 and 2005. *Biogeosciences*, 9(8), 3357–3380. <https://doi.org/10.5194/bg-9-3357-2012>
- Luyssaert, S., Ciais, P., Piao, S. L., Schulze, E.-D., Jung, M., Zaehle, S., et al. (2010). The European carbon balance. Part 3: Forests. *Global Change Biology*, 16(5), 1429–1450. <https://doi.org/10.1111/j.1365-2486.2009.02056.x>
- Madani, N., Kimball, J. S., & Running, S. W. (2017). Improving global gross primary productivity estimates by computing optimum light use efficiencies using flux tower data. *Journal of Geophysical Research: Biogeosciences*, 122(11), 2939–2951. <https://doi.org/10.1002/2017JG004142>
- Madani, N., & Parazoo, N. C. (2020). *Global monthly GPP from an improved light use efficiency model, 1982–2016*. ORNL DAAC. <https://doi.org/10.3334/ORNLDAAC/1789>
- Max-Planck-Institute for Biogeochemistry [MPI-BGC]. (n.d.). Data exchange portal. Retrieved from <https://www.bgc-jena.mpg.de/geodb/projects/Home.php>
- Mayorga, E., Seitzinger, S. P., Harrison, J. A., Dumont, E., Beusen, A. H. W., Bouwman, A. F., et al. (2010). Global nutrient export from waterSheds 2 (NEWS 2): Model development and implementation. *Environmental Modelling & Software*, 25(7), 837–853. <https://doi.org/10.1016/j.envsoft.2010.01.007>
- McDowell, N. G., Allen, C. D., Anderson-Teixeira, K., Aukema, B. H., Bond-Lamberty, B., Chini, L., et al. (2020). Pervasive shifts in forest dynamics in a changing world. *Science*, 368(6494), eaaz9463. <https://doi.org/10.1126/science.aaz9463>
- McDowell, N. G., Beerling, D. J., Breshers, D. D., Fisher, R. A., Raffa, K. F., & Stitt, M. (2011). The interdependence of mechanisms underlying climate-driven vegetation mortality. *Trends in Ecology & Evolution*, 26(10), 523–532. <https://doi.org/10.1016/j.tree.2011.06.003>
- McGrath, M. J., Petrescu, A. M. R., Peylin, P., Andrew, R. M., Matthews, B., Dentener, F., et al. (2023). The consolidated European synthesis of CO<sub>2</sub> emissions and removals for the European Union and United Kingdom: 1990–2020. *Earth System Science Data*, 15(10), 4295–4370. <https://doi.org/10.5194/essd-15-4295-2023>
- Mendonça, R., Müller, R. A., Clow, D., Verpoorter, C., Raymond, P., Tranvik, L. J., & Sobek, S. (2017). Organic carbon burial in global lakes and reservoirs. *Nature Communications*, 8(1), 1694. <https://doi.org/10.1038/s41467-017-01789-6>
- Meybeck, M., Dürr, H. H., & Vörösmarty, C. J. (2006). Global coastal segmentation and its river catchment contributors: A new look at land-ocean linkage. *Global Biogeochemical Cycles*, 20(1). <https://doi.org/10.1029/2005GB002540>
- Monteil, G., Broquet, G., Scholze, M., Lang, M., Karstens, U., Gerbig, C., et al. (2020). The regional European atmospheric transport inversion comparison, EUROCOM: First results on European-wide terrestrial carbon fluxes for the period 2006–2015. *Atmospheric Chemistry and Physics*, 20(20), 12063–12091. <https://doi.org/10.5194/acp-20-12063-2020>
- Moran, D., Pichler, P.-P., Zheng, H., Muri, H., Klenner, J., Kramel, D., et al. (2022). Estimating CO<sub>2</sub> emissions for 108000 European cities. *Earth System Science Data*, 14(2), 845–864. <https://doi.org/10.5194/essd-14-845-2022>

- Murguia-Flores, F., Arndt, S., Ganesan, A. L., Murray-Tortarolo, G., & Hornibrook, E. R. C. (2018). Soil methanotrophy model (MeMo v1.0): A process-based model to quantify global uptake of atmospheric methane by soil. *Geoscientific Model Development*, 11(6), 2009–2032. <https://doi.org/10.5194/gmd-11-2009-2018>
- Nabuurs, G.-J., Arets, E. J. M. M., & Schelhaas, M.-J. (2018). Understanding the implications of the EU-LULUCF regulation for the wood supply from EU forests to the EU. *Carbon Balance and Management*, 13(1), 18. <https://doi.org/10.1186/s13021-018-0107-3>
- Nabuurs, G.-J., Lindner, M., Verkerk, P. J., Gunia, K., Deda, P., Michalak, R., & Grassi, G. (2013). First signs of carbon sink saturation in European forest biomass. *Nature Climate Change*, 3(9), 792–796. <https://doi.org/10.1038/nclimate1853>
- O'Sullivan, M. (2022). TRENDYv10 DGVM output for: Process-oriented analysis of dominant sources of uncertainty in the land carbon sink [Dataset]. *Zenodo*. <https://doi.org/10.5281/zenodo.6884342>
- Palahí, M., Valbuena, R., Senf, C., Acil, N., Pugh, T. A. M., Sadler, J., et al. (2021). Concerns about reported harvests in European forests. *Nature*, 592(7856), E15–E17. <https://doi.org/10.1038/s41586-021-03292-x>
- Patacca, M., Lindner, M., Lucas-Borja, M. E., Cordonnier, T., Fidej, G., Gardiner, B., et al. (2023). Significant increase in natural disturbance impacts on European forests since 1950. *Global Change Biology*, 29(5), 1359–1376. <https://doi.org/10.1111/gcb.16531>
- Petrescu, A. M. R., McGrath, M. J., Andrew, R. M., Peylin, P., Peters, G. P., Ciais, P., et al. (2021). The consolidated European synthesis of CO<sub>2</sub> emissions and removals for the European Union and United Kingdom: 1990–2018. *Earth System Science Data*, 13(5), 2363–2406. <https://doi.org/10.5194/essd-13-2363-2021>
- Petrescu, A. M. R., Peters, G. P., Janssens-Maenhout, G., Ciais, P., Tubiello, F. N., Grassi, G., et al. (2020). European anthropogenic AFOLU greenhouse gas emissions: A review and benchmark data. *Earth System Science Data*, 12(2), 961–1001. <https://doi.org/10.5194/essd-12-961-2020>
- Petrescu, A. M. R., Qiu, C., Ciais, P., Thompson, R. L., Peylin, P., McGrath, M. J., et al. (2021). The consolidated European synthesis of CH<sub>4</sub> and N<sub>2</sub>O emissions for the European Union and United Kingdom: 1990–2017. *Earth System Science Data*, 13(5), 2307–2362. <https://doi.org/10.5194/essd-13-2307-2021>
- Petrescu, A. M. R., Qiu, C., McGrath, M. J., Peylin, P., Peters, G. P., Ciais, P., et al. (2023). The consolidated European synthesis of CH<sub>4</sub> and N<sub>2</sub>O emissions for the European Union and United Kingdom: 1990–2019. *Earth System Science Data*, 15(3), 1197–1268. <https://doi.org/10.5194/essd-15-1197-2023>
- Petz, K., Schulp, C. J. E., van der Zanden, E. H., Veerkamp, C., Jan Schelhaas, M.-, Nabuurs, G.-J., & Hengeveld, G. (2016). *Indicators and modelling of land use, land management and ecosystem services. Methodological documentation Nature Outlook*. PBL Netherlands Environmental Assessment Agency. PBL publication number: 2386.
- Randerson, J. T., van der Werf, G. R., Giglio, L., Collatz, G. J., & Kasibhatla, P. S. (2018). Global fire emissions database, version 4, (GFEDv4) [Dataset]. *ORNL DAAC*. <https://doi.org/10.3334/ORNLDAAC/1293>
- Roberts, J. F., Champion, A. J., Dawkins, L. C., Hodges, K. I., Shaffrey, L. C., Stephenson, D. B., et al. (2014). The XWS open access catalogue of extreme European windstorms from 1979 to 2012. *Natural Hazards and Earth System Sciences*, 14(9), 2487–2501. <https://doi.org/10.5194/nhess-14-2487-2014>
- Rosentreter, J. A., Laruelle, G. G., Bange, H. W., Bianchi, T. S., Busecke, J. J. M., Cai, W.-J., et al. (2023). Coastal vegetation and estuaries are collectively a greenhouse gas sink. *Nature Climate Change*, 13(6), 579–587. <https://doi.org/10.1038/s41558-023-01682-9>
- Santoro, M., & Cartus, O. (2021). ESA biomass climate change initiative (Biomass\_cci): Global datasets of forest above-ground biomass for the years 2010, 2017 and 2018 v3.
- Saunio, M., Stavert, A. R., Poulter, B., Bousquet, P., Canadell, J. G., Jackson, R. B., et al. (2020). The global methane budget 2000–2017. *Earth System Science Data*, 12(3), 1561–1623. <https://doi.org/10.5194/essd-12-1561-2020>
- Schelhaas, M.-J., Nabuurs, G.-J., & Schuck, A. (2003). Natural disturbances in the European forests in the 19th and 20th centuries. *Global Change Biology*, 9(11), 1620–1633. <https://doi.org/10.1046/j.1365-2486.2003.00684.x>
- Sedano, F., & Randerson, J. T. (2014). Multi-scale influence of vapor pressure deficit on fire ignition and spread in boreal forest ecosystems. *Biogeosciences*, 11(14), 3739–3755. <https://doi.org/10.5194/bg-11-3739-2014>
- Seidl, R., Schelhaas, M.-J., Rammer, W., & Verkerk, P. J. (2014). Increasing forest disturbances in Europe and their impact on carbon storage. *Nature Climate Change*, 4(9), 806–810. <https://doi.org/10.1038/nclimate2318>
- Senf, C., Buras, A., Zang, C. S., Rammig, A., & Seidl, R. (2020). Excess forest mortality is consistently linked to drought across Europe. *Nature Communications*, 11(1), 6200. <https://doi.org/10.1038/s41467-020-19924-1>
- Senf, C., Müller, J., & Seidl, R. (2019). Post-disturbance recovery of forest cover and tree height differ with management in Central Europe. *Landscape Ecology*, 34(12), 2837–2850. <https://doi.org/10.1007/s10980-019-00921-9>
- Senf, C., & Seidl, R. (2021a). Mapping the forest disturbance regimes of Europe. *Nature Sustainability*, 4(1), 63–70. <https://doi.org/10.1038/s41893-020-00609-y>
- Senf, C., & Seidl, R. (2021b). Post-disturbance canopy recovery and the resilience of Europe's forests. *Global Ecology and Biogeography*, 31(1), 25–36. <https://doi.org/10.1111/gcb.13406>
- Senf, C., & Seidl, R. (2021c). Storm and fire disturbances in Europe: Distribution and trends. *Global Change Biology*, 27(15), 3605–3619. <https://doi.org/10.1111/gcb.15679>
- Smith, T., Traxl, D., & Boers, N. (2022). Empirical evidence for recent global shifts in vegetation resilience. *Nature Climate Change*, 12(5), 477–484. <https://doi.org/10.1038/s41558-022-01352-2>
- Solazzo, E., Crippa, M., Guizzardi, D., Muntean, M., Choulga, M., & Janssens-Maenhout, G. (2021). Uncertainties in the emissions database for global atmospheric research (EDGAR) emission inventory of greenhouse gases. *Atmospheric Chemistry and Physics*, 21(7), 5655–5683. <https://doi.org/10.5194/acp-21-5655-2021>
- Stavert, A. R., Saunio, M., Canadell, J. G., Poulter, B., Jackson, R. B., Regnier, P., et al. (2022). Regional trends and drivers of the global methane budget. *Global Change Biology*, 28(1), 182–200. <https://doi.org/10.1111/gcb.15901>
- Tian, H., Lu, C., Ciais, P., Michalak, A. M., Canadell, J. G., Saikawa, E., et al. (2016). The terrestrial biosphere as a net source of greenhouse gases to the atmosphere. *Nature*, 531(7593), 225–228. <https://doi.org/10.1038/nature16946>
- Tian, H., Xu, R., Canadell, J. G., Thompson, R. L., Winiwarter, W., Suntharalingam, P., et al. (2020). A comprehensive quantification of global nitrous oxide sources and sinks. *Nature*, 586(7828), 248–256. <https://doi.org/10.1038/s41586-020-2780-0>
- Tian, H., Yang, J., Xu, R., Lu, C., Canadell, J. G., Davidson, E. A., et al. (2019). Global soil nitrous oxide emissions since the preindustrial era estimated by an ensemble of terrestrial biosphere models: Magnitude, attribution, and uncertainty. *Global Change Biology*, 25(2), 640–659. <https://doi.org/10.1111/gcb.14514>
- Tubiello, F. N., Salvatore, M., Rossi, S., Ferrara, A., Fitton, N., & Smith, P. (2013). The FAOSTAT database of greenhouse gas emissions from agriculture. *Environmental Research Letters*, 8(1), 015009. <https://doi.org/10.1088/1748-9326/8/1/015009>

- UNFCCC. (n.d.). GHG data from UNFCCC [Dataset]. *United Nations Climate Change*. Retrieved from <https://unfccc.int/topics/mitigation/resources/registry-and-data/ghg-data-from-unfccc>
- UNFCCC. (2022). National inventory submissions 2022. Retrieved from <https://unfccc.int/process-and-meetings/transparency-and-reporting-reporting-and-review/reporting-and-review-under-the-convention/greenhouse-gas-inventories-annex-i-parties/submissions/national-inventory-submissions-2022>
- van der Werf, G. R., Randerson, J. T., Giglio, L., van Leeuwen, T. T., Chen, Y., Rogers, B. M., et al. (2017). Global fire emissions estimates during 1997–2016. *Earth System Science Data*, *9*(2), 697–720. <https://doi.org/10.5194/essd-9-697-2017>
- Velthof, G. L., Lesschen, J. P., Webb, J., Pietrzak, S., Miatkowski, Z., Pinto, M., et al. (2014). The impact of the Nitrates Directive on nitrogen emissions from agriculture in the EU-27 during 2000–2008. *Science of the Total Environment*, *468–469*, 1225–1233. <https://doi.org/10.1016/j.scitotenv.2013.04.058>
- Wernick, I. K., Ciais, P., Fridman, J., Högberg, P., Korhonen, K. T., Nordin, A., & Kauppi, P. E. (2021). Quantifying forest change in the European Union. *Nature*, *592*(7856), E13–E14. <https://doi.org/10.1038/s41586-021-03293-w>
- Winkler, K., Fuchs, R., Rounsevell, M., & Herold, M. (2021). Global land use changes are four times greater than previously estimated. *Nature Communications*, *12*(1), 2501. <https://doi.org/10.1038/s41467-021-22702-2>
- Winkler, K., Yang, H., Ganzenmüller, R., Fuchs, R., Ceccherini, G., Duveiller, G., et al. (2023). Changes in land use and management led to a decline in Eastern Europe's terrestrial carbon sink. *Communications Earth & Environment*, *4*(1), 237. <https://doi.org/10.1038/s43247-023-00893-4>
- Yao, Y., Ciais, P., Viovy, N., Li, W., Cresto-Aleina, F., Yang, H., et al. (2021). A data-driven global soil heterotrophic respiration dataset and the drivers of its inter-annual variability. *Global Biogeochemical Cycles*, *35*(8), e2020GB006918. <https://doi.org/10.1029/2020GB006918>
- Yao, Y., Tian, H., Shi, H., Pan, S., Xu, R., Pan, N., & Canadell, J. G. (2020). Increased global nitrous oxide emissions from streams and rivers in the Anthropocene. *Nature Climate Change*, *10*(2), 138–142. <https://doi.org/10.1038/s41558-019-0665-8>
- Zaehle, S., & Friend, A. D. (2010). Carbon and nitrogen cycle dynamics in the O-CN land surface model: 1. Model description, site-scale evaluation, and sensitivity to parameter estimates. *Global Biogeochemical Cycles*, *24*(1). <https://doi.org/10.1029/2009GB003521>
- Zhao, M., Heinsch, F. A., Nemani, R. R., & Running, S. W. (2005). Improvements of the MODIS terrestrial gross and net primary production global data set. *Remote Sensing of Environment*, *95*(2), 164–176. <https://doi.org/10.1016/j.rse.2004.12.011>
- Zscheischler, J., Mahecha, M. D., Avitabile, V., Calle, L., Carvalhais, N., Ciais, P., et al. (2017). Reviews and syntheses: An empirical spatio-temporal description of the global surface-atmosphere carbon fluxes: Opportunities and data limitations. *Biogeosciences*, *14*(15), 3685–3703. <https://doi.org/10.5194/bg-14-3685-2017>